AD **4 2 1 8 8 9**

DEFENSE DOCUMENTATION CENTER

FOR

SCIENTIFIC AND TECHNICAL INFORMATION

CAMERON STATION, ALEXANDRIA, VIRGINIA

GENERAL MOTORS CORPORATION

Technical Report

ON THE THEORY OF THE RADAR-PLASMA ABSORPTION EFFECT

GM DEFENSE RESEARCH LABORATORIES

SANTA BARPARA, CALIFORNIA

AEROSPACE OPERATIONS DEPARTMENT

Copy No 62

GENERAL MOTORS CORPORATION

Technical Report

ON THE THEORY OF THE RADAR-PLASMA ABSORPTION EFFECT
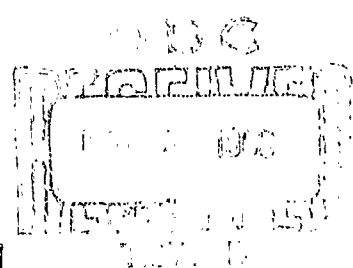
H.M. MUSAL, JR.

GM DEFENSE RESEARCH LABORATORIES

SANTA BARBARA, CALIFORNIA

AEROSPACE OPERATIONS DEPARTMENT

TR63-217A

JULY 1963

FOREWORD

This report is one of a series of related papers covering various aspects of a broad program to investigate the flow-field variables associated with hypersonic-velocity projectiles in free flight under controlled environmental condtions. This research is being conducted in the Flight Physics Range of General Motors Defense Research Laboratories; the work is supported by the Advanced Research Projects Agency under Contract No. DA-04-495-ORD-3567 (Z), and the contract is monitored by the Army Missile Command. It is intended that the series of reports generated under this program, when completed, shall form a background of knowledge of the phenomena involved in the basic study and thus aid in a better understanding of the data obtained in the investigation.

The reports submitted under this program fall into the following general categories:

1. Technical discussions of the theoretical and experimental aspects of selected areas of interest,

2. Data reports and compilations of experimental data derived in the investigation, and

3. Periodic progress reports.

The present report is one of those in the first category.

ABSTRACT

The usual manifestation of the phenomenon known as the radar absorption effect is the drastic reduction of the radar cross section of a body when it is surrounded by a plasma sheath having certain spatial configuration and electromagnetic properties. This effect has been observed during the atmospheric reentry of hypersonic test vehicles and in laboratory studies of models in hypersonic flight.

A brief review of the hypersonic aerodynamics, chemical physics, plasma physics, and electromagnetic wave scattering phenomena involved in the study of plasma effects on radar cross sections is given. It is shown that the effect of the plasma sheath on the radar cross section of a hypersonic body can be considered separately from the effect of the plasma trail left behind the body. Several theoretical models of electromagnetic wave scattering from plasma-covered bodies are formulated and analyzed. The theoretical results of these analyses show both absorption and enhancement effects that could be caused by the plasma sheath.

Theoretical predictions of plasma sheath effects calculated from the analyses of the theoretical models are compared with experimental results. It is seen that the measured absorption and enhancement are both significantly greater than predicted by the theoretical results.

Possible reasons for these discrepancies between theory and experiment are discussed.

It is concluded that the physical mechanisms that cause the absorption and enhancement effects observed experimentally are not yet completely understood and consequently not completely included in the theoretical models. Several possible additional factors are suggested for incorporation into more advanced theoretical models of electromagnetic wave scattering from plasma sheathed bodies in order to predict the radar absorption effect more accurately.

TABLE OF CONTENTS

TABLE OF CONTENTS (continued)

LIST OF ILLUSTRATIONS

LIST OF ILLUSTRATIONS
FOR APPENDIXES

LIST OF ILLUSTRATIONS (continued)

SECTION I
INTRODUCTION

One aspect of the general study of the interaction between electro-magnetic waves and plasmas that has received significant attention recently is the effect of a plasma sheath surrounding a body on the radar cross section of the body. [1 through 5]* Such a plasma sheath can be produced around a body in hypersonic flight through a gaseous atmosphere. Thus, interest in this subject arises in the consideration of the dynamic radar cross sections of reentry objects. Since certain characteristic effects are caused by the plasma sheath, it is also of interest to consider these effects as the keys to new plasma diagnostic techniques. For these two reasons, a thorough understanding of the causative mechanisms behind these effects and an adequate theoretical analysis that can quantitatively predict these effects are necessary.

In this report, the particular phenomenon known as the radar absorption effect is discussed. The usual manifestation of this effect is the drastic reduction of the radar cross section of a body when it is surrounded by a plasma sheath having certain spatial configuration and electromagnetic properties. This effect has been observed during the atmospheric reentry of hypersonic test vehicles [6] and in laboratory studies of the flow fields around bodies in hypersonic flight through various ambient gases. [7], [8] Up to the present time a quantitatively adequate theoretical analysis that predicts this effect under all the conditions that have been observed has not been available, although certain aspects of this effect are well understood and can be predicted with reasonably good accuracy. [5]

---

*Numbers in parentheses refer to references listed at the end of this report.

SECTION II

DESCRIPTION OF PHENOMENA

Study of the plasma sheath effect on radar cross sections involves interplay between the disciplines of hypersonic aerodynamics, chemical physics, plasma physics, and electromagnetic wave scattering. The simultaneous application of the first three disciplines is required in order to determine the configuration and physical properties of the plasma sheath formed around a body in hypersonic flight through an ambient atmosphere. The physical properties of the plasma sheath are in general described by the phase space distribution functions of all the constituents, which simplifies to the specification of composition, temperature, and density in the special case of thermodynamic and chemical equilibrium. Important parameters entering into this aspect of the phenomenon are the ambient gas density, temperature, and composition, and the body configuration, angle of attack, and speed. The latter two disciplines are then applied to determine the electromagnetic response of the plasma-sheathed body to the applied electromagnetic wave from the radar and thus determine the electromagnetic wave scattering. Important parameters entering into this aspect of the phenomenon are the configuration and physical properties of the body and the surrounding plasma sheath, the frequency of the incident electromagnetic wave, and the relative orientation between the body and the direction of propagation of the incident and scattered electromagnetic waves. As indicated, the aerodynamic, chemical, and plasma aspects of the problem can be decoupled from

the plasma and electromagnetic wave scattering aspects in most cases, in particular when the energy density of the electromagnetic field is negligible compared to the thermal and kinetic energy density of the flow field. This allows independent determination of the properties of the flow field and independent study of electromagnetic wave-plasma interaction and scattering from plasma-coated bodies. However, the final prediction of the details of plasma sheath effects in any given aerodynamic situation necessarily involves the combination of the results of computations from all these disciplines. It is important to emphasize that if any one of these computations is in error, then the final prediction will be incorrect.

Consider a body traveling through an ambient gaseous atmosphere at hypersonic speed. Energy lost by the body through aerodynamic forces acting on the body is transferred to the gas that is disturbed by the body. This energy transfer is manifested in the formation of a strong shock wave around the front of the high-speed body. The gas in the shock layer around the front of the body has received a large amount of energy that is distributed among the various degrees of freedom of the gas particles. Some excitation, dissociation, and ionization of the gas particles will result, thus producing radiation and free electrons. A significant amount of the radiation, from the infrared through the ultraviolet, is radiated out of the shock layer. The ultraviolet radiation may produce additional ionization ahead of the shock front (precursor ionization) when it is absorbed by the ambient gas particles. Also, some of the high-energy free electrons may diffuse ahead of the shock front, causing additional precursor ionization. As the partially ionized gas in the shock layer flows from the front of the body (the stagnation region) around to the sides of the

body it expands and cools, thereby reducing the free electron concentration. This thin layer of partially ionized gas (plasma) surrounding the hypersonic body constitutes the plasma sheath. When the flowing plasma reaches the rear of the body it rapidly expands to fill the volume swept out behind the body, and further expansion to ambient pressure also occurs very rapidly. The effect of this expansion is to reduce the free electron concentration in the plasma left behind the body (the trail or wake) very rapidly, so that shortly behind the body this quantity may be orders of magnitude smaller than in the stagnation region. Farther behind the body the free electron concentration in the trail decreases by diffusion, attachment, and recombination processes at a much slower rate.

This simple picture of the flow field may be complicated by the formation of a recompression zone behind the body, and the addition of foreign particles to the flow field by the ablation of material from the body surface. Determination of the exact variation of the free electron concentration as well as other particle specie concentrations around the body and in the trail requires detailed consideration, in both the equilibrium and non-equilibrium regimes, of the aerodynamic and chemical processes involved. These considerations lie at current frontiers of knowledge in both sciences.

When an electromagnetic wave propagates in a region containing free electrons (such as a plasma) the electric and magnetic fields of the wave influence the motion of the free electrons, which in turn extract energy from the electromagnetic wave. This absorbed energy is either returned to the electromagnetic field as coherent scattered radiation (with a broadened frequency spectrum due to doppler and

other effects) or converted to thermal energy (both non-coherent radiant energy and random kinetic energy). Thermalization of the energy is the result of "collisions" between the free electrons and other particles in the plasma. When the free electron concentration in the plasma is very small the coherent scattered radiation does not change the total electromagnetic field significantly, the energy losses are small, and an incident electromagnetic wave propagates almost unaffected by the "transparent" plasma. If the free electron concentration is sufficiently large, the coherent scattered radiation and energy losses contribute significantly to the description of the total electromagnetic field.

In order to facilitate quantitative discussion of electromagnetic wave-plasma interaction it is convenient to introduce the concepts of plasma frequency and electron collision frequency. The plasma frequency is a measure of the free electron concentration, and is given in Appendix A-1. The physical significance of the plasma frequency is that, if there are no electron collisons with other particles, an electromagnetic wave with a frequency higher than the plasma frequency will propagate in the plasma, while if the wave frequency is lower than the plasma frequency propagation is not possible (the electric and magnetic fields merely "diffuse" in the plasma). The electron collision frequency is just the average number of collisions per second between each free electron and other particles in the plasma required to account for the energy losses. From a detailed viewpoint, the concept of electron collision frequency is really somewhat of an artificiality. In a plasma in which the collision frequency is not zero (losses are present), electromagnetic wave propagation is always possible although with greatly increased

attenuation when the wave frequency is less than the plasma frequency. Thus, if the electromagnetic wave frequency is much greater than both the plasma frequency and the electron collision frequency the plasma appears essentially transparent to the wave, while if the plasma frequency approaches or exceeds the wave frequency the wave suffers significant scattering (and absorption if the electron collision frequency also approaches or exceeds the wave frequency).

Now consider an electromagnetic wave (such as a radar pulse) incident on the plasma-sheathed body and its plasma trail. If the radar frequency is sufficiently higher than the stagnation region plasma frequency and electron collision frequency, the incident radar wave will be unaffected by any of the plasma since at all other locations around and behind the body the plasma frequency and electron collision frequency are usually lower than in the stagnation region. Scattering of this incident electromagnetic wave will thus be caused by the body alone, and the radar cross section will be the free-space radar cross section of the body. If the radar frequency is lowered (or the electron concentration is increased, due to higher ambient gas density and/or higher body speed) the radar wave will first be affected by the plasma in the stagnation region, and with continued radar frequency reduction (or continued electron concentration increase) the radar wave will be affected progressively by more of the plasma sheath around the sides of the body. Throughout this regime the trail, although present, will usually be essentially transparent to the radar wave and consequently will not contribute to the radar cross section; the plasma sheath surrounding the body will then determine, to a great extent, the effective radar cross section.

If the electron collision frequency is very small compared to both the radar frequency and plasma frequency, the plasma sheath will appear reflective, approaching the appearance of a solid reflective coating when the plasma frequency exceeds the radar frequency. If, on the other hand, the electron collision frequency is comparable to the radar frequency and plasma frequency, the plasma sheath will appear absorptive. Hence, in this regime the plasma-sheathed body will appear to be a reflective or absorptive object having the configuration of the outer surface of the plasma sheath, the expansion zone behind the body may give a small additional contribution, and the trail will be essentially transparent.

Further reduction of the radar frequency (or increase of the electron concentration) will cause the interaction between the incident electro-magnetic wave and the plasma in the trail to become significant, and thus the trail will begin to contribute to the total radar cross section. The effective length of the trail in which significant microwave-plasma interaction occurs will tend to increase as the radar frequency is reduced or the electron concentration left behind the body increases. It is important to note, however, that this interaction may take the form of either scattering or absorption, depending on the magnitude of the electron collision frequency, and therefore it does not immediately follow that the radar cross section of the trail will necessarily increase under these conditions. In the parameter regime in which the trail does contribute significantly to the total effective radar cross section the variations due to the contribution from the plasma-sheathed body may be negligible in comparison to the variations due to the contribution from the plasma trail.

Consideration of the phenomena described in the preceding paragraphs suggests an initial subdivision of the problem into essentially independent determinations of the plasma sheath effect on the radar cross section of the body and the radar cross section of the plasma trail as an additional target element, from which the total effective radar cross section of the complex target can be determined by appropriate summation. This subdivision is particularly useful if the significant parameter sensitivities of the sheath effect and the trail effect occur in different parameter regimes.

Determination of the plasma sheath effect on the radar cross section of the body (and the radar cross section of the plasma trail) is accomplished by first the determination of the physical properties of the plasma and their spatial variation (the "boundaries" of the plasma), and then the determination of the electromagnetic wave scattering characteristics from which the radar cross section is derived. Effective decoupling of the physical properties and "boundaries" determination from the electromagnetic scattering determination depends upon the condition that the incident electromagnetic wave does not significantly alter the physical properties or the spatial variation of the plasma. This is usually the case in normal radar applications, since the coherent energy supplied by the incident radar wave is negligible compared to the normal thermal and kinetic energy level in the plasma.

If the details of the frequency spectrum broadening of the scattered coherent electromagnetic energy are not to be considered, the physical properties of the plasma and the details of the energy transfer mechanisms can usually be subsumed in a phenomenological description

of the propagation of the incident electromagnetic wave. This
phenomenological approach consists of the assignment of effective
constitutive parameters (dielectric constant and conductivity) to the
plasma, as well as any other media involved, and the subsequent
treatment of the electromagnetic behavior on a classical electro-
magnetic field theory basis. Thus, the plasma is considered to be a
lossy (and in general, nonlinear, anisotropic, and inhomogeneous)
dielectric material.

The analytical determination of the scattering of an incident electro-
magnetic wave by localized spatial distributions of material
characterized by electromagnetic constitutive parameters is a
classical boundary-value problem in electromagnetic field theory.
The complete description of the scattering effects can be expressed
in terms of boundary-matched sets of solutions to Maxwell's equations
(one set of solutions for each of the regions involved). Information
about the nature of this solution in the high-frequency regime can be
obtained from a geometrical optics solution to the problem. The results
of a geometrical optics solution to the problem must be used with
caution, however, since incomplete or highly misleading interpretations
are possible if the applicability criteria are not satisfied. Even though
its applicability may be limited, a geometrical optics solution should
not be excluded a priori since it can be obtained with relative ease
compared to the rigorous solution of the electromagnetic boundary-
value problem. Often, certain characteristic features of the solution
can be easily seen from the geometrical optics solution even when the
exact solution is extremely complicated.

SECTION III

MODELS OF PHENOMENA, ANALYTIC APPROACHES, AND THEORETICAL RESULTS

It is obvious from the preceding discussion that the complete physical situation is too complicated to analyze in comprehensive detail initially. Part of the difficulty of a comprehensive analysis lies in the cross-coupling between the different scientific disciplines involved, each of which has its own unsolved problems. Thus, to provide an initial approach to the determination of the plasma sheath effect on the radar cross section of a body, simple models characterizing the main features of the structure and properties of a plasma-sheathed body were evolved. Furthermore, in order to expedite the initial determination of the behavior of these models and to simplify the interpretation of the analytical results, simple analytic approaches to the various aspects of the behavior were used.

Basic Model

The body configuration chosen to represent typical blunt-nosed hypersonic vehicles, for frontal aspects, is the sphere. In order to make the electromagnetic wave scattering analysis tractable the sphere is assumed to be perfectly reflective. This represents a realistic approximation for metallic bodies. This assumption, however, makes the model not directly applicable to the consideration of ablative-dielectric-coated vehicles.

It is assumed that all ionization around the front of the sphere is confined within the shock layer. Thus, the bow shock wave around the front of the sphere defines the outer boundary of the plasma sheath. In this case, the effect of precursor ionization, if any, is not considered.

The determination of the exact shape of the bow shock wave formed around the front of a body in hypersonic flight through a gaseous atmosphere involves lengthy and complicated aerodynamic computation, even for relatively simple body configurations. In order to avoid this complication, it is assumed that the plasma sheath forms a constant-thickness layer around the sphere. If only the frontal view of the sphere is considered (the stagnation region) this approximation appears to be reasonably in accord with the actual physical picture. [9, 10, 11] An explicit, exact formula for the calculation of the plasma sheath thickness at the stagnation point (shock wave detachment distance) has not been obtained up to the present time; however, approximate formulas are available. [12, 13, 14]

The physical properties of the plasma sheath that determine its electromagnetic wave interaction behavior are subsumed in the specification of an effective dielectric constant and conductivity of the plasma. Thus, the spectral broadening of the scattered electromagnetic energy [15] is not considered. The effective electromagnetic constitutive parameters (dielectric constant and conductivity) of the plasma are derived from the consideration of the propagation of a small-amplitude plane transverse electromagnetic wave through an unbounded uniform plasma with no externally applied magnetic field, considering the effect of only the free electrons. This analysis yields

linear and isotropic constitutive parameters, given in Appendix A-1,
dependent only on the plasma frequency, electron collision frequency,
and incident wave frequency. Thus, the anisotropic effects in the
plasma introduced by the application of a magnetic field are not
considered. The spatial variation (homogeneity) of the plasma con-
stitutive parameters throughout the plasma sheath must be known
explicitly in order to determine the electromagnetic wave scattering
behavior. This requires determination of the spatial variation of
electron concentration and electron collision frequency throughout
the plasma sheath, which is a complicated and lengthy aerophysical
computation. In order to avoid this complication, it is assumed that
the constitutive parameters of the plasma are spatially uniform
(homogeneous) throughout the plasma sheath.

As a result of the simplifying approximations detailed in the preceding
paragraphs, the initial theoretical investigation of the plasma sheath
effect on the radar cross section of a hypersonic body is reduced to
the problem of determining how the radar cross section of a perfectly
reflective body is changed when it is coated with a uniform-thickness
layer of linear, isotropic, homogeneous lossy dielectric material.
In the case of the spherical body, an exact analytic solution
is available (see Appendix A-2), but the interpretation of the
mathematical results is very difficult without extensive numerical
computation. In keeping with the precept of a simplified approach
to the initial study of the behavior of the plasma sheath effect, the
short-wavelength (or high-frequency) regime was selected, thus
allowing the application of a geometrical optics approach to the
determination of the radar cross section of both the bare sphere and
the dielectric-coated (plasma-sheathed) sphere. The steps in this

analytic approach are detailed in Appendixes A-3 through A-7. This approach considers the propagation of an electromagnetic wave from a radar toward the dielectric-coated metallic sphere where partial reflection of the wave back toward the radar occurs at the outer surface of the dielectric coating. Partial transmission (penetration) of the incident wave into the dielectric coating also occurs, and this transmitted wave is attenuated as it propagates through the dielectric coating to the sphere surface where it is reflected so that it propagates, with additional attenuation, back to the outer surface of the dielectric coating. At the outer surface of the dielectric coating the attenuated wave is partially transmitted out of the dielectric coating toward the radar and partially reflected back into the dielectric coating, where the attenuated propagation, sphere surface reflection, etc. cycle is repeated over and over again. The total electromagnetic wave returned to the radar from the dielectric-coated sphere thus consists of the coherent superposition of the wave reflection from the dielectric surface and an infinite number of decreasing-intensity wave contributions emerging from the dielectric surface due to the multiple reflections within the dielectric layer. The intensity of the total returned electromagnetic wave is the measure of the radar cross section. The geometrical optics approach used here accounts for electromagnetic wave interference and thus predicts scintillation effects that arise from this phenomenon. This geometrical optics approach is valid when the size and radii of curvature of the body are much larger than the wavelength of the incident electromagnetic wave; in general, it gives the direct specular contribution to the radar cross section, but does not account for surface or ducted waves which may also contribute to the radar cross section.

14

When this analysis is applied to the situation where the dielectric represents a plasma (see Appendix A-8), several interesting results are obtained. In particular, the most significant result of the analysis is the prediction of conditions under which the radar cross section of the plasma-covered metallic sphere vanishes. These conditions therefore define complete "radar absorption", and a radar absorption effect will occur whenever these conditions are approached. The amount of absorption (decrease of radar cross section) that occurs in any given situation is dependent on how closely the complete absorption conditions are approached in that situation. It can be seen from Appendix A-8 that the normalized plasma frequency required for complete absorption is of the order of unity for small (less than unity) values of normalized electron collision frequency, and varies approximately as the square root of the normalized electron collision frequency for large (greater than unity) values of normalized electron collision frequency. The minimum plasma-layer thickness for which complete absorption can occur is of the order of one-third of the free-space wavelength of the radar wave when the normalized electron collision frequency is large, and increases at a moderate rate as the normalized electron collision frequency is decreased below unity. These results are comparable to the results obtained from the rigorous analysis of the case of an infinite, flat, metallic sheet covered with a uniform layer of lossy plasma (see Appendix A-9).

Advanced Model

In the basic model considered in the previous section, the spatial variation of the plasma properties throughout the plasma sheath around the hypersonic body was neglected. This appears to be one of the most obvious deficiencies of the basic model. Actually, the plasma properties vary spatially in both the angular (azimuthal) direction around the body and the radial direction away from the body surface. In general, both the plasma frequency and the electron collision frequency decrease in the azimuthal direction away from the stagnation point. The radial variation can, in general, be more complicated. It is possible for the plasma frequency to increase, reach a maximum, and then decrease in the radial direction away from the body surface. The electron collision frequency around the front of the body is usually essentially constant from the body surface out to the shock front, where it decreases abruptly to the value for the ambient gas.

If chemical equilibrium is maintained in the shock layer, the plasma frequency in the shock layer around the front of the body also is relatively constant from the body surface out to the shock front, where it decreases rapidly to zero unless significant precursor ionization is present. Such precursor ionization effectively extends the radial range of non-zero plasma frequency outside the shock front, although usually with a much smaller value than in the shock layer and with a smoothly decreasing magnitude outward in the radial direction. If chemical equilibrium is not maintained in the shock layer, two different forms of radial variation of the plasma frequency are possible. In one case, the plasma frequency begins to increase inside the shock front and continues monotonically increasing

toward the body surface. The gradient of plasma frequency depends on the chemical reaction rates involved in the production of free electrons from the neutral gas particles. In the other case, the plasma frequency also begins to increase inside the shock front but reaches a maximum from which it decreases in the direction toward the body surface. This "overshoot" may be significantly large compared to the magnitude of the plasma frequency near the body surface. The details of this spatial variation again depend on the chemical reactions occurring in the gas behind the shock front. Here again, precursor ionization may be present with a generally similar effect to the case where chemical equilibrium is maintained.

Some general idea of how radial and azimuthal gradients in the electromagnetic properties of the plasma sheath may modify the solution obtained for the basic model (uniform plasma layer) can be obtained by separate consideration of gradients in the two directions. Here all the simplifications of the basic model are employed except that the plasma layer is assumed to have either radially or azimuthally non-uniform electromagnetic properties. Some work has been reported [16] on the scattering of electromagnetic waves by a dielectric-coated metallic sphere, where the dielectric coating is uniform in thickness but has radial variation of its electromagnetic properties. Considering this model in regard to the radar absorption effect, it is possible for a lossy dielectric layer with a radial gradient to reduce the magnitude of the backscattered electromagnetic wave, and hence the radar cross section, more than it would be reduced by an equivalent uniform lossy dielectric layer. In terms of the plasma parameters, if the plasma frequency decreases smoothly in the radial direction away from

the sphere surface from a value larger to a value significantly smaller than the radar frequency and the electron collision frequency is moderately large compared to the radar frequency, considerable absorption will occur provided also that the distance over which the plasma frequency decreases is significantly large compared to the radar wavelength. If the change in plasma frequency occurs over a distance that is a small fraction of the radar wavelength, no significant difference between this case and the uniform-plasma-layer situation will exist. Thus, for a plasma sheath that is only a small fraction of a radar wavelength in thickness, the effect of a radial gradient may be neglected by simply using an average value of the plasma frequency in the layer for the basic model analysis.

The effect of azimuthal variation of the electromagnetic properties of the dielectric coating around a metallic sphere on the electromagnetic wave scattering characteristics of the dielectric-coated sphere is analyzed in Appendixes A-10 through A-13. In this analysis all the assumptions made in the analysis of the basic model are made except uniformity of the dielectric properties, the short-wavelength (or high-frequency) regime is similarly considered, and the geometrical optics approach is also used to determine the radar cross section of the non-uniform lossy dielectric-coated metallic sphere. The variation of the dielectric properties is assumed to be symmetrical about an axis of symmetry, and the radar cross section looking along this axis is found. This corresponds to looking at a plasma-sheathed hypersonic sphere from the nose-on aspect.

Several interesting results are obtained from this analysis of the electromagnetic wave scattering characteristics of this non-uniform lossy dielectric-coated metallic sphere. Here again, as in the situation where the dielectric layer is uniform, conditions can be found for which the radar cross section will vanish. These conditions are similar to those obtained for the uniform dielectric situation. In addition, the dielectric layer acts as a lens which can either focus or de-focus the back-scattered electromagnetic wave and thus greatly increase as well as decrease the radar cross section. This is a new effect not predicted by the basic model (uniform dielectric). The focusing mechanism potentially can explain increases in the radar cross section which also have been observed. [7] Unfortunately, when strong focusing is present the applicability criteria of the geometrical optics approach are violated and the quantitative results become questionable. This does not mitigate the possibility for the physical mechanism (gradients) to produce such increases in radar cross section; it simply means that a more refined analysis must be used to obtain accurate quantitative predictions in this situation.

In order to determine appropriate spatial variations of dielectric properties that correspond to the variations of the plasma properties in the plasma sheath around the front of a hypersonic sphere, some flow field studies and computations are necessary. These are outlined in Appendix A-14. The results of these calculations show, as expected, that the plasma frequency and the electron collision frequency in the plasma sheath both decrease monotonically in going from the stagnation point around to the sides of the body. However, the electromagnetic wave relative phase factor in the plasma layer can either decrease or increase initially in going from the stagnation point

around to the sides of the body (see Appendix A-14). It is this angular variation of the relative phase factor that can cause focusing or de-focusing of the back-scattered electromagnetic wave at nose-on aspect.

In general, when the plasma frequency is less than the radar frequency the angular variation of the relative phase factor is such as to cause de-focusing, and when the plasma frequency is greater than the radar frequency the angular variation of the relative phase factor is such as to cause focusing. The exact ratio of plasma frequency to radar frequency at which transition from de-focusing to focusing occurs depends on the gradient of electron collision frequency. Specifically, when there is no angular variation of the electron collision frequency this transition occurs when the plasma frequency is the square root of two times the radar frequency. As the gradient of electron collision frequency increases, the ratio of plasma frequency to radar frequency at which this transition occurs increases. Since the plasma frequency in the plasma sheath increases with increasing speed of the body, it follows that the de-focusing effect will occur at a lower speed than that for which the focusing effect will occur.

When the sphere flow field analysis and the non-uniform lossy dielectric-coated metallic sphere wave scattering analysis are combined (see Appendix A-15) and applied to the plasma-sheathed sphere problem, several interesting results additional to those obtained for the case of the uniform plasma coating are obtained. It is found that the usual flow field spatial variations of the plasma sheath electromagnetic properties can produce gradients in the equivalent dielectric coating such

that both de-focusing and focusing of the nose-on back-scattered electromagnetic wave are possible. The relative parameter regimes in which these effects occur have been outlined in the preceeding paragraph. The net effect of de-focusing and focusing on the radar cross section depends very sensitively on the exact phase and amplitude relationships between all the component back-scattered waves that add coherently to give the total back-scattered wave whose amplitude is the measure of the radar cross section. Potentially, both de-focusing and focusing gradients can either decrease or increase the radar cross section compared to that obtained for the equivalent "zero-gradient" situation. In general, however, a de-focusing gradient cannot increase the radar cross section to a value greater than that obtained when the plasma coating is perfectly reflective. It can, of course, greatly decrease the radar cross section and consequently enhance any radar absorption effect. A focusing gradient can greatly increase the radar cross section above the value obtained when the plasma coating is perfectly reflective. It can also cause a pronounced decrease when the amplitude and relative phase relations between the component back-scattered waves are just right. Whether de-focusing or focusing will have a significant effect depends on how much of the net back-scattered power has passed through the plasma layer where it is affected by the de-focusing or focusing gradients.

In other words, if the incident wave does not penetrate into the plasma layer significantly, it cannot be significantly affected by the gradients, and consequently the back-scattered wave cannot exhibit significant de-focusing or focusing effects. At low body speeds the plasma frequency in the plasma sheath is low and consequently much

of the incident wave power passes through the plasma layer. It is under these conditions that the usual radar absorption effect occurs and that de-focusing gradients exist. Thus, it may be expected that de-focusing gradients will usually enhance the absorption effect. At high body speeds the plasma frequency in the plasma sheath is high and consequently very little of the incident wave power penetrates into the plasma layer. It is under this condition that focusing gradients exist. Consequently, because there is so little power available to be focused, it is not likely that the radar cross section will be greatly increased by focusing gradients.

SECTION IV

APPLICATION OF THEORETICAL RESULTS TO HYPERSONIC BODIES AND COMPARISON WITH EXPERIMENTAL RESULTS

Some experimental measurements of the radar cross sections of hypersonic bodies in a free-flight ballistic range have been reported,[7] under conditions where a radar absorption effect would be expected. These observations confirmed the existence of the absorption effect under controlled environmental conditions. It was found, however, that the measured absorption in some cases was considerably greater than predicted by the simplest theoretical model, as exemplified by the "basic model" of the previous section of this work. Comparisons of the experimental results from Reference 7 with the theoretical predictions from the "basic model" analysis of the phenomenon are shown in Figures 1, 2 and 3.

The details of the experimental program, whose results are shown in Figures 1, 2 and 3, are given in full in Reference 7 and will not be repeated here. It should be noted, however, that two different hypersonic body configurations were used in the experimental work. One model (copper-capped model) was a short plastic cylinder (10 mm long and 20 mm in diameter) whose forward end was rounded. This rounded nose was covered with a copper cap (13 mm nose radius) which served as a heat shield. The other body (copper sphere) was a plastic sphere covered with a copper skin (15 mm in diameter) which also served as a heat shield. The flight stability of the copper-capped models was very good, as evidenced by spark photographs of the
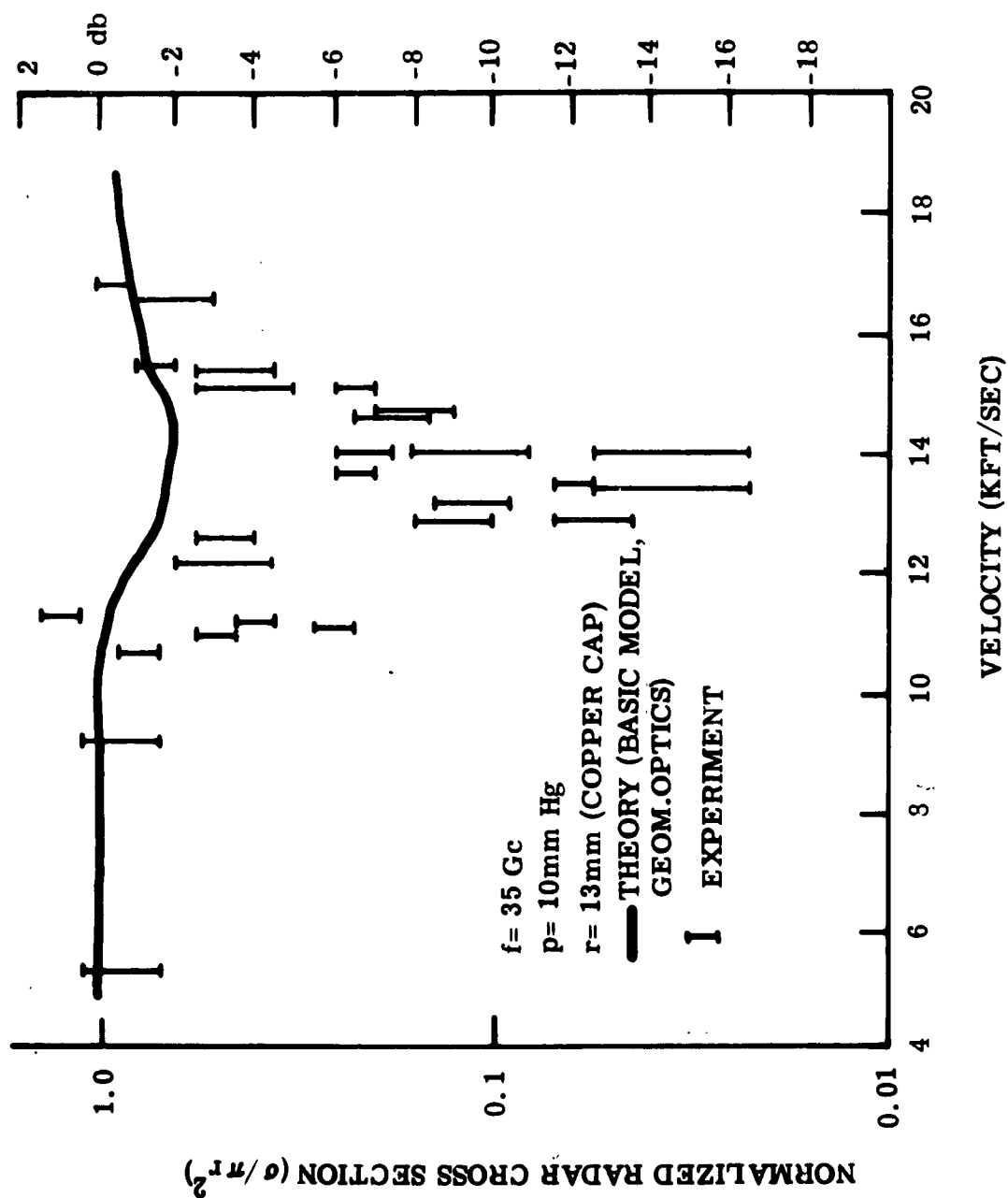
Figure 1   Nose-On Radar Cross Section of a Copper-Capped Model
in Flight vs Velocity, 35 Gc
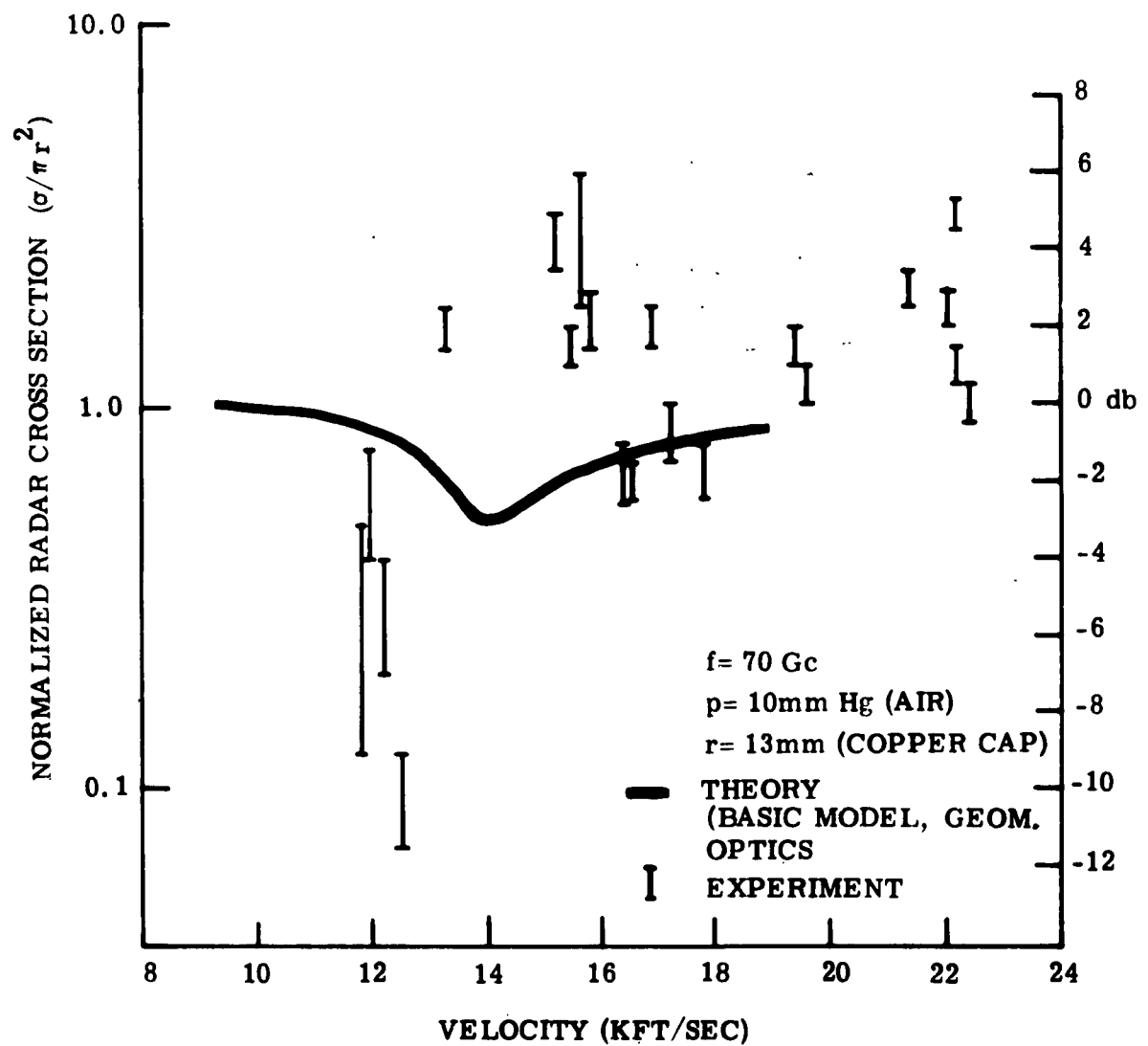
Figure 2   Nose-On Radar Cross Section of a Copper-Capped Model
in Flight vs Velocity, 70 Gc
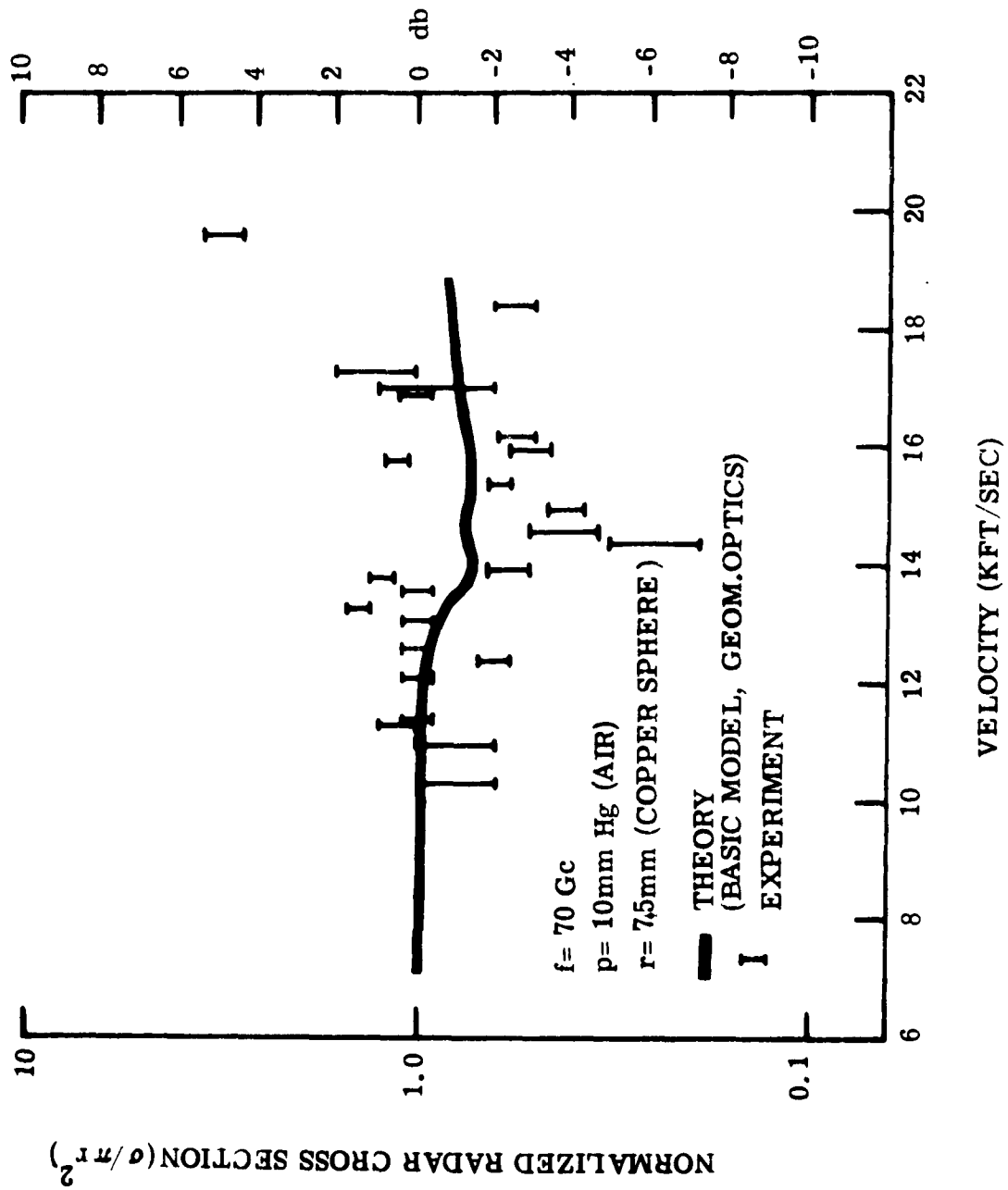
Figure 3   Nose-On Radar Cross Section of a Copper Sphere in
Flight vs Velocity, 70 Gc

models taken along the flight path. The structural integrity of the copper heat shields of both types of models throughout their flights was verified at the end of each flight by flash X-ray photographs. In the execution of the experimental program the ambient air pressure in the flight chamber was held constant at 10 mm Hg. The models were observed in flight by a CW doppler radar at the velocities shown by the data points. The vertical extent covered by each data point shows the extent of the variation of the measured radar cross section over the length of the flight path under observation (approximately 30 feet).

An outline of the method of calculation of the theoretical predictions shown in Figures 1, 2 and 3 is as follows. In order to use the "basic model" analysis to calculate the nose-on radar cross section of a plasma-sheathed blunt metallic body, it is necessary to know the plasma frequency and the electron collision frequency at the stagnation point and the thickness of the plasma layer around the nose of the body. Charts are available [17] showing the flow field properties of a blunt body in hypersonic flight through air over a range of ambient air density and flight velocity, and these charts were used to obtain the plasma frequency and electron collision frequency at the stagnation point as functions of body velocity for an ambient air pressure of 10 mm Hg. The derivation of the charts is based on the condition that chemical equilibrium is maintained in the flow field. In order to check the applicability of these charts for the small bodies used in the experimental work, special non-equilibrium flow field calculations were carried out for these small body sizes at specific velocities within the range encountered in the experimental work. It was found (see Appendix A-14) that near-equilibrium

conditions prevailed in the flow field near the body around the nose region of the bodies, and consequently the chart values of plasma properties are reasonably accurate even for the small bodies used in the experimental work. The plasma frequency and electron collision frequency at the stagnation point as functions of body velocity at an ambient air pressure of 10 mm Hg, obtained from the charts and used in the theoretical calculations, are shown in Appendix A-14. The value of plasma layer thickness used in the calculations is the actual measured value of shock detachment distance as a function of body velocity, taken from Reference 7 and shown in Appendix A-14; this value is in good agreement with other published theoretical and experimental work.[12, 13, 14]

Using the above input data, the theoretical prediction curves of nose-on radar cross section as a function of body velocity shown in Figures 1, 2 and 3 were calculated from equation (8.1) of Appendix A-8, which is the geometrical optics approximation. This calculation embodies the "basic model" assumption that the plasma layer can be considered to be spatially uniform. It can be seen that in all cases the measured absorption is greater than predicted by this theoretical approach.

In order to remove any doubt about the validity of the use of the geo- metrical optics approximation in deriving the theoretical curves shown in Figures 1, 2 and 3, the rigorous field theory solution of the "basic model" was obtained (see Appendix A-2). Using the same input data as for the geometrical optics calculation, the variation of the nose-on radar cross section as a function of body velocity was calcu- lated from the rigorous field theory solution, and is shown in Figures 4 and 5.
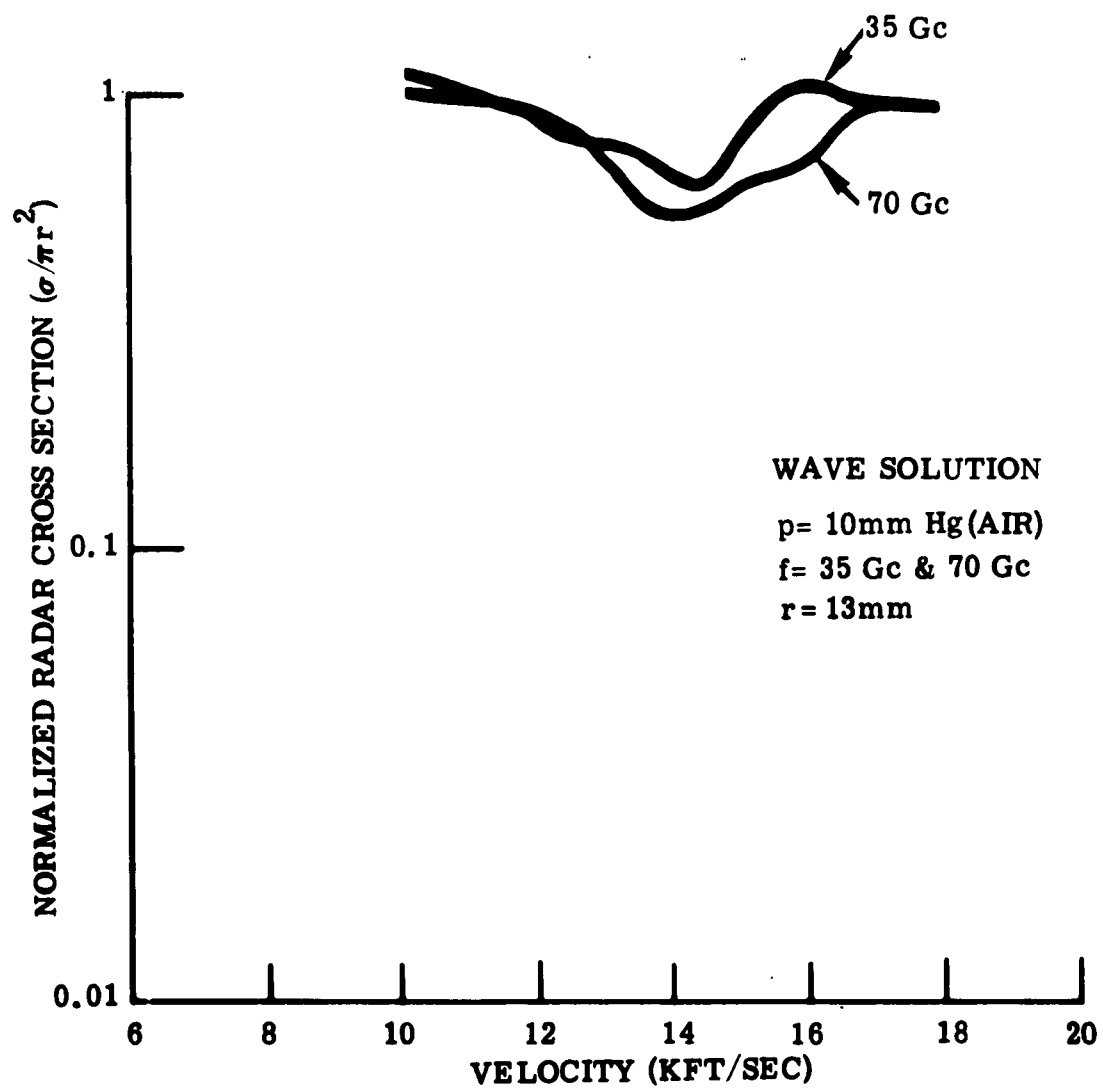
Figure 4   Wave Solution for Copper-Capped Model, 35 and 70 Gc
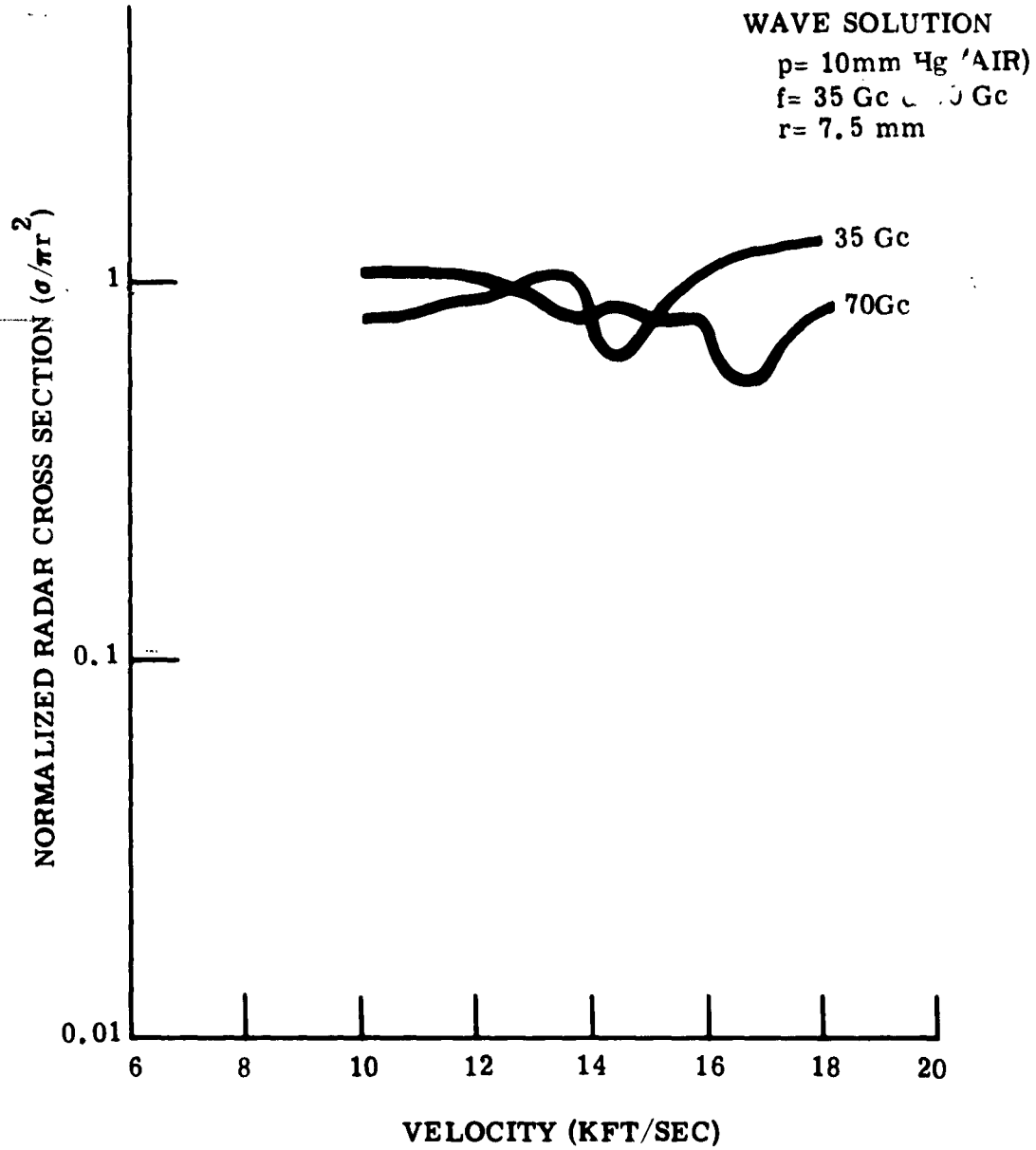
Figure 5   Wave Solution for Copper Sphere, 35 and 70 Gc

It can be seen from Figures 4 and 5 that there is little significant difference between the rigorous field theory approach and the geometrical optics approach in theoretically predicting the amount of absorption according to the "basic model" assumptions. It appears, therefore, that the "basic model" is deficient in characterizing the essential mechanisms that cause the large amount of absorption in the parameter regime covered by the experimental results.

It was pointed out earlier that one of the obvious deficiencies in the "basic model" is that it does not account for the gradients in the plasma properties in the plasma sheath around the nose of the body. Such gradients could, in principle, cause focusing or de-focusing of the back-scattered radar wave. The "advanced model" was formulated to incorporate this additional mechanism, and the nose-on radar cross section of this model was found using the geometrical optics approach (see Appendix A-15). In order to use this analysis to predict the amount of absorption that will occur, it is necessary to have analytic expressions for the gradients of plasma frequency and electron collision frequency in the flow field in the angular direction away from the stagnation point in the vicinity of the stagnation point. Some discussion and analysis of this aspect of the situation is given in Appendix A-14. It is shown there that the variations of plasma frequency and electron collision frequency in the angular direction near the stagnation point can be approximated by parabolic functions of the angle around the nose away from the stagnation point. Using the coefficients of these parabolic representations obtained from the non-equilibrium flow field analysis (see Appendix A-14) together with the plasma properties at the stagnation point used in the previous calculations, the variation of the nose-on

radar cross section as a function of body velocity predicted by the "advanced model" was calculated from Equation (15.1) of Appendix A-15 and is shown in Figures 6 and 7.

It can be seen, by comparison between Figures 1, 2 and 3 and Figures 6 and 7, that the "advanced model" predicts a somewhat different absorption behavior as a function of sphere velocity, but it does not account for the very large amount of absorption observed experimentally. Some enhancement effects due to focusing of the back-scattered radar wave are evident in the "advanced model" theoretical results. It should be noted that these theoretical results are based on the geometrical optics approach. In view of the good agreement between the results of the geometrical optics approach and the results of the rigorous wave theory approach in the analysis of the "basic model", it is reasonable to expect the geometrical optics approach to be applicable in the analysis of the "advanced model" also. Since the "advanced model" results do not predict a large amount of absorption it appears, therefore, that the presence of angular gradients in the plasma properties is not the significant mechanism causing the large amount of absorption in the parameter regime covered by the experimental results.
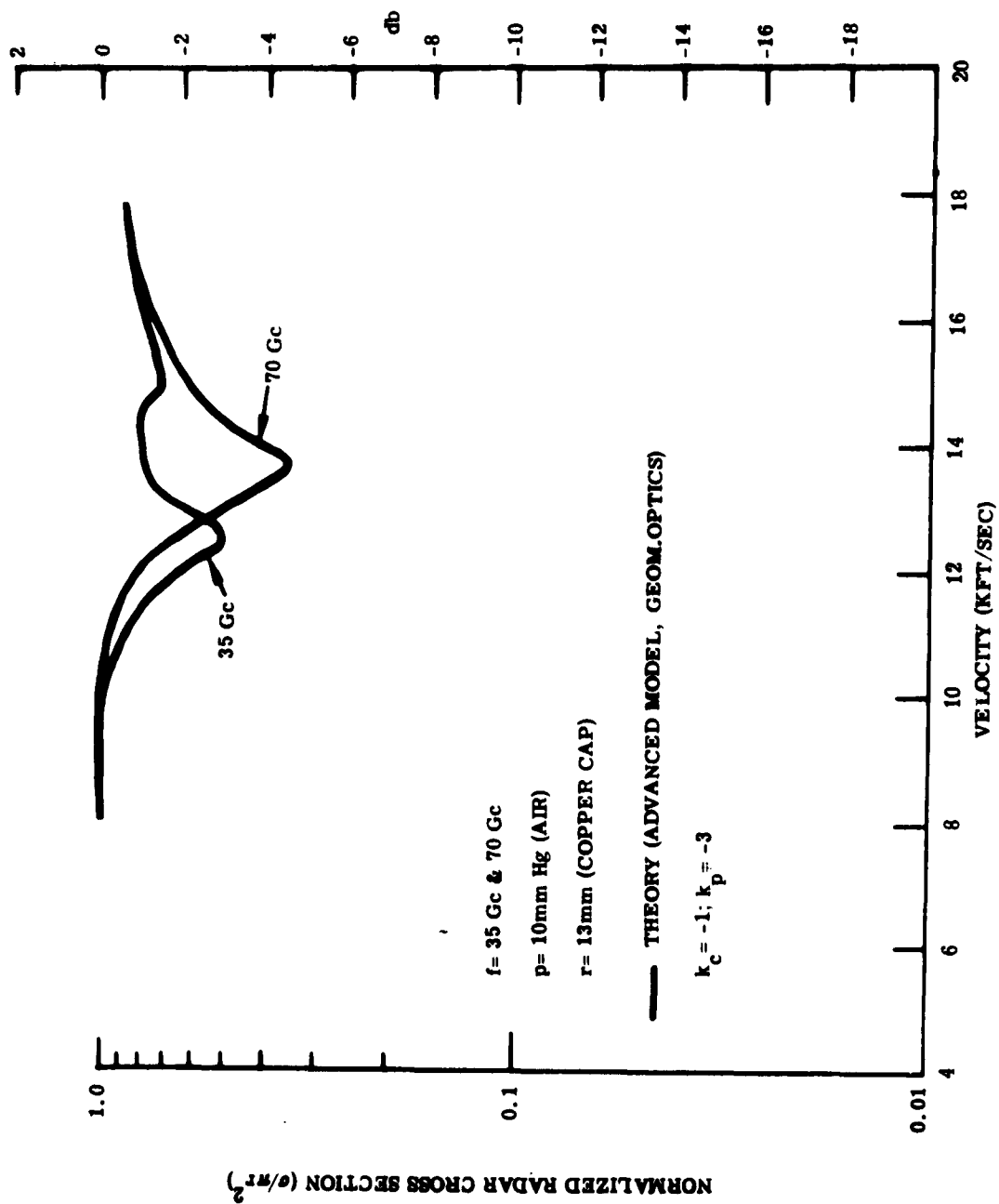
Figure 6   Geometrical Optics Solution for Copper-Capped Model, 35 & 70 Gc
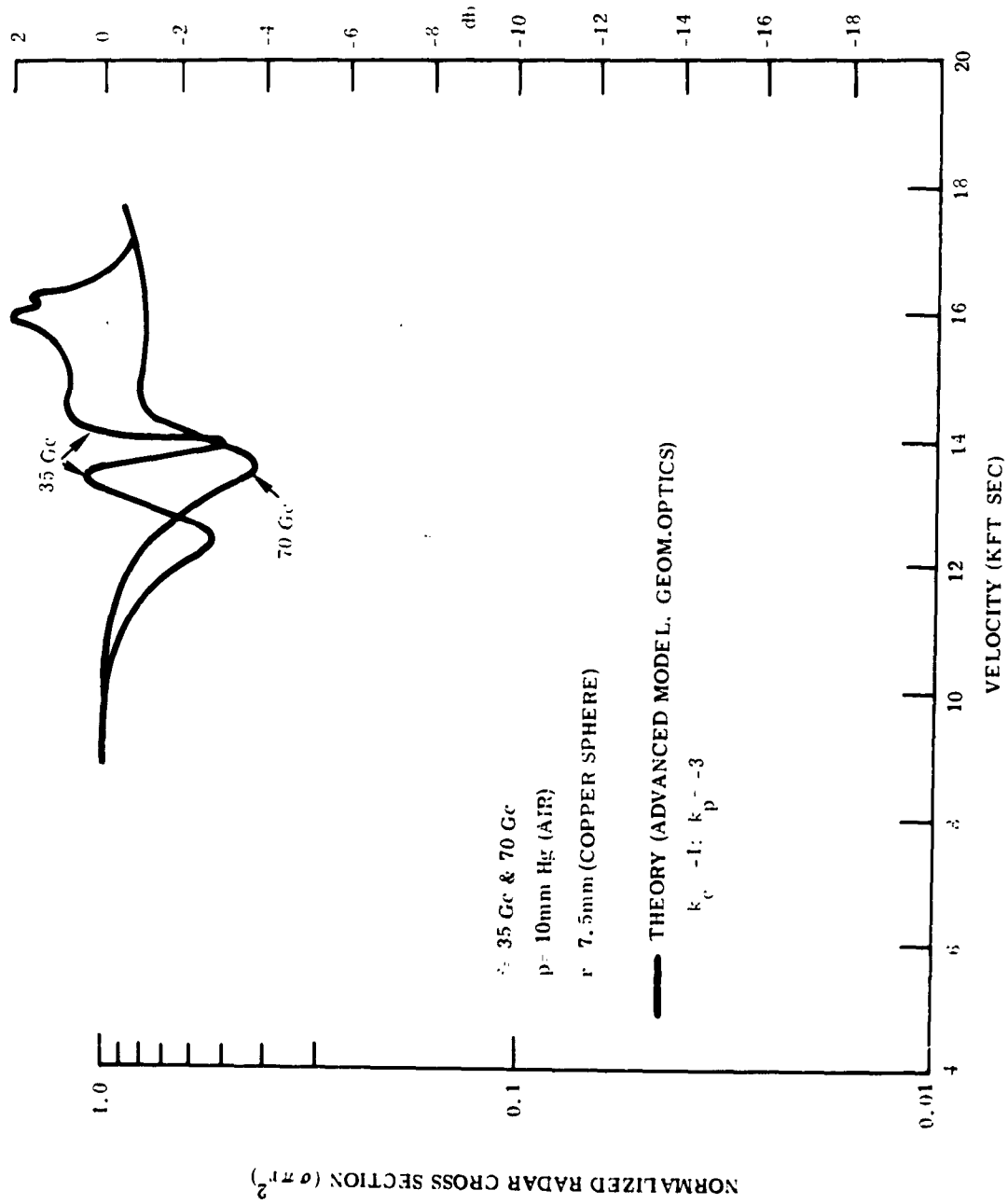
Figure 7 Geometrical Optics Solution for Copper Sphere, 35 & 70 Gc

SECTION V

DISCUSSION OF RESULTS

The comparisons between the experimental results available from
ballistic range studies of the effect of the plasma sheath on the nose-
on radar cross sections of blunt metallic bodies and the theoretical
predictions based on the theoretical models of the phenomenon for-
mulated in this report show that distinct discrepancies between theory
and experiment exist. Anomalous absorption and enhancement are
both seen in the experimental results. That is, the maximum absorption
measured is significantly greater than predicted by either the "basic
model" or the "advanced model", and the maximum enhancement in
the cases where it appears is significantly greater than predicted
by the "advanced model". These results seem to indicate that either
the numerical values of the plasma parameters used in the theoretical
calculations were in error or that the theoretical models are deficient
in representing a dominant mechanism involved in the phenomenon.
Such deficiencies may involve either (or both) the aerodynamic or
(and) the electromagnetic aspects of the situation.

Consider first the effects of variation of the numerical values of the
plasma parameters used in the theoretical calculations. The para-
meters involved are the plasma frequency, the electron collision
frequency, and the thickness of the plasma layer. The effects of
altered plasma properties on the theoretical predictions of the
"basic model" are shown in Figures 8, 9 and 10. The plasma
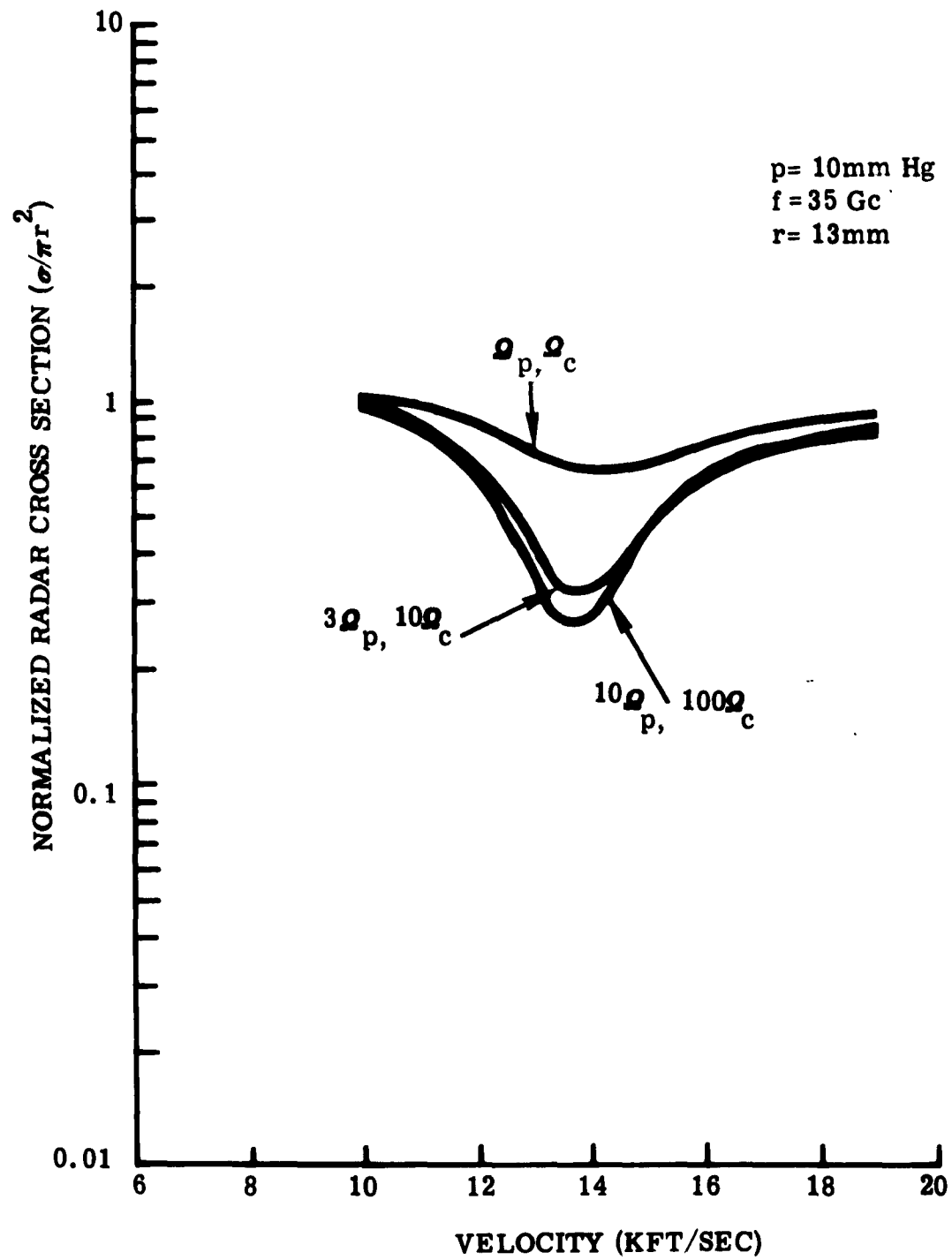
Figure 8   Effect of Plasma Frequency and Collision Frequency
Changes on Radar Absorption, Copper-Capped Model, 35 Gc
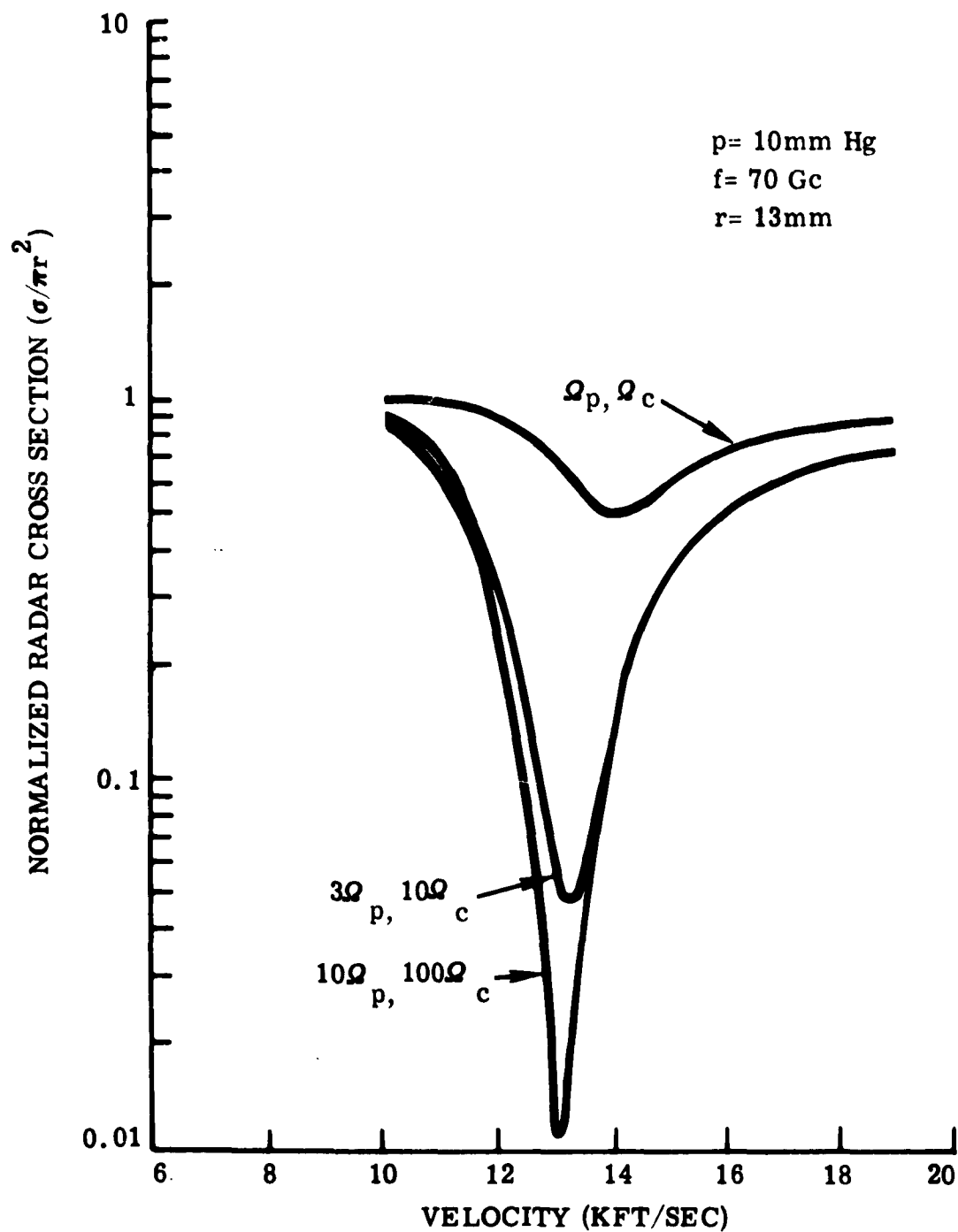
Figure 9   Effect of Plasma Frequency and Collision Frequency
Changes on Radar Absorption, Copper-Capped Model, 70 Gc
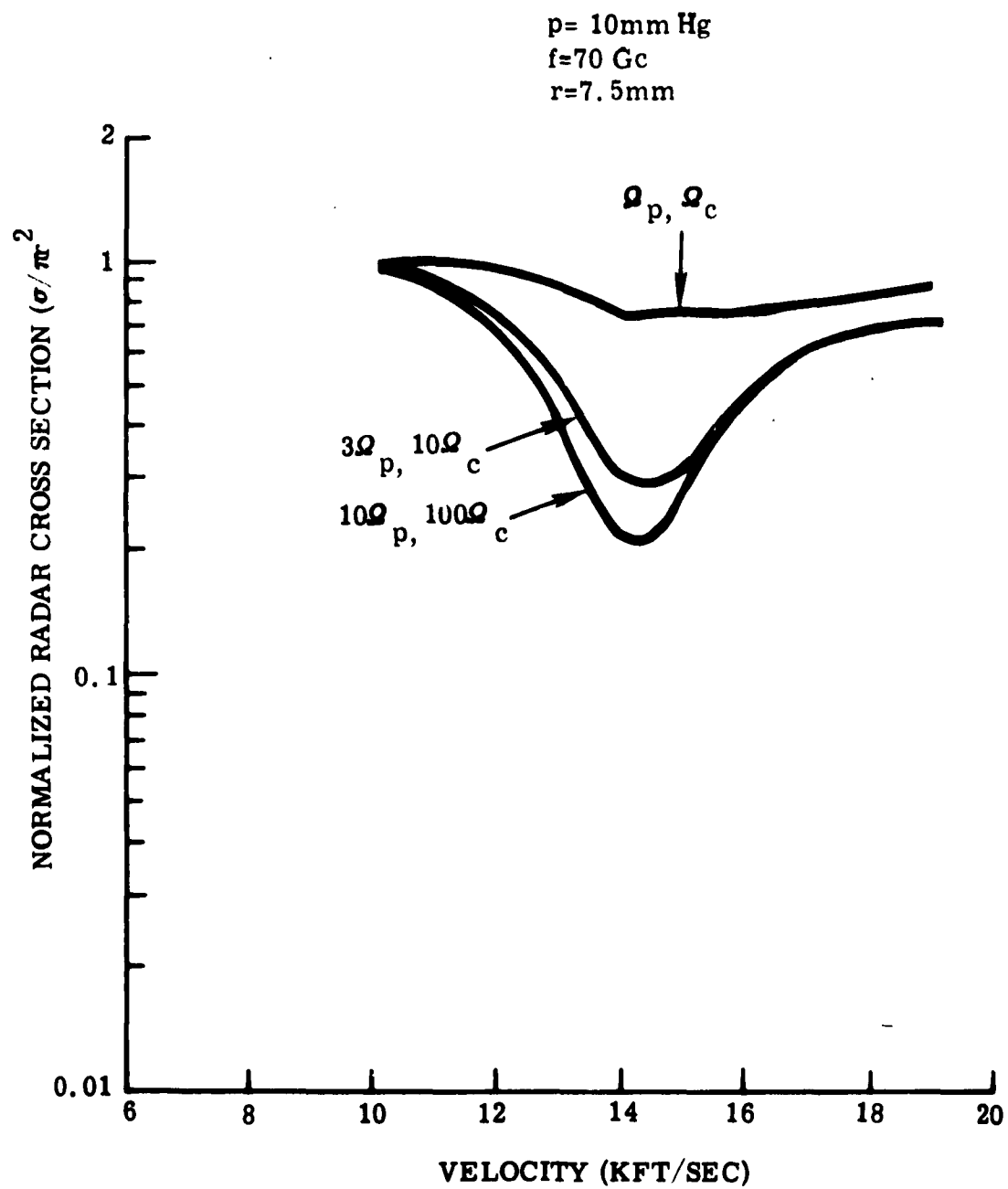
Figure 10   Effect of Plasma Frequency and Collision Frequency Changes
on Radar Absorption, Copper Sphere, 70 Gc

frequency and electron collision frequency have been increased in
such proportions as to increase the maximum absorption at approxi-
mately a fixed velocity. Factors of increase in plasma frequency and
electron collision frequency of up to 10 and 100, respectively, are
considered. It is apparent from Figures 8, 9 and 10 that this alone
is not sufficient to resolve the experimental-theoretical discrepancy,
and such large deviations from the values used in the original calcu-
lations are not at all justified. It appears, therefore, that the dis-
crepancy is not due to the use of incorrect values of plasma frequency
or electron collision frequency in the theoretical calculations. The
effects of variation of the numerical value of the plasma layer thick-
ness on the theoretical predictions of the "basic model" are shown in
Figures 11, 12 and 13. The value of thickness used in the calculations
shown is increased by factors of 2, 3 and 4 above the values used in
the original calculations. These curves show that maximum absorption
of the same order of magnitude as the experimental results is pre-
dicted when the plasma sheath thickness used in the calculations is
approximately three times the value originally used. This is consistent
with the requirements for vanishing radar cross section given in
Appendix A-8, since the tripled thickness is approximately one or
two halves of the radar wavelength at 35 Gc or 70 Gc, respectively,
for the copper-capped model and approximately one-half the radar
wavelength at 70 Gc for the copper sphere. It should be noted that
the numerical values of plasma sheath thickness used in the original
theoretical prediction calculations are actually the shock detachment
distances measured from photographs of the actual flow fields. These
measured shock detachment distances are in good agreement with
other published data and cannot be in error by more than 20 percent.
Hence, if the ionization is confined to the region behind the shock
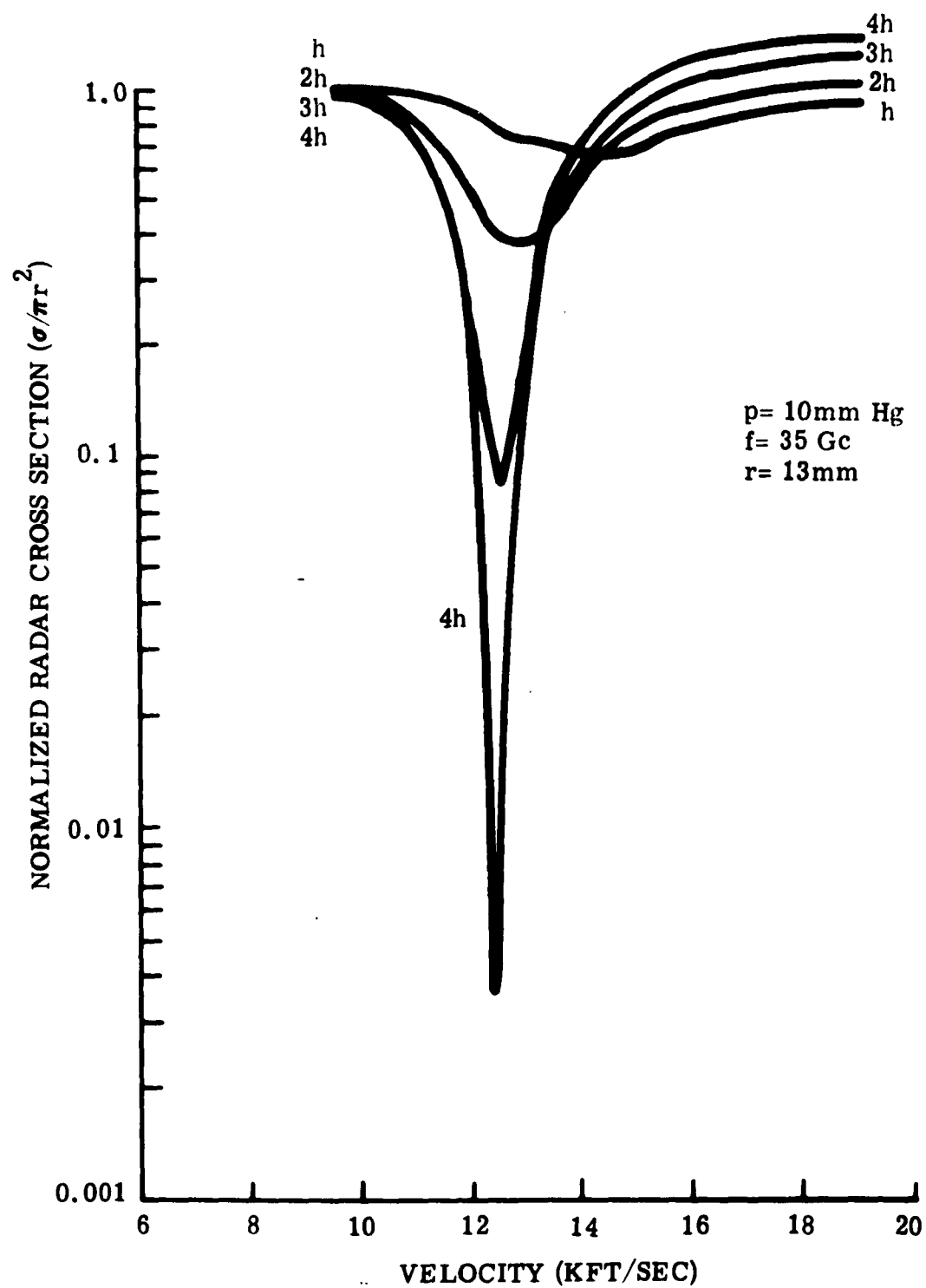
Figure 11   Effect of Changes in Stand-Off Distance on Radar Absorption,
Copper-Capped Model, 35 Gc
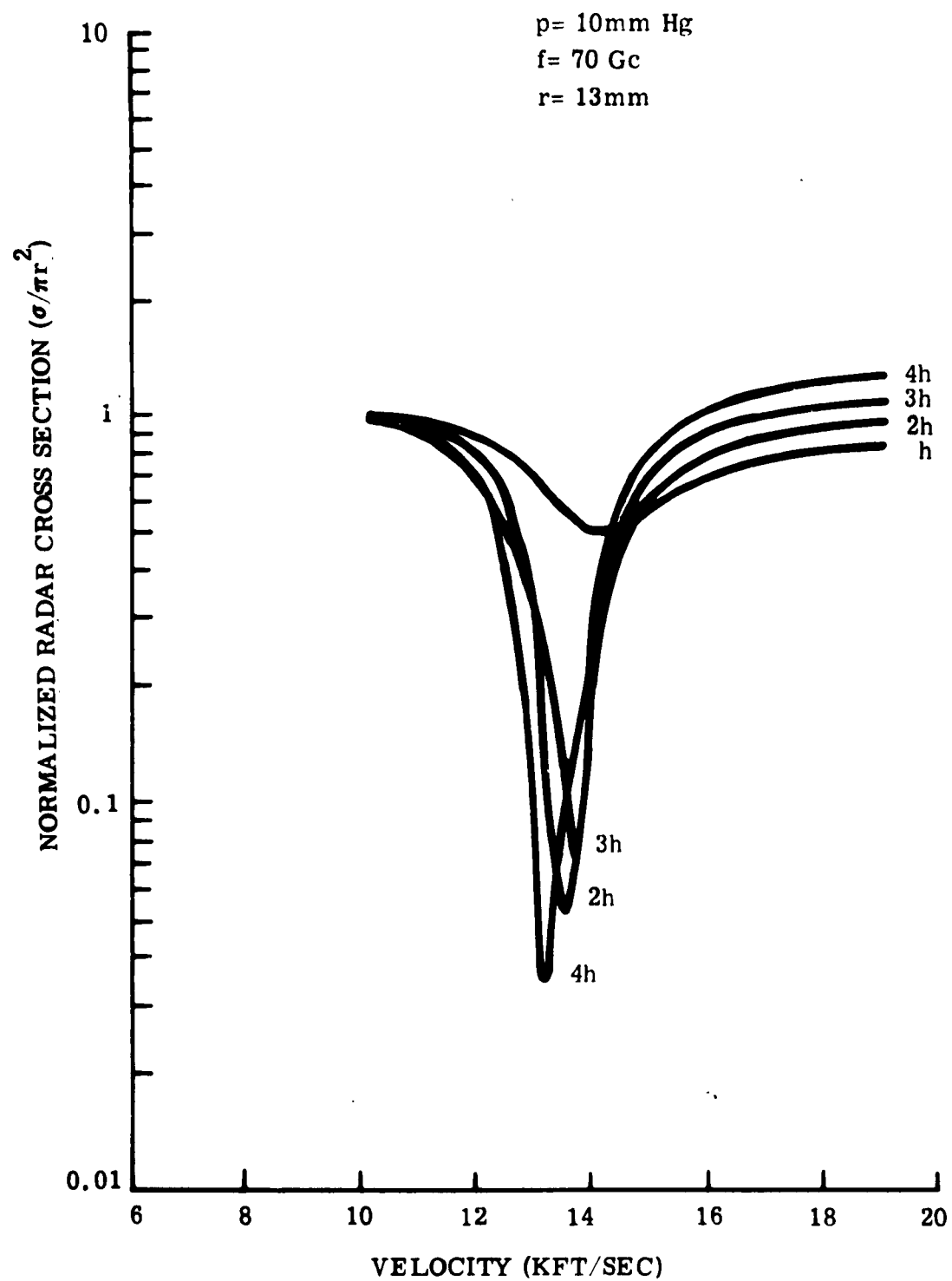
Figure 12   Effect of Changes in Stand-Off Distance on Radar Absorption, Copper-Capped Model, 70 Gc
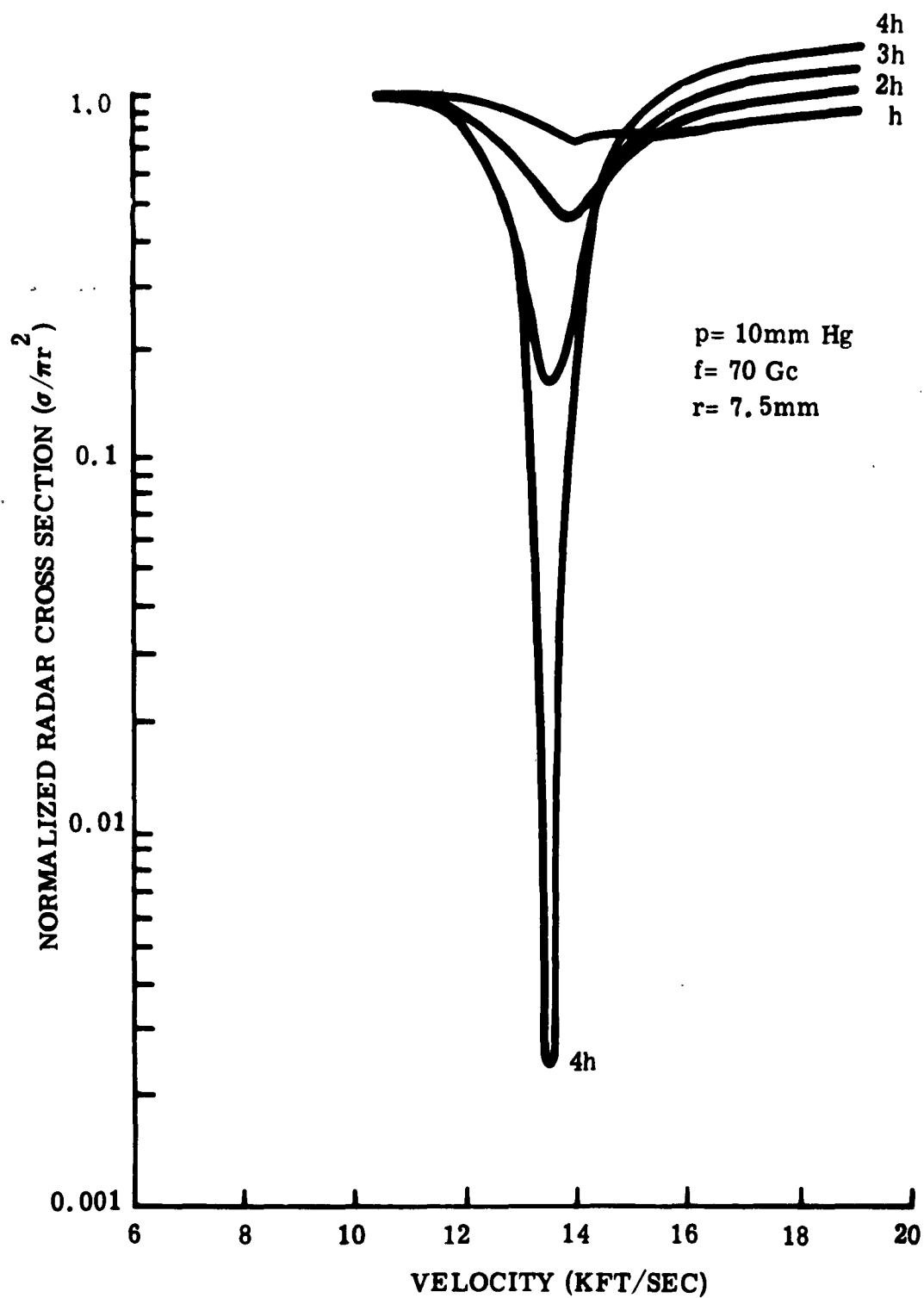
Figure 13   Effect of Changes in Stand-Off Distance on Radar
Absorption, Copper Sphere, 70 Gc

front, the plasma layer is too thin (by a factor of approximately three) to account for the measured absorption.

The theoretical models formulated here of the phenomena involved in the effect of the plasma sheath on the radar cross sections of blunt metallic bodies have not considered the possibility of the presence of ionization outside of the shock front around the nose of the body. Such precursor ionization could be produced by either (or both) electron diffusion ahead of the shock front or (and) ultraviolet photoionization of the air ahead of the luminous shock front. Precursor ionization ahead of the shock front effectively increases the plasma sheath thickness to a value greater than the shock detachment distance. The plasma frequency in a precursor ionization region caused by either electron diffusion or by photoionization will decrease smoothly in the radial direction away from the body. Such a transition region between free space and the shock front around the nose of the body can, if the parameters are appropriate, significantly influence the scattering of an incident electromagnetic wave and consequently affect the radar cross section.

Two mechanisms by which such a transition region can significantly decrease the radar cross section are (1) the actual absorption of the incident wave power in the transition region (real absorption) and (2) the reflection and refraction or diffraction of the incident wave in the transition region into directions other than the back-scattering direction (deviative absorption). Real absorption requires that the transition region be lossy, which implies that the electron collision frequency as well as the plasma frequency are not negligible compared to the radar frequency. Some analysis of this situation was given in

Reference 7, where it was shown that in order to produce significant absorption in a transition region with constant electron collision frequency and exponentially decreasing plasma frequency the e-folding distance had to be greater than one-fourth of the radar wavelength, and the peak plasma frequency and electron collision frequency had to be greater than one-tenth of the radar frequency.

An analysis of the deviative absorption situation has not yet been made, but it is reasonable to expect in this situation also that in order to produce a significant effect the peak plasma frequency would have to be at least one-tenth of the radar frequency or greater. A more refined examination of this matter is planned. At the present time there is a serious lack of extensive quantitative information about the amount of precursor ionization that may be present at various flight conditions. However, some preliminary measurements of precursor ionization have been made [18] and it appears from these measurements that the peak plasma frequency in the precursor region is too low at the flight conditions encountered in the experimental work to give significant interaction effects. At higher velocities and for lower radar frequencies the effect of precursor ionization will be more significant, and may account for some of the absorption effects observed during the atmospheric reentry of hypersonic test vehicles [6].

Because the plasma layer is so thin compared to the wavelength of the incident radar wave in the experimental regime studied in Reference 7, gradients within the layer in the radial direction away from the body could not greatly influence the overall scattering

behavior. Hence, the fact that such gradients have not been included in the theoretical models could not greatly alter the conclusions drawn so far. In principle, however, such gradients could considerably affect the scattering behavior when they extend over a region which is of the order of a wavelength in size.

Another physical mechanism, not incorporated in any of the theoretical models so far, that could possibly account for both the anomalous absorption and the increases in radar cross section is the coupling of the transverse electromagnetic radar wave with longitudinal plasma waves (electroacoustic waves). The anomalous absorption could result when strong coupling between the waves exists and the electroacoustic waves are highly damped, thus forming an effective "sink" for the coherent energy. Increases in the radar cross section could result if the electroacoustic waves resonate within the plasma sheath. These ideas are speculative at this time, but work is planned to substantiate (or deny) these possibilities.

The possibility is under study that peculiar diffraction effects may cause the anomalous absorption and the increase in radar cross section. It is possible that the copper-capped plastic model may give rise to some strong real diffraction effects both with and without the plasma sheath present. Studies of this model and configurational variations of it are being made in a static radar cross section range in order to answer this question.

SECTION VI
CONCLUSION

Several theoretical models of radar wave scattering from plasma-sheathed blunt metallic bodies have been formulated and analyzed. The results of the analyses show that the theoretical models potentially can account for both extreme absorption and enhancement under appropriate conditions. Predictions of the effects of the plasma sheath on radar cross sections based on these theoretical models have been compared with experimental results. The theoretical models fail to predict correctly the amount of absorption and enhancement observed experimentally for the particular values of parameters involved. The apparent reason for failure of the theory to give numerical results consistent with experimental results is that the plasma layer thickness used in the numerical calculations, as deduced from the most reasonable aerodynamic considerations, is too small to yield significant absorption or enhancement effects. It appears, therefore, that the physical mechanism that causes the absorption and enhancement effects observed experimentally is not yet completely understood and consequently is not included in the theoretical models. Further work on the theoretical models is necessary to incorporate into them the additional factors mentioned earlier in this work, and experiments over a wider range of parameters should be carried out to better define the theoretical-experimental relationship.

REFERENCES

(1)   Antenna Laboratory, Dept. of Electrical Engineering, Ohio State University Research Foundation, Geometrical Optics Approximations for the Effects of Shock Waves on Spherical Geometrics, by R. B. Green, Report 768-9, Columbus, Ohio, 15 August 1959.

(2)   Bendix Corporation, Bendix Systems Division, The Plasma Sheath Effect on the Radar Cross Section of a Hypersonic Sphere as Predicted by Lossless Geometrical Optics and The Plasma Sheath Effect on the Radar Cross Section of a Hypersonic Sphere as Predicted by Loss-Inclusive Geometrical Optics, by H. M. Musal, Jr., Research Notes 1 and 13, Ann Arbor, Michigan, 1 March 1960 and 1 July 1960.

(3)   Radiation Laboratory, Dept. of Electrical Engineering, University of Michigan, Plasma Sheath Surrounding a Conducting Spherical Satellite and the Effect on Radar Cross Section, by K. M. Chen, Studies in Radar Cross Sections XLIII, Ann Arbor, Michigan, October 1960.

(4)   Antenna Laboratory, Dept. of Electrical Engineering, Ohio State University Research Foundation, Coherent Scattering of a Metallic Body in the Presence of an Ionized Shell, by L. Peters, Jr., and W. G. Swarner, Report 1116-4, Columbus, Ohio, 7 March 1961.

(5)   H. M. Musal, Jr., "Plasma Effects on the Radar Cross Sections of Reentry Objects," Seventh Annual Radar Symposium Record, University of Michigan, Ann Arbor, Michigan, June 1961, pp. 351−373.

(6)   Lincoln Laboratory, Massachusetts Institute of Technology, Reentry Physics and Project PRESS Programs, Semiannual Technical Summary Report to the Advanced Research Projects

Agency, Lexington, Massachusetts, 30 June 1962, pp. III-1 to III-19.

(7) General Motors Corporation, Defense Research Laboratories, The Radar Absorption Effect as Measured in a Flight Physics Range, by H. M. Musal, Jr., P. E. Robillard, and R. I. Primich, TR62-209B, Santa Barbara, California, December 1962.

(8) Canadian Armament Research and Development Establishment, Status Report on the Reentry Physics Program, CARDE Technical Memorandum 740, Valcartier, Quebec, 31 December 1962, p. 14.

(9) I. E. Vas, S. M. Bogdonoff, and A. G. Hammitt, "An Experimental Investigation of the Flow over Simple Two-Dimensional and Axially Symmetric Bodies at Hypersonic Speeds," Jet Propulsion, 28, 2, February 1958, pp. 97−104.

(10) E. D. Martin, "Inviscid Hypersonic Flow Around Spheres and Circular Cylinders," Journal of the Aero/Space Sciences, Readers Forum, 26, 8, August 1959, pp. 529−530.

(11) Royal Aircraft Establishment, Measurement of the Sonic Line, Bow Shock Wave Shape, and Stand-off Distance For Blunt-Nosed Bodies at M = 6.8, by W. K. Osborne and J. F. W. Crane, Technical Note No: AERO. 2707, Farnborough, England, August 1960.

(12) H. Serbin, "Supersonic Flow Around Blunt Bodies," Journal of Aeronautical Sciences, Readers Forum, 25, 1, January 1958, pp. 58−59.

(13) Aerodynamics Division, N. P. L., An Analysis of Shock Detachment Distance in Supersonic Flow, by C. S. Sinnott, A. R. C. 21, 078, 11 June 1959.

(14) J. L. Stollery and D. J. Maull, "A Note on Shock Detachment Distance," Journal of the Royal Aeronautical Society, Technical Notes, 64, June 1960, pp. 357−359.

(15) S. Zivanovic, 'Reradiation Spectrum Broadening of Harmonically Driven Plasma Electrons," in Engineering Aspects of Magnetohydrodynamics, Columbia University Press, 1962, pp. 390−404.

(16)   Antenna Laboratory, Dept. of Electrical Engineering, Ohio
         State University Research Foundation, Electromagnetic
         Scattering by Radially Inhomogeneous Spheres, by R. J. Garbacz,
         Report 1223-3, Columbus, Ohio, 9 January 1962.

(17)   General Motors Corporation, Defense Research Laboratories,
         Plasma Frequency and Electron Collision Frequency Charts for
         Hypersonic Vehicle Equilibrium Flow Fields in Air, by H. M.
         Musal, Jr., SP62-232, Santa Barbara, California, October 1962.

(18)   S. Zivanovic, "Investigation of Precursor Ionization in Front of
         the Shock Waves of Hypersonic Projectiles," (to be presented at
         the Conference on Physics of Entry into Planetary Atmospheres,
         MIT, Cambridge, Mass., 26 – 28 August 1963).

APPENDIXES

APPENDIX A-1

ELECTROMAGNETIC CONSTITUTIVE PARAMETERS OF PLASMA

In the phenomenological viewpoint of the interaction between electromagnetic waves and matter it is customary to consider all nonionized media to be completely characterized (electromagnetically) by the constitutive parameters

1. permeability (μ),
2. capacitivity (ϵ), and
3. conductivity (σ).

It is highly advantageous to extend this concept to include ionized media, particularly plasma. Plasma is essentially a gaseous mixture of electrically neutral and charged particles of atomic or sub-atomic size exhibiting essentially no net charge density. If a plasma has a sufficiently large number of each type of particle per unit applicable volume, the concept of configuration space density has meaning and the velocity distribution of the particles in a unit applicable volume can be described by a velocity space density. The configuration and velocity space densities (phase space density) describe the dynamic properties of the plasma. If the time variation of the phase space density from causes other than the incident electromagnetic wave is very small during one cycle of the incident wave, the concept of constitutive parameters can be applied to the plasma.

The electromagnetic constitutive parameters of the plasma are assumed here to be the same as the effective constitutive parameters derived under the condition of a small-signal plane transverse electromagnetic wave propagating through an unbounded uniform (homogeneous) plasma with no externally applied electric or magnetic fields (isotropic), considering the effects of only the free electrons and assuming a constant electron collision frequency. This derivation is well documented in the literature,[1] the results of which give the plasma permeability μ_p,

$$(1.1) \qquad \mu_p = \mu_v$$

where

$$\mu_v = \text{free-space permeability,}$$

the plasma capacitivity ϵ_p,

$$(1.2) \qquad \epsilon_p = \epsilon_v \epsilon_r = \epsilon_v \left[1 - \frac{N_e \, q_e^2}{\epsilon_v \, m_e \left(\omega^2 + \nu_c^2 \right)} \right]$$

where

ϵ_v = free-space capacitivity,

ϵ_r = plasma dielectric constant,

N_e = plasma electron concentration,

q_e = electron charge,

m_e = electron mass,

ω = incident electromagnetic wave angular frequency ($2 \pi f$),

ν_c = plasma electron collision frequency,

and the plasma conductivity σ_p ,

(1.3) $\qquad \sigma_p = \dfrac{N_e \, q_e^2 \, \nu_c}{m_e \left(\omega^2 + \nu_c^2 \right)}$

These equations can be written in more compact form by introducing the relative conductivity σ_r ,

(1.4) $\qquad \sigma_r = \dfrac{\sigma_p}{\epsilon_v \, \omega}$

and the plasma frequency ω_p ,

(1.5) $\qquad \omega_p = q_e \left[\dfrac{N_e}{\epsilon_v \, m_e} \right]^{1/2}$

The plasma dielectric constant ϵ_r and relative conductivity σ_r can now be expressed in the forms

(1.6) $\qquad \epsilon_r = 1 - \dfrac{\omega_p^2}{\omega^2 + \nu_c^2}$

(1.7) $\qquad \sigma_r = \dfrac{\nu_c}{\omega} \dfrac{\omega_p^2}{\omega^2 + \nu_c^2}$

It is convenient to introduce a normalized plasma frequency Ω_p given by

$$(1.8) \qquad \Omega_p = \frac{\omega_p}{\omega}$$

and a normalized electron collision frequency Ω_c given by

$$(1.9) \qquad \Omega_c = \frac{\nu_c}{\omega}$$

in terms of which equations (1.6) and (1.7) can be written in the forms

$$(1.10) \qquad \epsilon_r = 1 - \frac{\Omega_p^2}{1 + \Omega_c^2}$$

$$(1.11) \qquad \sigma_r = \Omega_c \frac{\Omega_p^2}{1 + \Omega_c^2}$$

It can be shown [2] that the electromagnetic wave propagation factor γ_p for a plane transverse electromagnetic wave propagating through an unbounded, homogeneous, isotropic plasma characterized by the above three electromagnetic constitutive parameters is given by

$$(1.12) \qquad \gamma_p = \alpha_p + j\beta_p = j\omega \left(\epsilon_r \mu_r \right)^{1/2} \left(\epsilon_r - j\sigma_r \right)^{1/2}$$

where the attenuation factor α_p is given by

$$(1.13) \quad \alpha_p = \frac{\omega \left(\epsilon_v \, \mu_v\right)^{1/2}}{\sqrt{2}} \left[-\epsilon_r + \left(\epsilon_r^2 + \sigma_r^2\right)^{1/2} \right]^{1/2}$$

and the phase factor β_p is given by

$$(1.14) \quad \beta_p = \frac{\omega \left(\epsilon_v \, \mu_v\right)^{1/2}}{\sqrt{2}} \left[\epsilon_r + \left(\epsilon_r^2 + \sigma_r^2\right)^{1/2} \right]^{1/2}$$

The free-space wavelength λ_v of an electromagnetic wave is

$$(1.15) \quad \lambda_v = \frac{2\pi}{\beta_v} = \frac{2\pi}{\omega \left(\epsilon_v \, \mu_v\right)^{1/2}}$$

which can be used to simplify equations (1.12), (1.13), and (1.14) to

$$(1.16) \quad \gamma_p = j \, \frac{2\pi}{\lambda_v} \left(\epsilon_r - j \sigma_r\right)^{1/2}$$

$$(1.17) \quad \alpha_p = \frac{\pi \sqrt{2}}{\lambda_v} \left[- \epsilon_r + \left(\epsilon_r^2 + \sigma_r^2 \right)^{1/2} \right]^{1/2}$$

$$(1.18) \quad \beta_p = \frac{\pi \sqrt{2}}{\lambda_v} \left[\epsilon_r + \left(\epsilon_r^2 + \sigma_r^2 \right)^{1/2} \right]^{1/2}$$

It is also convenient to define a relative attenuation factor α_r given by

$$(1.19) \quad \alpha_r = \frac{\alpha_p}{\beta_v} = \frac{1}{\sqrt{2}} \left[-\epsilon_r + \left(\epsilon_r^2 + \sigma_r^2 \right)^{1/2} \right]^{1/2}$$

and a relative phase factor β_r given by

$$(1.20) \quad \beta_r = \frac{\beta_p}{\beta_v} = \frac{1}{\sqrt{2}} \left[\epsilon_r + \left(\epsilon_r^2 + \sigma_r^2 \right)^{1/2} \right]^{1/2}$$

In terms of the normalized plasma frequency Ω_p and the normalized electron collision frequency Ω_c , equations (1.16), (1.17), and (1.18) are

$$(1.21) \quad \gamma_p = j \frac{2\pi}{\lambda_v} \left[1 - \frac{\Omega_p^2}{1 - j\Omega_c} \right]^{1/2}$$

$$(1.22) \quad \alpha_p = \frac{\pi\sqrt{2}}{\lambda_r} \left\{ \frac{\left[\Omega_c^2 + \left(1 - \Omega_p^2\right)^2 \right]^{1/2} \left(1 + \Omega_c^2\right)^{1/2} - \Omega_c^2 - \left(1 - \Omega_p^2\right)}{1 + \Omega_c^2} \right\}^{1/2}$$

$$(1.23) \quad \beta_p = \frac{\pi\sqrt{2}}{\lambda_r} \left\{ \frac{\left[\Omega_c^2 + \left(1 - \Omega_p^2\right)^2 \right]^{1/2} \left(1 + \Omega_c^2\right)^{1/2} + \Omega_c^2 + \left(1 - \Omega_p^2\right)}{1 + \Omega_c^2} \right\}^{1/2}$$

so that the relative attenuation factor α_r and the relative phase factor β_r for a plasma can be written in the forms

$$(1.24) \quad \alpha_r = \left\{ \frac{\left[\Omega_c^2 + \left(1 - \Omega_p^2\right)^2 \right]^{1/2} \left(1 + \Omega_c^2\right)^{1/2} - \Omega_c^2 - \left(1 - \Omega_p^2\right)}{2 \left(1 + \Omega_c^2\right)} \right\}^{1/2}$$

$$(1.25) \quad \beta_r = \left\{ \frac{\left[\Omega_c^2 + \left(1 - \Omega_p^2\right)^2 \right]^{1/2} \left(1 + \Omega_c^2\right)^{1/2} + \Omega_c^2 + \left(1 - \Omega_p^2\right)}{2 \left(1 + \Omega_c^2\right)} \right\}^{1/2}$$

The relationship between the electromagnetic wave wavelength in the plasma λ_p and the free-space wavelength λ_r is

$$(1.26) \qquad \lambda_p = \frac{2\pi}{\beta_p} = \frac{\lambda_v}{\beta_r}$$

(1) E. C. Jordan, Electromagnetic Waves and Radiating Systems,
     Prentice-Hall, 1950, pp. 659—662.

(2) Bendix Systems Division, Wave Propagation, Reflection,
     and Transmission in a Lossy Semi-Infinite Cold Plasma,
     By G. T. Flesher, Research Note 8, Ann Arbor, Michigan,
     20 June 1960.

APPENDIX A-2

ELECTROMAGNETIC WAVE BACK-SCATTERING CROSS SECTION OF A METALLIC SPHERE COATED WITH A UNIFORM LOSSY DIELECTRIC

.The rigorous wave theory determination of the scattering of an incident linearly polarized plane transverse electromagnetic wave by a uniform isotropic spherical body with a concentric uniform isotropic spherical coating, both of which may have arbitrary constitutive parameters, immersed in an arbitrary uniform isotropic surrounding medium, has been reported in the literature. [1] This solution can be specialized to the case where the inner spherical body is a perfect conductor (metal), the coating has arbitrary dielectric constant and conductivity (lossy dielectric) but a permeability the same as free space, and the surrounding medium is free space. The back-scattered plane transverse electromagnetic wave is linearly polarized in the same direction as the incident wave. The electromagnetic wave back-scattering cross section (radar cross section) σ of this special composite configuration is given by

$$(2.1) \qquad \sigma = \frac{\lambda_v^2}{4\pi} \left| \sum_{n=1}^{\infty} (-1)^n (2n+1)(a_n - b_n) \right|^2$$

where

λ_v = free-space wavelength of the incident wave, and

a_n, b_n = scattering amplitude coefficients.

The scattering amplitude coefficients are given by

$$(2.2) \quad a_n = \frac{\begin{vmatrix} 0 & z_n^{(1)}(Nc) & z_n^{(3)}(Nc) \\ Nz_n^{(1)}(d) & z_n^{(1)}(Nd) & z_n^{(3)}(Nd) \\ \eta_n^{(1)}(d) & \eta_n^{(1)}(Nd) & \eta_n^{(3)}(Nd) \end{vmatrix}}{\begin{vmatrix} 0 & z_n^{(1)}(Nc) & z_n^{(3)}(Nc) \\ -Nz_n^{(3)}(d) & z_n^{(1)}(Nd) & z_n^{(3)}(Nd) \\ -\eta_n^{(3)}(d) & \eta_n^{(1)}(Nd) & \eta_n^{(3)}(Nd) \end{vmatrix}}$$

$$(2.3) \quad b_n = \frac{\begin{vmatrix} 0 & \eta_n^{(1)}(Nc) & \eta_n^{(3)}(Nc) \\ N\eta_n^{(1)}(d) & \eta_n^{(1)}(Nd) & \eta_n^{(3)}(Nd) \\ z_n^{(1)}(d) & z_n^{(1)}(Nd) & z_n^{(3)}(Nd) \end{vmatrix}}{\begin{vmatrix} 0 & \eta_n^{(1)}(Nc) & \eta_n^{(3)}(Nc) \\ -N\eta_n^{(3)}(d) & \eta_n^{(1)}(Nd) & \eta_n^{(3)}(Nd) \\ -z_n^{(3)}(d) & z_n^{(1)}(Nd) & z_n^{(3)}(Nd) \end{vmatrix}}$$

The factor N is the complex index of refraction of the lossy dielectric coating, and is given by

$$(2.4) \qquad N = (\epsilon_r - j\sigma_r)^{1/2}$$

where

$$\epsilon_r = \frac{\epsilon_d}{\epsilon_v} = \text{dielectric constant of dielectric}$$

$$\sigma_r = \frac{\sigma_d}{\epsilon_v \omega} = \text{relative conductivity of dielectric}$$

ϵ_d = capacitivity of dielectric

σ_d = conductivity of dielectric

ϵ_v = capacitivity of free space

ω = angular frequency of incident wave ($2 \pi f$).

The quantities c and d in the arguments of the functions in equation (2.1) are defined by

$$(2.5) \qquad c = \frac{2 \pi r}{\lambda_v}$$

$$(2.6) \qquad d = \frac{2 \pi (r + \ell)}{\lambda_v}$$

where

$\qquad r$ = radius of metal sphere

$\qquad \ell$ = thickness of dielectric coating

The function $z_n^{(1)}(X)$ is the spherical Bessel function of the first kind, of integer order n, and complex argument X. This function is related to the ordinary Bessel function of the first kind, of order $n + \frac{1}{2}$, and complex argument X by

$$(2.7) \qquad z_n^{(1)} X = \left(\frac{\pi}{2X}\right)^{\frac{1}{2}} J_{n+\frac{1}{2}}(X)$$

The function $z_n^{(3)}(X)$ is the spherical Bessel function of the third kind, of integer order n, and complex argument X. This function is related to the ordinary Hankel function of the second kind, of order $n + 1/2$, and complex argument X by [2]

$$(2.8) \qquad z_n^{(3)}(X) = \left(\frac{\pi}{2X}\right)^{1/2} H_{n+1/2}^{(2)}(X)$$

The functions $\eta_n^{(1)}(X)$ and $\eta_n^{(3)}(X)$ are defined by

$$(2.9) \qquad \eta_n^{(1)}(X) = \frac{\left[X z_n^{(1)}(X)\right]'}{X}$$

$$(2.10) \qquad \eta_n^{(3)}(X) = \frac{\left[X z_n^{(3)}(X)\right]'}{X}$$

where the prime indicates differentiation with respect to the argument X.

The complicated nature of this solution precludes observation of the behavior of the radar cross section as a function of the input variables r, $\hbar$, ϵ_r, σ_r, ω, and λ_r merely by inspection. Computation on an electronic digital computer is the only practical way in which to obtain numerical values of the solution for study, because of the lengthy calculation involved. Even with this approach, there are parameter regimes in which the solution, as given in the form of equation (2.1) et seq, does not converge well and consequently

the accuracy of the numerical result is poor. This occurs when r is very large compared to λ_r and/or the magnitude of N is very small compared to unity. In these parameter regimes other analytic forms of the solution must be used.

In order to adapt the above analytic solution to the special case where the dielectric coating represents a lossy plasma, it is merely necessary to express N in terms of the plasma variables, giving

$$(2.11) \qquad N = \left(1 - \frac{\Omega_p^2}{1 - j\Omega_c} \right)^{1/2}$$

where Ω_p and Ω_c are defined in Appendix 1.

(1)   A. L. Aden and M. Kerker, "Scattering of Electromagnetic Waves from Two Concentric Spheres," Journal of Applied Physics, Vol. 22, No. 10, October 1951, pp. 1242–1246.

(2)   A. Erdelyi, editor, Higher Transcendental Functions, Vol. II, McGraw-Hill, 1953, pp. 9 – 10.

APPENDIX A-3

GEOMETRICAL OPTICS APPROACH TO THE DETERMINATION OF ELECTROMAGNETIC WAVE SCATTERING CROSS SECTION

The electromagnetic wave scattering cross section σ of an object is defined in terms of the ratio of the scattered wave average power density at the receiver location $\overline{S}_R$ to the incident wave average power density at the object location $\overline{S}_i$ by

$$(3.1) \qquad \sigma = 4\pi \, R_R^2 \, \frac{\overline{S}_R}{\overline{S}_i}$$

where

R_R = distance between object location and receiver location.

In order for this definition to be complete, the polarization characteristics of the incident and scattered waves at the object and receiver locations, respectively, must also be specified. When the incident wave is linearly polarized in some reference direction, then in general the scattered wave will have a component polarized in this same direction (parallel-polarized) and a component polarized in the orthogonal direction (cross-polarized).

The definition given in equation (3.1) can be written to give the parallel-polarized and the cross-polarized components of the scattering cross section by using the parallel-polarized and the cross-polarized components of the scattered wave average power density at the receiver location.

The analytical determination of the scattering of an incident electro-
magnetic wave by a localized macroscopic region with known constitu-
tive parameters and spatial configuration is a boundary-value problem
in electromagnetic field theory. The solution of the scattering problem
gives the scattered wave at a receiver location when the incident wave
at the object location is specified. The complete description of the
scattering effects can be expressed in terms of boundary-matched sets
of solutions to Maxwell's equations (one set of solutions for each of the
regions involved). Information about the nature of this solution can be
obtained from a geometrical optics solution to the problem. The results
of a geometrical optics solution to the problem must be used with
caution, however, since incomplete or highly misleading results are
possible if the applicability criteria are not met. Even though its
applicability may be limited, a geometrical optics solution should not
be excluded a priori since it can be obtained with relative ease com-
pared to the rigorous solution of the electromagnetic boundary-value
problem.

It can be shown [1] from Maxwell's equations that the geometrical
optics (ray theory) solution is reasonably accurate when

(1) the fractional change in the constitutive parameters over a
     distance of one wavelength is small (for continuously varying
     constitutive parameters) or if the total change in the constitu-
     tive parameters takes place over a distance very much smaller
     than one wavelength (for an abrupt boundary between two
     regions), and

(2) the fractional change in the spacing between adjacent rays
     over a distance along the rays of one wavelength is small. This

means that the geometrical optics solution is open to
question if

    (a) the rays pass through a focus, or

    (b) the rays are reflected or refracted at a surface with a
size or radius of curvature that is not large compared
to the wavelength.

The geometrical optics approach can be used to determine the total
electric field intensity at a receiver location, from which the average
power density can be determined. To accomplish this, it is necessary
to consider

    (1) the length of each ray path from the incident wave front to the
receiver location (to obtain the transmission phase shift and
attenuation, and the change in polarization characteristics if
anisotropic media are traversed),

    (2) the magnitude changes, phase shifts, and polarization
characteristics changes that occur at the boundaries encountered
by each ray path (expressed by the reflection and transmission
factors), and

    (3) the magnitude changes that occur along each ray path due to
geometrical divergence of the ray bundle (expressed by the
geometrical divergence factor)

in order to determine the magnitude, phase, and polarization relation-
ships between the components that add up to give the total electric field
intensity at the receiver location.

Using the ray path field intensity addition technique, the total scattered
wave average power density arriving at a receiver location S_R is given
by

$$(3.2) \qquad \overline{S}_R = \frac{|E_R|^2}{2 Z_{OR}}$$

where

E_R = peak value of total electric field intensity at receiver location (linearly polarized)

Z_{OR} = characteristic impedance of medium (lossless) in which receiver is located.

The total electric field intensity at the receiver location E_R is the sum of the contributions from all the ray paths that terminate at the receiver location.

$$(3.3) \qquad E_R = \sum_{k=1}^{K} E_{Rk}$$

where

E_{Rk} = electric field intensity of kth ray path at receiver location (linearly polarized)

Note that equations (3.2) and (3.3) can be written for each of two orthogonally polarized electric field intensities.

In the scattering situation, all ray paths that reach the receiver location originate from incident wave ray paths, hence the initial ray path electric field intensity of all ray paths is the incident wave (linearly polarized) electric field intensity E_i. The incident wave average power density is given by

$$(3.4) \qquad \overline{S}_i = \frac{|E_i|^2}{2 Z_{oi}}$$

where

Z_{0i} = characteristic impedance of medium (lossless) in which wave source is located.

In general, each ray path will encounter boundaries at which it is either reflected or transmitted, and consequently the magnitude, phase, and polarization characteristics of the ray path electric field intensity will be affected by the reflection or transmission factors at these boundaries. The curvature of the boundaries encountered by each ray path introduces an overall geometrical divergence factor, which affects the ray path average power density. Transmission along each ray path introduces a phase shift between the incident wave electric field intensity and the electric field intensity of that ray path at the receiver location. This phase shift can be measured between two conveniently located reference planes, one perpendicular to the incident wave propagation direction and in the same medium as the incident wave source, and the other perpendicular to the scattered wave propagation direction and in the same medium as the receiver location but located a fixed distance from the receiver location (preferably as close to the scattering body as possible). Transmission through lossy media causes attenuation of the electric field intensity along the ray path. Transmission through anisotropic media causes changes in the polarization characteristics along the ray path.

When all the media involved are isotropic, uniform (changes in constitutive parameters occur only at sharp boundaries between regions), and no changes in polarization characteristics occur at the boundaries, a general formulation for the scattering cross section can be made. Simultaneous consideration of the effects of all reflections, transmissions,

geometrical divergence, phase shifts, and losses along the kth ray path (in which there are a total of R_k reflections at the surfaces r, a total of T_k transmissions at the surfaces t, a total of B_k uniform media traversed, a total of A_k uniform lossy media traversed, and the source and receiver locations are in the same lossless medium), gives

$$E_{Rk} = \frac{E_i}{D_{iRk}^{1/2}} \prod_{r=1}^{R_k} \rho_{kr} \prod_{t=1}^{T_k} \tau_{kt} \prod_{b=1}^{B_k}$$

(3.5)

$$e^{-j\beta_{kb} L_{kb}} \prod_{a=1}^{A_k} e^{-\alpha_{ka} L_{ka}}$$

where

$$D_{iRk} = \text{geometrical divergence factor for } k^{th} \text{ ray path}$$
$$\rho_{kr} = r^{th} \text{ surface reflection factor in the } k^{th} \text{ ray path}$$
$$\tau_{kt} = t^{th} \text{ surface transmission factor in the } k^{th} \text{ ray path}$$
$$\alpha_{ka} = \text{attenuation factor along } k^{th} \text{ ray path in } a^{th} \text{ medium}$$
$$L_{ka} = \text{length of } k^{th} \text{ ray path in } a^{th} \text{ medium}$$
$$\beta_{kb} = \text{phase factor along } k^{th} \text{ ray path in } b^{th} \text{ medium}$$
$$L_{kb} = \text{length of } k^{th} \text{ ray path in } b^{th} \text{ medium}$$

Equations (3.2) through (3.5), for Z_{0i} and Z_{0R} equal, give

(3.6)
$$\frac{\bar{S}_R}{\bar{S}_i} = \left| \sum_{k=1}^{K} D_{iRk}^{-1/2} \prod_{r=1}^{R_k} \rho_{kr} \prod_{t=1}^{T_k} \tau_{kt} \prod_{b=1}^{B_k} e^{-j\beta_{kb} L_{kb}} \prod_{a=1}^{A_k} e^{-\alpha_{ka} L_{ka}} \right|^2$$

which can be substituted into equation (3.1) to give

$$\sigma = 4\pi R_R^2 \left| \sum_{k=1}^{K} D_{iRk}^{-1/2} \prod_{r=1}^{R_k} \rho_{kr} \prod_{t=1}^{T_k} \tau_{kt} \right.$$
$$\left. \prod_{b=1}^{B_k} e^{-j\beta_{kb} L_{kb}} \prod_{a=1}^{A_k} e^{-\alpha_{ka} L_{ka}} \right|^2$$

(3.7)

Thus the electromagnetic wave scattering cross section can be expressed in terms of a geometrical optics solution of the scattering problem, using a ray path field intensity addition technique.

---

(1) D.E. Kerr, <u>Propagation of Short Radio Waves</u>, McGraw-Hill, 1951, pp. 53–58.

APPENDIX A-4

ELECTROMAGNETIC WAVE REFLECTION AND TRANSMISSION AT LOSSY DIELECTRIC BOUNDARIES

It is assumed that the boundaries between the lossy dielectric and the adjacent media are plane, and furthermore that all the media involved can be completely characterized (electromagnetically) by the three constitutive parameters: capacitivity ϵ , permeability μ , and conductivity σ . The media bounding the lossy dielectric are assumed to be either free space (a lossless dielectric) or infinitely conductive material (perfect reflector), and the lossy dielectric (a dielectric with nonzero conductivity) is assumed to have free space permeability.

The reflection and transmission of electromagnetic waves at plane interfaces between dielectrics (both lossless and lossy) and perfect reflectors have been given some attention in the literature. [1] The generalized Snell's Law gives the directions of the reflected and transmitted waves at the interface when the direction of the incident wave is specified. The propagation direction vectors of the incident wave, reflected wave, transmitted wave, and the surface normal are co-planar, this common plane being defined as the plane of incidence. This is shown in Figure A4-1 for a wave propagating from free space through a lossy dielectric slab and into free space again. The generalized Snell's Law for the relationships shown in Figure A4-1 gives

(4.1)
$$\theta_{iv} = \theta_{rv} = \theta_{tv}$$
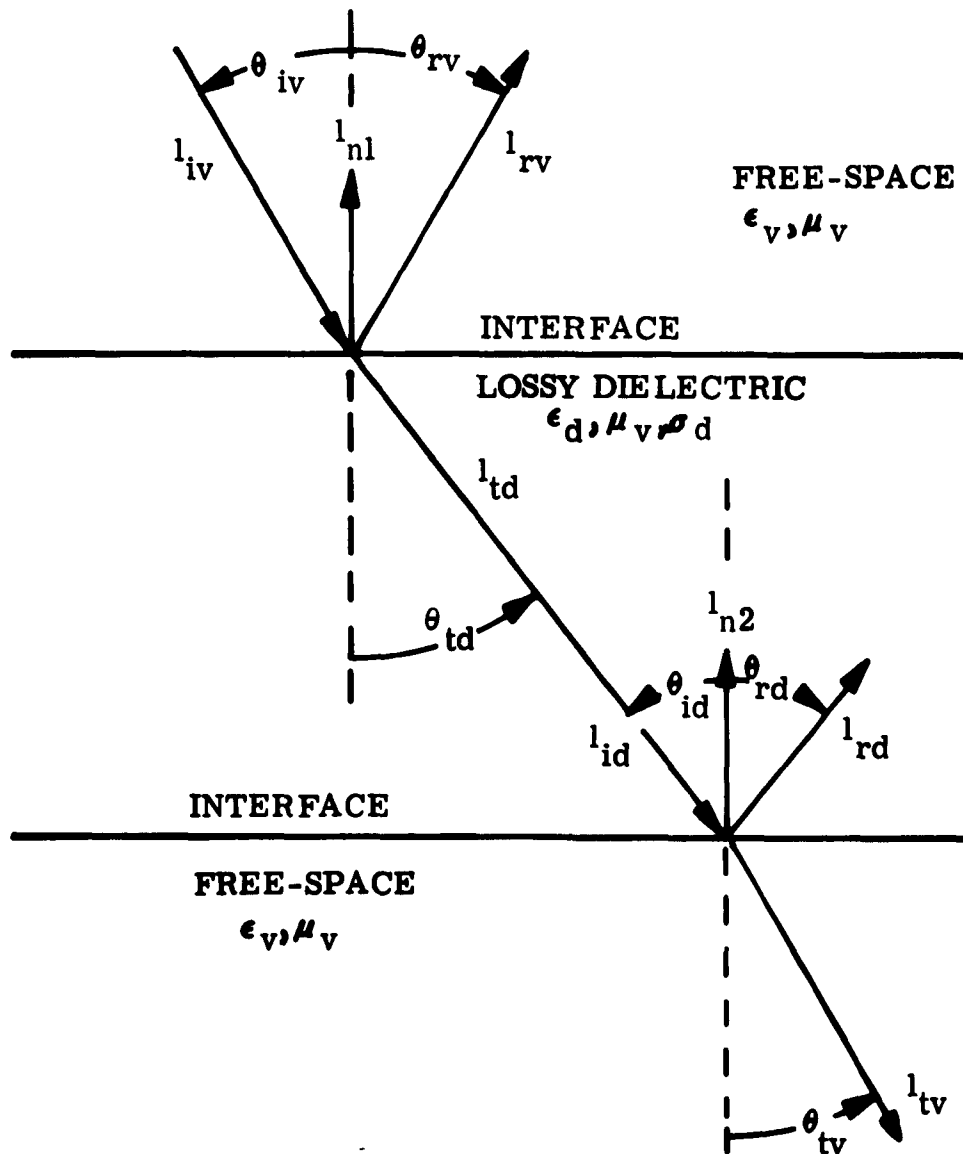
Figure A4-1   Reflection – Refraction Geometry for Interfaces
Between Free Space and Lossy Dielectric

(4.2) $\quad \theta_{td} = \theta_{id} = \theta_{rd}$

(4.3) $\quad \sin \theta_{td} = \dfrac{\sqrt{2} \ \sin \theta_{iv}}{\left\{ \epsilon_r + \sin^2 \theta_{iv} + \left[\sigma_r^2 + \left(\epsilon_r - \sin^2 \theta_{iv} \right)^2 \right]^{1/2} \right\}^{1/2}}$

(4.4) $\quad \sin \theta_{tv} = \dfrac{1}{\sqrt{2}} \ \sin \theta_{id} \left[\epsilon_r + \left(\epsilon_r^2 + \dfrac{\sigma_r^2}{\cos^2 \theta_{id}} \right)^{1/2} \right]^{1/2}$

where

ϵ_r = dielectric constant

σ_r = relative conductivity.

The dielectric constant and relative conductivity are given by

(4.5) $\quad \epsilon_r = \epsilon_d / \epsilon_v$

(4.6) $\quad \sigma_r = \sigma_d / \epsilon_v \omega$

where

ϵ_d = dielectric capacitivity

ϵ_v = free-space capacitivity

ω = incident electromagnetic wave angular frequency ($2\pi f$)

σ_d = dielectric conductivity.

The electromagnetic wave reflection (ρ) and transmission (τ) factors for an interface between two media relate the magnitude and phase of the reflected (E_r) and transmitted (E_t) electromagnetic wave electric field intensities at the interface to the incident electromagnetic wave electric field intensity (E_i) at the interface, that is,

$$(4.7) \qquad \rho = \frac{E_r}{E_i} \Bigg|_{\text{at interface}}$$

$$(4.8) \qquad \tau = \frac{E_t}{E_i} \Bigg|_{\text{at interface}}$$

where E_r, E_t, and E_i are complex quantities. The reflection and transmission factors for an interface are, in general, functions of the constitutive parameters of the media on the two sides of the interface, the angle of incidence, and the electric field polarization with respect to the plane of incidence. For normal incidence ($\theta_{iv} = 0$) only the first of the above three functional dependencies enters the equations explicitly. The reflection factor (ρ_{12}) and the transmission factor (τ_{12}) for an electromagnetic wave propagating normally from medium (1) to medium (2) are given by

$$(4.9) \qquad \rho_{12} = \frac{Z_{02} - Z_{01}}{Z_{02} + Z_{01}}$$

$$(4.10) \qquad \tau_{12} = \frac{2Z_{02}}{Z_{02} + Z_{01}}$$

where

Z_{01} = characteristic impedance of medium (1),

Z_{02} = characteristic impedance of medium (2).

The characteristic impedance of a lossless dielectric is

$$(4.11) \qquad Z_0 = \left(\frac{\mu}{\epsilon} \right)^{1/2}$$

the characteristic impedance of a lossy dielectric is

$$(4.12) \qquad Z_0 = \left(\frac{\mu}{\epsilon - j \frac{\sigma}{\omega}} \right)^{1/2}$$

and the characteristic impedance of a perfect reflector is

$$(4.13) \qquad Z_0 = 0$$

The reflection factor (ρ_{vd}) and transmission factor (τ_{vd}) for an electromagnetic wave propagating normally from free space into a lossy dielectric having free-space permeability, using equations (4.9) through (4.12), are

$$(4.14) \qquad \rho_{vd} = \frac{1 - \left(\epsilon_r - j \sigma_r \right)^{1/2}}{1 + \left(\epsilon_r - j \sigma_r \right)^{1/2}}$$

$$(4.15) \qquad \tau_{vd} = \frac{2}{1 + \left(\epsilon_r - j \sigma_r \right)^{1/2}}$$

The reflection factor (ρ_{dv}) and transmission factor (τ_{dv}) for an electromagnetic wave propagating normally from a lossy dielectric having free-space permeability into free space, using equations (4.9) through (4.12), are

$$(4.16) \qquad \rho_{dv} = \frac{\left(\epsilon_r - j \sigma_r \right)^{1/2} - 1}{\left(\epsilon_r - j \sigma_r \right)^{1/2} + 1}$$

$$(4.17) \qquad \tau_{dv} = \frac{2 \left(\epsilon_r - j \sigma_r \right)^{1/2}}{\left(\epsilon_r - j \sigma_r \right)^{1/2} + 1}$$

It can be seen from equations (4.14) through (4.17) that

(4.18) $\qquad \rho_{dr} = - \rho_{rd}$

(4.19) $\qquad \tau_{rd} = 1 + \rho_{rd}$

(4.20) $\qquad \tau_{dr} = 1 - \rho_{rd}$

The reflection factor (ρ_{dr}) and transmission factor (τ_{dr}) for an electromagnetic wave propagating normally from a lossy dielectric to a perfect reflector, using equations (4.9), (4.10), (4.12) and (4.13), are

(4.21) $\qquad \rho_{dr} = -1$

(4.22) $\qquad \tau_{dr} = 0$

In the special case where the lossy dielectric represents a plasma, it is merely necessary to express ϵ_r and σ_r in terms of the plasma variables. Thus, the reflection factor (Γ_p) for an electromagnetic wave propagating normally from free space into a plasma is given by

(4.23) $\qquad \Gamma_p \equiv \rho_{rp} = \dfrac{1 - \left(1 - \dfrac{\Omega_p^2}{1 - j\,\Omega_c} \right)^{1/2}}{1 + \left(1 - \dfrac{\Omega_p^2}{1 - j\,\Omega_c} \right)^{1/2}}$

where Ω_p and Ω_c are the plasma variables and are defined in Appendix 1. Equations (4.18) through (4.20) allow all the other pertinent reflection and transmission factors for the interface to be expressed in terms of Γ_+ , just as in the case of the lossy dielectric.

(1) J. A. Stratton, <u>Electromagnetic Theory</u>, McGraw-Hill, 1941,
     pp. 500—524.

APPENDIX A-5

RAY PATH GEOMETRY FOR BACK-SCATTERING BY A UNIFORM LOSSY DIELECTRIC-COATED METALLIC SPHERE

It is assumed that the scattering object consists of a perfectly reflective sphere coated with a uniform layer of lossy dielectric material. The ray path geometry of a plane electromagnetic wave incident on these concentric spherical boundaries and the resultant scattered wave ray path geometry, necessary for the determination of the scattering cross section, can be completely defined by the ray paths in the plane of incidence (as defined in Appendix 4). A normal view of the plane of incidence, showing the equatorial section of the spherical boundaries, is shown in Figure A5-1. The angles of refraction of the ray paths shown are indicative of a dielectric constant with a value less than unity in the coating. Three characteristic ray path configurations are apparent, but only the contributions to the scattered wave due to "single-transit" paths through the dielectric are detailed (with the exception of the "vds$_\infty$" path, which makes an infinite number of transits through the dielectric). It should be noted that contributions to the scattered wave also come from rays that have been carried around the back of the sphere in the dielectric coating. The geometrical details of each of the three characteristic ray paths must be known in order to determine the relationship between the incident wave and the scattered wave.

Consider the "v" ray path, in which the ray is reflected from the outer surface of the dielectric coating. This path is detailed in Figure A5-2.
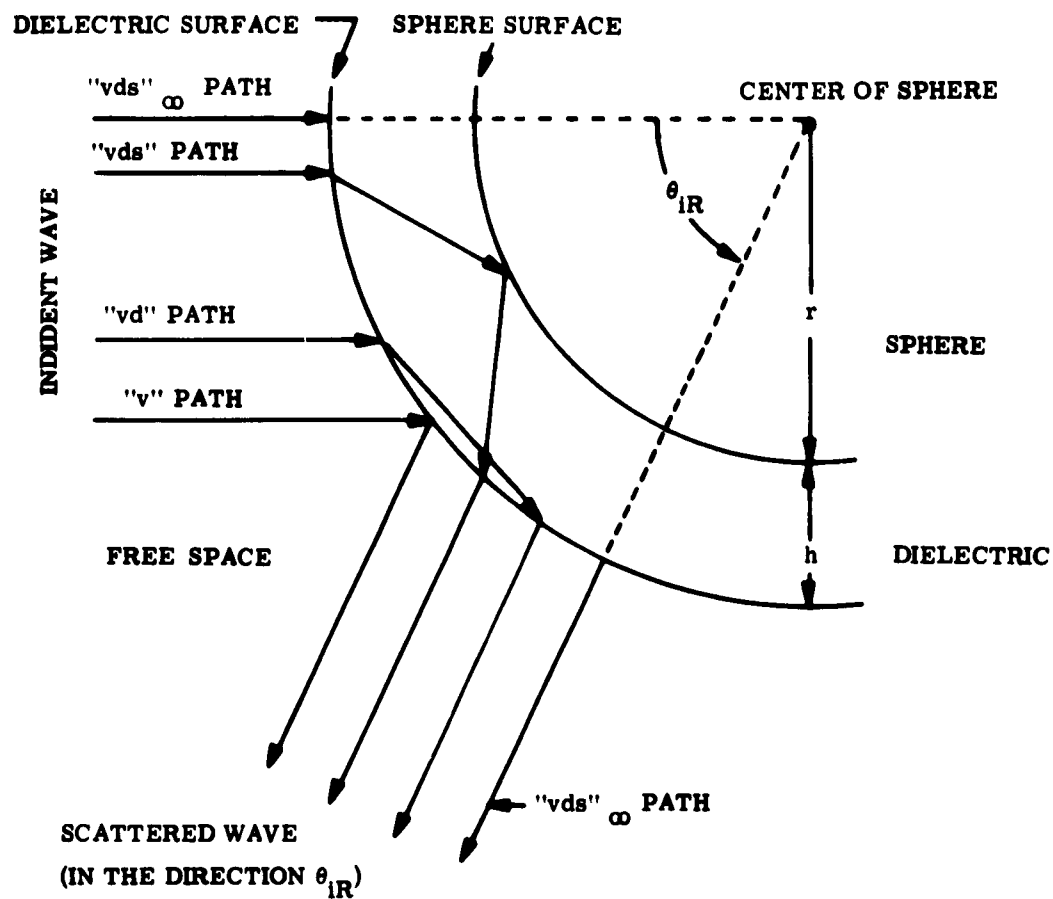
Figure A5-1   Ray Path Geometry in the Plane of Incidence
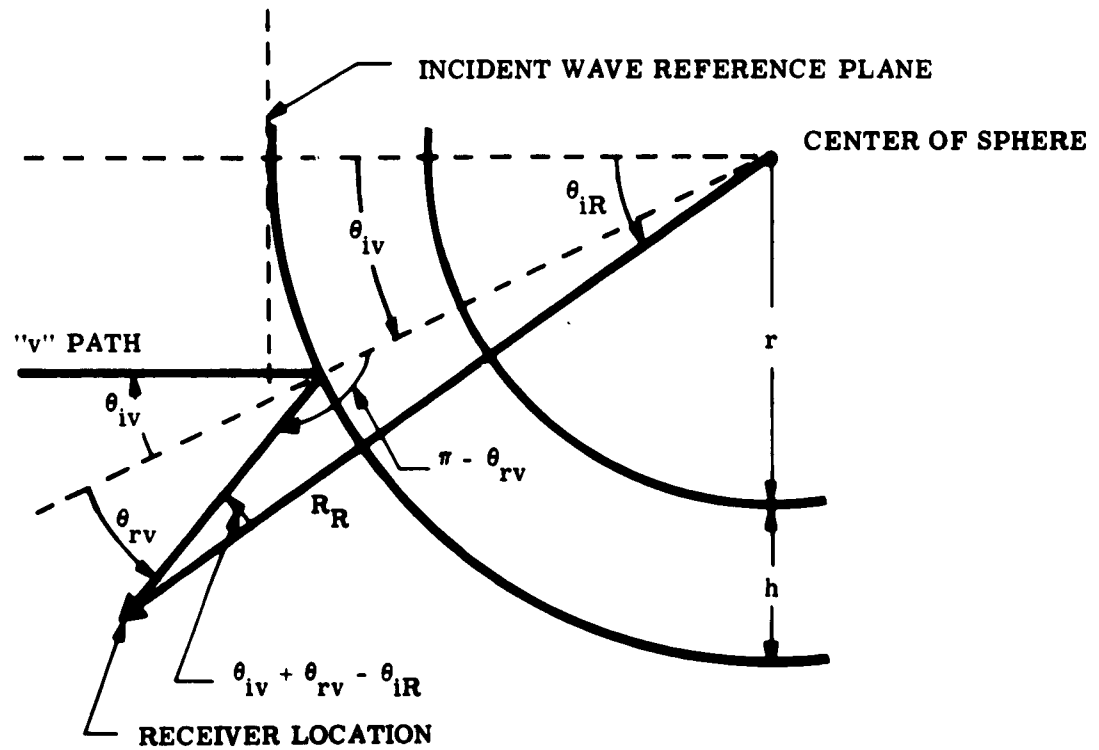
Figure A5-2   Characteristic Ray Path "v"

Appendix 4 gives

$$(5.1) \qquad \theta_{rv} = \theta_{iv}$$

and the law of sines for a plane triangle, with equation (5.1), gives

$$(5.2) \qquad \frac{r + h}{\sin \left(2\,\theta_{iv} - \theta_{ir} \right)} = \frac{R_R}{\sin \left(\pi - \theta_{iv} \right)}$$

which can be expanded and arranged to give

$$(5.3) \qquad \sin \left(2\,\theta_{iv} - \theta_{ir} \right) = \frac{r + h}{R_R} \sin \theta_{iv}$$

The "far-field" condition gives

$$(5.4) \qquad \sin \left(2\,\theta_{iv} - \theta_{ir} \right) = \lim_{R_R \to \infty} \left[\frac{r + h}{R_R} \sin \theta_{iv} \right] = 0$$

which means that

$$(5.5) \qquad \theta_{ir} = 2\,\theta_{iv}$$

The length of the "v" ray path is most conveniently measured from an incident wave reference plane perpendicular to the direction of pro-pagation of the incident wave and tangent to the outer surface of the dielectric coating, as shown in Figure A5-2. The lengths of the ray path in free space and in the dielectric from this reference plane to

the receiver location must both be determined. From Figure A5-2 it is obvious that the length of the ray path in the dielectric (L_{Dv}) is zero.

$$(5.6) \qquad L_{Dr} = 0$$

The ray path length in free space from the incident reference plane to the dielectric surface (ℓ_1) is given by

$$(5.7) \qquad \ell_1 = (r + h)(1 - \cos \theta_{ir})$$

and the ray path length in free space from the dielectric surface to the receiver location (ℓ_2), using equation (5.1), is given by

$$(5.8) \qquad \ell_2 = (r + h) \cos(\pi - \theta_{ir}) + R_R \cos(2\theta_w - \theta_{ir})$$

It is convenient to establish a scattered wave reference plane perpendicular to the direction of propagation of the scattered wave and located a distance $\left| R_R - (r + h) \right|$ from the receiver location. The ray path length from the dielectric surface to this reference plane (ℓ_3) is given by

$$(5.9) \qquad \ell_3 = (r + h)(1 - \cos \theta_{ir}) + R_R \left[\cos(2\theta_{ir} - \theta_{ir}) - 1 \right]$$

The "far-field" condition can be evaluated through the use of equation (5.3) and l'Hospital's rule, giving

(5.10) $\quad\lim\limits_{R_R \to \infty} \quad \ell_3 = \left(r + \hbar\right)\left(1 - \cos\theta_{iv}\right)$

The total ray path length in free-space between the two reference planes (L_{Vv}), for the "far-field" condition, is given by

(5.11) $\quad L_{Vv} = 2\left(r + \hbar\right)\left(1 - \cos\theta_{iv}\right)$

For the back-scattering condition ($\theta_{ir} = 0$) it follows that

(5.12) $\quad L_{Vr} = 0$

Consider the "vds" ray path, in which the ray is transmitted through the outer dielectric surface, passes through the dielectric coating until it meets the sphere surface, is reflected from the sphere surface, again passes through the dielectric coating until it meets the outer dielectric surface, and is transmitted through the outer dielectric surface to the receiver location. In general, such a ray path may traverse the dielectric coating 2m times before emerging. This path is detailed in Figure A5-3. Appendix 4 gives

(5.13) $\quad \sin\theta_{td} = \dfrac{\sqrt{2}\ \sin\theta_{iv}}{\left\{\epsilon_r + \sin^2\theta_{iv} + \left[\sigma_r^2 + \left(\epsilon_r - \sin^2\theta_{iv}\right)^2\right]^{\frac{1}{2}}\right\}^{\frac{1}{2}}}$

(5.14) $\quad \theta_{ids} = \theta_{rds}$

A5-6
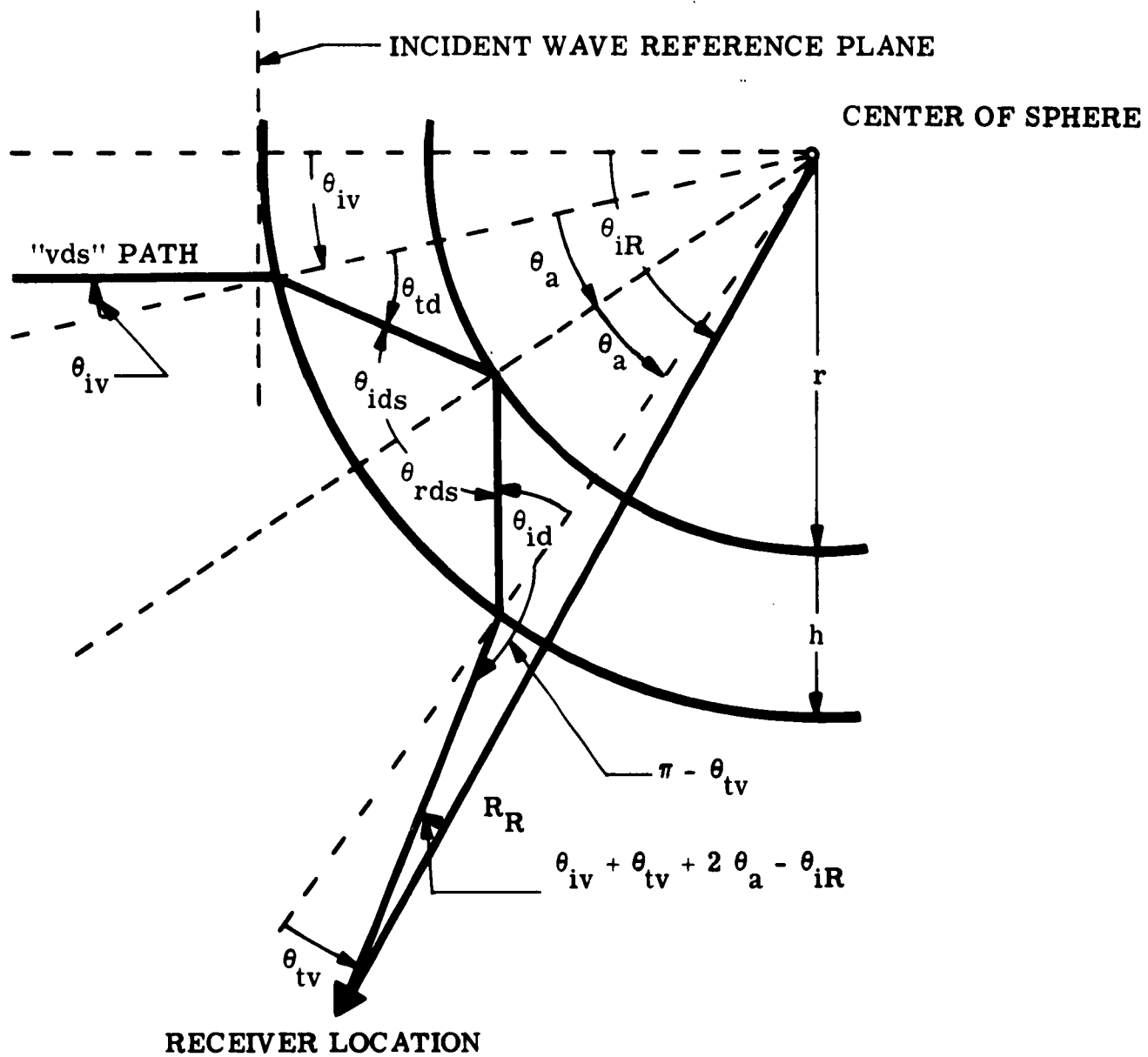
Figure A5-3   Characteristic Ray Path "vds"

$$(5.15) \quad \sin \theta_{tv} = \frac{1}{\sqrt{2}} \sin \theta_{id} \left[\epsilon_r + \left(\epsilon_r^2 + \frac{\sigma_r^2}{\cos^2 \theta_{id}} \right)^{1/2} \right]^{1/2}$$

By symmetry, it can be seen that

$$(5.16) \quad \theta_{td} = \theta_{id}$$

and

$$(5.17) \quad \theta_{tv} = \theta_{iv}$$

The law of sines gives

$$(5.18) \quad \frac{r + h}{\sin \left(\theta_{iv} + \theta_{tv} + 2\theta_a - \theta_{ir} \right)} = \frac{R_R}{\sin \left(\pi - \theta_{tv} \right)}$$

which can be simplified to

$$(5.19) \quad \frac{r + h}{\sin \left(2\theta_{iv} + 2\theta_a - \theta_{ir} \right)} = \frac{R_R}{\sin \theta_{iv}}$$

The "far-field" condition gives

$$(5.20) \quad \sin \left(2\theta_{iv} + 2\theta_a - \theta_{ir} \right) = \lim_{R_R \to \infty} \left[\frac{r + h}{R_R} \sin \theta_{iv} \right] = 0$$

which means that

$$(5.21) \quad \theta_{ir} = 2 \left(\theta_{iv} + \theta_a \right)$$

in the specific case shown in Figure A5-3, but in general

$$(5.22) \qquad \theta_{iRm} = 2 \left(\theta_{iv} + m\,\theta_a \right) \qquad\qquad m = 1, 2, 3, \cdots$$

for multiple transits through the dielectric coating. The law of sines also gives

$$(5.23) \qquad \frac{r}{\sin \theta_{td}} = \frac{r + h}{\sin \left(\pi - \theta_{td} - \theta_a \right)}$$

which can be reduced to

$$(5.24) \qquad \frac{r}{\sin \theta_{td}} = \frac{r + h}{\sin \left(\theta_{td} + \theta_a \right)}$$

and solved to give

$$(5.25) \qquad \cos \theta_a = \left(\frac{r+h}{r} \right) \sin^2 \theta_{td} \\ + \left(1 - \sin^2 \theta_{td} \right)^{1/2} \left[1 - \left(\frac{r+h}{r} \right)^2 \sin^2 \theta_{td} \right]^{1/2}$$

Using equation (5.13) in equation (5.25) gives

$$(5.26) \qquad \cos \theta_a = \left[\left[\epsilon_r + \sin^2 \theta_{iv} + \left[\sigma_r^2 + \left(\epsilon_r - \sin^2 \theta_{iv} \right)^2 \right]^{1/2} \right]^{1/2} \right]^{-1} \\ \left\{ 2 \left(\frac{r+h}{r} \right) \sin^2 \theta_{iv} + \left[\left[\epsilon_r - \sin^2 \theta_{iv} + \left[\sigma_r^2 + \left(\epsilon_r - \sin^2 \theta_{iv} \right)^2 \right]^{1/2} \right] \right]^{1/2} \\ \epsilon_r + \sin^2 \theta_{iv} + \left[\sigma_r^2 + \left(\epsilon_r - \sin^2 \theta_{iv} \right)^2 \right]^{1/2} - 2 \left(\frac{r+h}{r} \right)^2 \sin^2 \theta_{iv} \right\}^{1/2}$$

which can be inverted to give θ_a for substitution into equation (5.22) to give θ_{iRm} in terms of θ_{iv} , in the form

$$
(5.27) \quad
\begin{aligned}
\theta_{iRm} &= 2\,\theta_{iv} \\
&+ 2\,m\,\,\text{arc cos}\,\left[\!\!\left[\, \epsilon_r + \sin^2\theta_{iv} + \left[\, \sigma_r^2 + (\epsilon_r - \sin^2\theta_{iv})^2 \right]^{1/2}\right]\!\!\right]^{-1}
\end{aligned}
$$

$$
\left\{ 2\left(\frac{r+\ell}{r}\right)\sin^2\theta_{iv} + \left[\!\!\left[\,\epsilon_r - \sin^2\theta_{iv} + \left[\,\sigma_r^2 + (\epsilon_r - \sin^2\theta_{iv})^2\right]^{1/2}\right]\!\!\right]^{1/2}\right.
$$

$$
\left. \left[\!\!\left[\,\epsilon_r + \sin^2\theta_{iv} + \left[\,\sigma_r^2 + (\epsilon_r - \sin^2\theta_{iv})^2\right]^{1/2} - 2\left(\frac{r+\ell}{r}\right)^2 \sin^2\theta_{iv}\right]\!\!\right]^{1/2}\right\}
$$

The length of the "vds" ray path is measured between the same two reference planes established for the "v" ray path. From Figure A5-3 it can be seen that the ray path length in the dielectric (L_{Dvds}), for one round trip, is given by

$$
(5.28) \quad L_{Dvds} = 2\,r\,\frac{\sin\theta_a}{\sin\theta_{td}}
$$

In general the "vds" ray path makes m round trips through the dielectric coating, thus the total ray path length in the dielectric (L_{Dvdsm}) is given by

$$
(5.29) \quad L_{Dvdsm} = 2\,m\,r\,\frac{\sin\theta_a}{\sin\theta_{td}}
$$

which can be expanded, thru the use of equations (5.13) and (5.26), to give

$$(5.30) \quad L_{Dvdsm} = 2mr\left[\!\!\left[\epsilon_r + \sin^2\theta_{iv} + \left[\sigma_r^2 + |\epsilon_r - \sin^2\theta_{iv}|^2\right]^{1/2}\right]\!\!\right]^{-1/2}$$

$$\left\{\left(\frac{r+\hbar}{r}\right)\left[\!\!\left[\epsilon_r - \sin^2\theta_{iv} + \left[\sigma_r^2 + (\epsilon_r - \sin^2\theta_{iv})^2\right]^{1/2}\right]\!\!\right]^{1/2}\right.$$

$$\left. - \left[\!\!\left[\epsilon_r + \sin^2\theta_{iv} + \left[\sigma_r^2 + (\epsilon_r - \sin^2\theta_{iv})^2\right]^{1/2} - 2\left(\frac{r+\hbar}{r}\right)^2\sin^2\theta_{iv}\right]\!\!\right]^{1/2}\right\}$$

For the back-scattering condition ($\theta_{iRm} = 0$), equation (5.30) reduces to

$$(5.31) \qquad L_{Dvdsm} = 2m\hbar$$

The ray path length in free space from the incident reference plane to the dielectric surface (ℓ_1) is given by

$$(5.32) \qquad \ell_1 = (r + \hbar)(1 - \cos\theta_{iv})$$

and the ray path length in free space from the dielectric surface to the receiver location (ℓ_2), using equation (5.17), is given by

$$(5.33) \qquad \ell_2 = (r+\hbar)\cos(\pi - \theta_{iv}) + R_R\cos(2\theta_{iv} + 2\theta_a - \theta_{iv})$$

The ray path length from the dielectric surface to the scattered wave reference plane (ℓ_3), using equation (5.33), is given by

$$(5.34) \quad \ell_3 = (r + \ell)(1 - \cos \theta_{iv}) + R_R \left[\cos (2\theta_{iv} + 2\theta_a - \theta_{ir}) - 1 \right]$$

The "far-field" condition can be evaluated through the use of equation (5.19) and l'Hospital's rule, giving

$$(5.35) \quad \lim_{R_R \to \infty} \ell_3 = (r + \ell)(1 - \cos \theta_{iv})$$

The total ray path length in free space between the two reference planes (L_{Vvdsm}), for the "far-field" condition, is given by

$$(5.36) \quad L_{Vvdsm} = 2 (r + \ell)(1 - \cos \theta_{iv})$$

For the back-scattering condition ($\theta_{iRm} = 0$), equation (5.36) reduces to

$$(5.37) \quad L_{Vvdsm} = 0$$

Consider the "vd" ray path, in which the ray is transmitted through the outer dielectric surface, passes through the dielectric coating until it again meets the outer dielectric surface, and is transmitted through the outer dielectric surface to the receiver location. In order for such a ray path to contribute to the back-scattering it must encircle the metal sphere at least once. When the dielectric-coating thickness is small compared to the sphere radius, then the ray path must meet the outer dielectric surface many times in going around the sphere. At each of these internal reflections the intensity is decreased, so that after going completely around the back of the sphere the intensity is greatly reduced, and hence the contribution from such a ray path may be neglected.

APPENDIX A-6

DIVERGENCE FACTOR FOR BACK-SCATTERING BY A UNIFORM LOSSY DIELECTRIC-COATED METALLIC SPHERE

The geometrical divergence factor (between two points on a ray path) is defined as the limit of the ratio of the cross sections (at the two points) of a ray bundle containing the specified ray as the bundle shrinks to the single specified ray. The physical significance of the geometrical divergence factor is that it accounts for the variation of the average power density along a ray bundle carrying constant power due to the variation of the cross-sectional area of the bundle along its length for the limiting condition of zero cross-sectional area of the bundle (a single ray).[1] If the first point lies in an initial plane perpendicular to the ray path and the second point lies in a receiver plane perpendicular to the ray path, the geometrical divergence factor between these two locations (D_{iR}) is given by

$$(6.1) \qquad D_{iR} = \lim_{A_i \to 0} \frac{A_R}{A_i}$$

where A_i is the cross-section area of a ray bundle in the initial plane and A_R is the cross-section area of the same ray bundle in the receiver plane. This divergence factor is independent of the shape of the ray bundle cross section, hence any form convenient to the geometry of the problem may be used.

It is assumed here that the scattering object consists of a perfectly reflective sphere coated with a uniform layer of lossy dielectric material. The geometrical divergence factor for a plane electromagnetic wave incident on these concentric spherical boundaries, necessary for the determination of the scattering cross section, is determined by the ray path geometry (as derived in Appendix 5). The geometrical configuration used to define a typical ray bundle that can be used in the explicit formulation of equation (6.1) for concentric spherical boundaries is shown in Figure A6-1.

The initial area A_i is plane and parallel to the xy plane, hence it is perpendicular to the incident rays from the source. Figure A6-2 details A_i, which is the area of the non-mutual part of a sector of two concentric circles. It may be seen from Figure A6-1 that

$$(6.2) \qquad \rho = \left(r + \ell \right) \sin \theta_{iv}$$

and

$$(6.3) \qquad \rho + \Delta\rho = \left(r + \ell \right) \sin \left(\theta_{iv} + \Delta\theta_{iv} \right)$$

from which it follows that

$$(6.4) \qquad A_i = \frac{\Delta\phi}{2} \left(r + \ell \right)^2 \left[\sin^2 \left(\theta_{iv} + \Delta\theta_{iv} \right) - \sin^2 \theta_{iv} \right]$$

The receiving area A_R is on the surface of a sphere with center at the object location and radius R_R, hence it is perpendicular to the scattered

PLANE OF INCIDENCE= x z
SOURCE DIRECTION= z
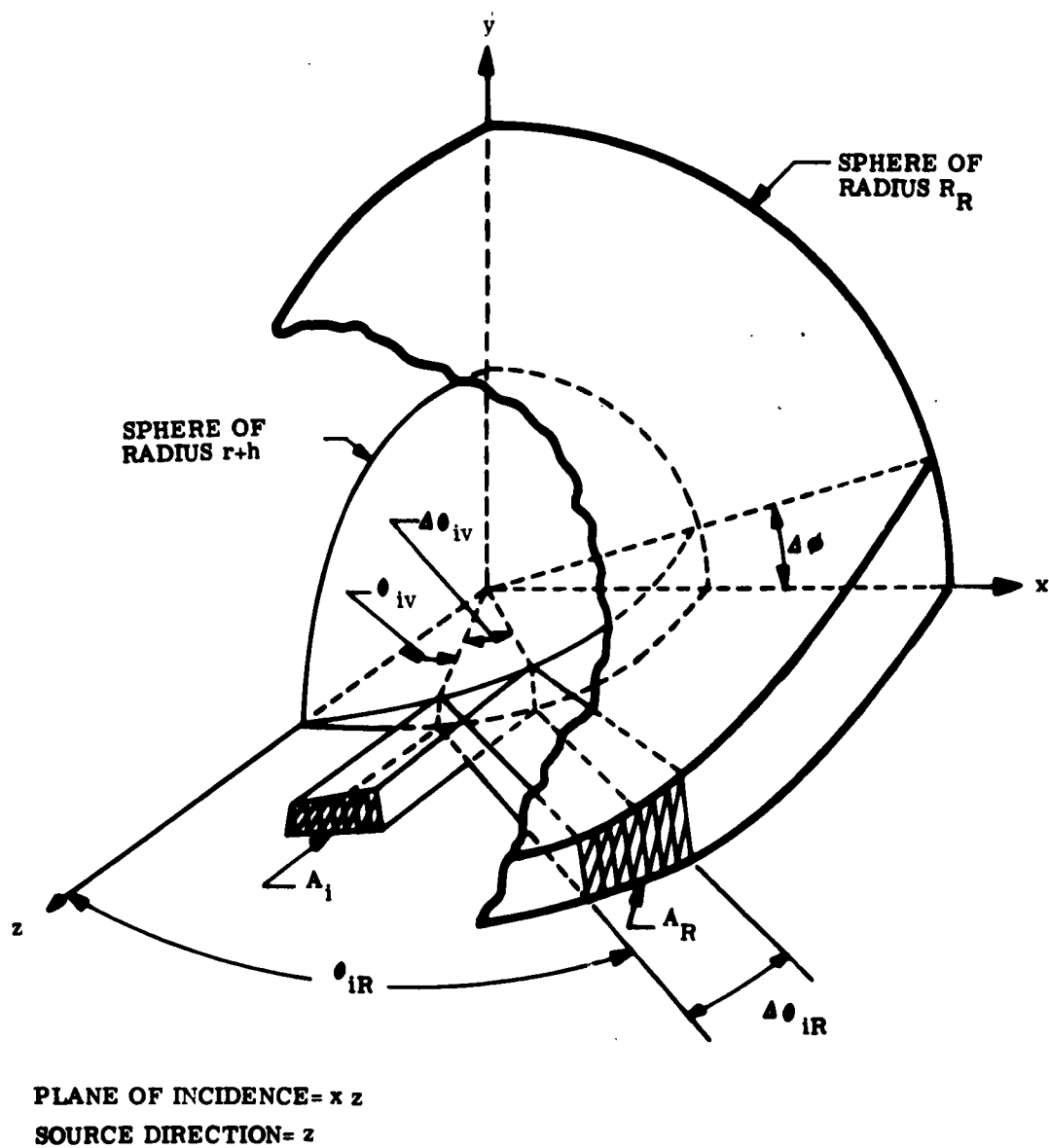
Figure A6-1   Ray Bundle Configuration
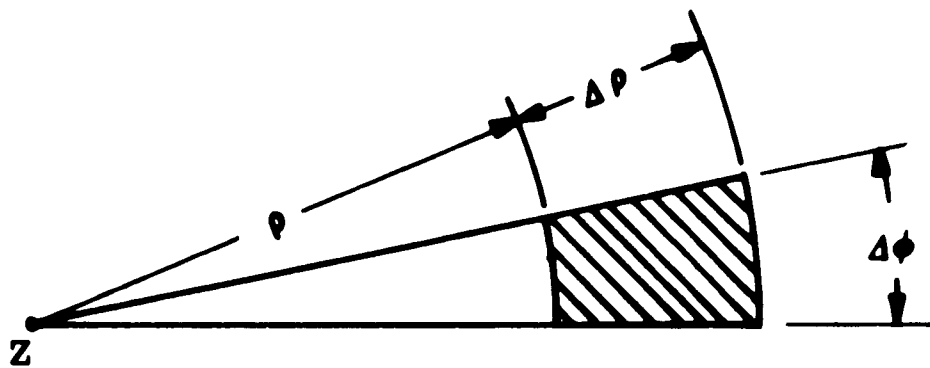
Figure A6-2   Details of Initial Area A_i

rays from the object when R_R is very much larger than the dimensions of the object. Figure A6-3 details A_R, which is a fraction of the area of the spherical zone defined by the planes $z = a$ and $z = b$. It may be seen from Figure A6-3 that

$$(6.5) \qquad a = R_R \cos \theta_{iR}$$

and

$$(6.6) \qquad b = R_R \cos \left(\theta_{iR} + \Delta \theta_{iR} \right)$$

from which it follows that

$$(6.7) \qquad A_R = \Delta \phi \, R_R^2 \left[\cos \theta_{iR} - \cos \left(\theta_{iR} + \Delta \theta_{iR} \right) \right]$$

Using equations (6.4) and (6.7), the geometrical divergence factor for the concentric spherical boundaries becomes

$$(6.8) \qquad D_{iR} = \frac{2 R_R^2}{(r + \hbar)^2} \lim_{\Delta \theta_{iv} \to 0} \frac{\cos \theta_{iR} - \cos \left(\theta_{iR} + \Delta \theta_{iR} \right)}{\sin^2 \left(\theta_{iv} + \Delta \theta_{iv} \right) - \sin^2 \theta_{iv}}$$

In which it is necessary to express θ_{iR} explicitly in terms of θ_{iv} before the limit can be taken. For the back-scattering condition, equation (6.8) reduces to
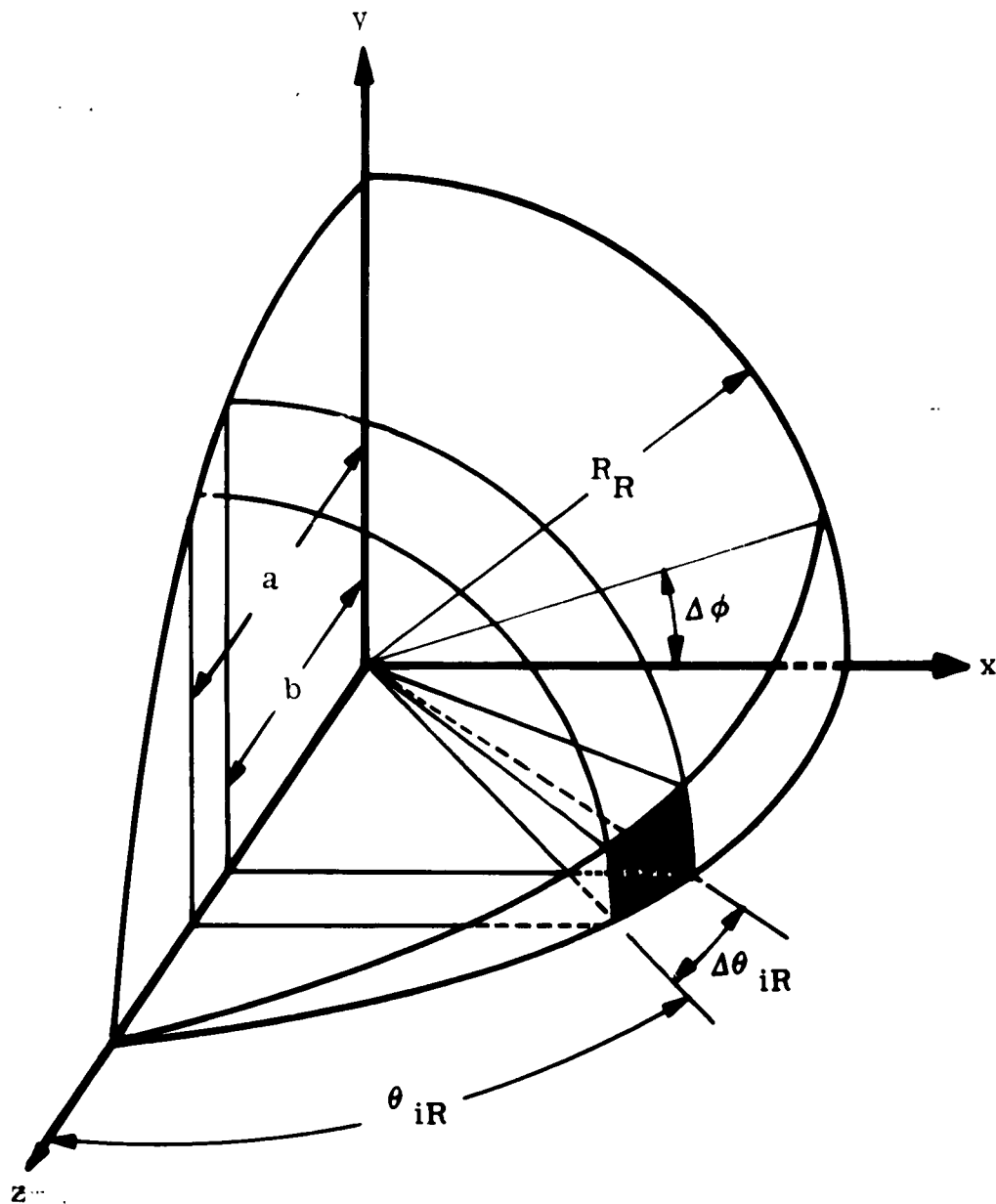
Figure A6-3   Details of Receiving Area A_R

$$(6.9) \qquad D_{iR} = \frac{2 R_R^2}{(r+\hbar)^2} \lim_{\Delta \theta_{iv} \to 0} \frac{1 - \cos \Delta \theta_{iR}}{\sin^2 \Delta \theta_{iv}}$$

The two different functional relationships between θ_{iR} and θ_{iv} are given in Appendix 5 for the two different characteristic ray paths that contribute to the back-scattering cross section, thus leading to a different divergence factor for each of the two different characteristic ray paths.

The back-scattering geometrical divergence factor for the "v" ray path is given by

$$(6.10) \qquad D_{iRv} = \frac{2 R_R^2}{(r+\hbar)^2} \lim_{\Delta \theta_{iv} \to 0} \frac{1 - \cos 2\Delta \theta_{iv}}{\sin^2 \Delta \theta_{iv}}$$

which can be simplified to give

$$(6.11) \qquad D_{iRv} = \frac{4 R_R^2}{(r+\hbar)^2}$$

The back-scattering geometrical divergence factor for the "vds" ray path is given by

$$(6.12)$$

$$D_{iRrds m} = \frac{2 R_R^2}{(r+\hbar)^2} \lim_{\Delta \theta_{iv} \to 0} \left[\sin^2 \Delta \theta_{iv} \right]^{-1} \left\{ 1 - \cos 2 \right.$$

$$\left\{ \Delta \theta_{iv} + m \arccos \left[\left| \epsilon_r + \sin^2 \Delta \theta_{iv} + \left[\sigma_r^2 + (\epsilon_r - \sin^2 \Delta \theta_{iv})^2 \right]^{1/2} \right| \right]^{-1} \right\}$$

$$\left\{ 2 \left(\frac{r+h}{r} \right) \sin^2 \Delta \theta_{iv} + \left[\left[\epsilon_r - \sin^2 \Delta \theta_{iv} + \left[\sigma_r^2 + \left(\epsilon_r - \sin^2 \Delta \theta_{iv} \right)^2 \right]^{1/2} \right] \right]^{1/2} \right.$$

$$\left. \left[\left[\epsilon_r + \sin^2 \Delta \theta_{iv} + \left[\sigma_r^2 + \left(\epsilon_r - \sin^2 \Delta \theta_{iv} \right)^2 \right]^{1/2} - 2 \left(\frac{r+h}{r} \right)^2 \sin^2 \Delta \theta_{iv} \right] \right]^{1/2} \right\} \right\}$$

which, thru the application of l'Hospital's rule, can be evaluated to give

(6.13) $$D_i R v d s m = \frac{4 R R_R^2}{(r+h)^2} \left[1 + m \frac{h}{r} \frac{\sqrt{2}}{\left[\epsilon_r + \left(\epsilon_r^2 + \sigma_r^2 \right)^{1/2} \right]^{1/2}} \right]^2$$

Using the relative phase factor β_r , as defined in Appendix 1, simplifies equation (6.13) to

(6.14) $$D_i R v d s m = \frac{4 R R_R^2}{(r+h)^2} \left[1 + m \frac{h}{r} \frac{1}{\beta_r} \right]^2$$

---

(1)   S. Silver, Microwave Antenna Theory and Design, McGraw-Hill, 1949, pp. 112 – 114.

APPENDIX A-7

GEOMETRICAL OPTICS ELECTROMAGNETIC WAVE BACK-SCATTERING CROSS SECTION OF A UNIFORM LOSSY DIELECTRIC-COATED METALLIC SPHERE

Detailed here is the theoretical determination of the electromagnetic wave back-scattering cross section (radar cross section) of a perfectly reflective sphere coated with a uniform layer of lossy dielectric material via the geometrical optics approach using the ray path field intensity addition technique.

Using the ray path field intensity addition technique, the general expression for the back-scattering cross section (from Appendix 3) is given by

$$(7.1) \qquad \sigma = 4\pi R_R^2 \left| \sum_{k=1}^{K} D_i R_k^{-1/2} \prod_{r=1}^{R_k} \rho_{kr} \prod_{t=1}^{T_k} \tau_{kt} \prod_{\ell=1}^{B_k} e^{-j\beta_{k\ell} L_{k\ell}} \prod_{a=1}^{A_k} e^{-\alpha_{ka} L_{ka}} \right|^2$$

The sum over k can be expanded into two sums, each over one of the two different characteristic ray paths ("v" and "vds"; see Appendix 5). This is reasonably accurate when the coating thickness (h) is small compared to the sphere radius (r) because the effects of encircling ray paths are negligible in this case.

Inspection of the characteristic ray paths shows that the sum of all the contributions from the "v" characteristic ray path reduces to a single term, while the sum of the contributions from the "vds" characteristic ray path consists of an infinite number of terms. Expanding the sum over k into sums over the two different characteristic ray path contributions gives

$$
(7.2) \quad \sigma = 4 \pi R_R^2 \left| \rho_{vd} D_{iRv}^{-\frac{1}{2}} e^{-j\beta_v L_{Vv}} \right.
$$

$$
+ \sum_{m=1}^{\infty} D_{iRvdsm}^{-\frac{1}{2}} \prod_{r=1}^{R_{vdsm}} \rho_{vdsmr} \prod_{t=1}^{T_{vdsm}} T_{vdsmt}
$$

$$
\left. \prod_{\ell=1}^{B_{vdsm}} e^{-j\beta_{vds\ell} L_{vdsm\ell}} \prod_{a=1}^{A_{vdsm}} e^{-\alpha_{vdsa} L_{vdsma}} \right|^2
$$

Examination of the "vds" characteristic ray path shows that

$$
(7.3) \quad \prod_{r=1}^{R_{vdsm}} \rho_{vdsmr} = (-1)^m (\rho_{dv})^{m-1}
$$

$$
(7.4) \quad \prod_{t=1}^{T_{vdsm}} T_{vdsmt} = T_{vd} T_{dv}
$$

$$
(7.5) \quad \prod_{\ell=1}^{B_{vdsm}} e^{-j\beta_{vds\ell} L_{vdsm\ell}} = e^{-j\beta_v L_{Vvdsm}} e^{-j\beta_c L_{Dvdsm}}
$$

$$(7.6) \quad \prod_{a=1}^{A_{vdsm}} e^{-\alpha_{vdsa} L_{vdsma}} = e^{-\alpha_{\alpha} L_{Dvdsm}}$$

Appendix 4 shows for normal incidence that

$$(7.7) \quad \rho_{dv} = -\rho_{vd}$$

$$(7.8) \quad T_{vd} T_{dv} = 1 - \rho_{vd}^{2}$$

and Appendix 5 shows for the back-scattering condition that

$$(7.9) \quad L_{Vv} = 0$$

$$(7.10) \quad L_{Vvdsm} = 0$$

$$(7.11) \quad L_{Dvdsm} = 2m\hbar$$

Using Equations (7.3) through (7.11) in equation (7.2) gives

$$(7.12) \quad \sigma = 4\pi R_{R}^{2} \left| \rho_{vd} D_{iRv}^{-\frac{1}{2}} \right.$$

$$\left. - \frac{|1 - \rho_{vd}^{2}|}{\rho_{vd}} \sum_{m=1}^{\infty} D_{iRvdsm}^{-\frac{1}{2}} \left[\rho_{vd} e^{-j\beta_{d} 2\hbar} e^{-\alpha_{d} 2\hbar} \right]^{m} \right|^{2}$$

The explicit forms of the various factors in equation (7.12) are necessary for completion of the formula.

Appendix A-4 shows for normal incidence that

$$(7.13) \qquad \rho_{vd} = \frac{1 - \left(\epsilon_r - j\sigma_r \right)^{1/2}}{1 + \left(\epsilon_r - j\sigma_r \right)^{1/2}}$$

and Appendix A-6 shows for the back-scattering condition that

$$(7.14) \qquad D_{iRv}^{-1/2} = \frac{\left(r + \ell \right)}{2 R_R}$$

$$(7.15) \qquad D_{iRvdsm}^{-1/2} = \frac{\left(r + \ell \right)}{2 R_R} \left[1 + m \frac{\ell}{r} \frac{1}{\beta_r} \right]^{-1}$$

It can be shown [1] that the phase factor (β_d) and attenuation factor (α_d) for a plane electromagnetic wave propagating normally into a lossy dielectric medium are the same as those derived for plane electromagnetic wave propagation in the unbounded lossy dielectric medium. These factors are

$$(7.16) \qquad \beta_d = \frac{\sqrt{2} \, \pi}{\lambda_v} \left[\epsilon_r + \left(\epsilon_r^2 + \sigma_r^2 \right)^{1/2} \right]^{1/2}$$

$$(7.17) \qquad \alpha_d = \frac{\sqrt{2} \, \pi}{\lambda_v} \left[-\epsilon_r + \left(\epsilon_r^2 + \sigma_r^2 \right)^{1/2} \right]^{1/2}$$

The relationship between the electromagnetic wave wavelength in the lossy dielectric medium (λ_d) and the free-space wavelength (λ_v) is

$$(7.18) \qquad \lambda_d = \frac{2\pi}{\beta_d} = \frac{\sqrt{2}\,\lambda_v}{\left[\epsilon_r + \left(\epsilon_r^2 + \sigma_r^2\right)^{1/2}\right]^{1/2}} = \frac{\lambda_v}{\beta_r}$$

Using equations (7.14) and (7.15) in equation (7.12), and normalizing with respect to the radar cross section of the uncoated sphere (πr^2), gives

$$(7.19) \quad \frac{\sigma}{\pi r^2} = \left(1 + \frac{\hbar}{r}\right)^2 \left| \rho_{vd} - \frac{\left(1 - \rho_{vd}^2\right)}{\rho_{vd}} \right.$$

$$\sum_{m=1}^{\infty} \left[1 + m\frac{\hbar}{r}\frac{1}{\beta_r}\right]^{-1} \left[\rho_{vd}\, e^{-j\beta_d 2\hbar}\, e^{-\alpha_d 2\hbar}\right]^m \Bigg|^2$$

where ρ_{vd} , β_d , and α_d are given by equations (7.13), (7.16), and (7.17) respectively.

Note that when

$$(7.20) \qquad \rho_{vd} = \frac{\left(1 - \rho_{vd}^2\right)}{\rho_{vd}}$$

$$\sum_{m=1}^{\infty} \left[1 + m\frac{\hbar}{r}\frac{1}{\beta_r}\right]^{-1} \left[\rho_{vd}\, e^{-j\beta_d 2\hbar}\, e^{-\alpha_d 2\hbar}\right]^m$$

the radar cross section of the uniform lossy dielectric-coated metallic sphere will vanish.

A useful approximation to equation (7.19) for the radar cross section of a uniform lossy dielectric-coated metallic sphere can be made if the condition

$$(7.21) \qquad \frac{\ell}{r}\frac{1}{\beta_r} << 1$$

is met. Under this condition, the approximation

$$(7.22) \qquad 1 + m\frac{\ell}{r}\frac{1}{\beta_r} \cong \left(1 + \frac{\ell}{r}\frac{1}{\beta_r}\right)^m$$

can be made, which modifies equation (7.19) to the form

$$(7.23) \qquad \frac{\sigma}{\pi r^2} \cong \left(1 + \frac{\ell}{r}\right)^2 \left| \rho_{vd} - \frac{(1-\rho_{vd}^2)}{\rho_{vd}} \sum_{m=1}^{\infty}\left[\frac{\rho_{vd}\,e^{-j\beta_d 2\ell}\,e^{-\alpha_d 2\ell}}{1 + \frac{\ell}{r}\frac{1}{\beta_r}}\right]^m \right|^2$$

Using the formula

$$(7.24) \qquad \sum_{m=1}^{\infty} x^m = \frac{x}{1-x}$$

the sum in equation (7.23) can be closed, giving

$$(7.25) \qquad \frac{\sigma}{\pi r^2} \cong \left(1 + \frac{\hbar}{r}\right)^2 \left| \frac{\rho_{vd} - \dfrac{e^{-j\beta_d 2\hbar} e^{-\alpha_d 2\hbar}}{1 + \dfrac{\hbar}{r}\dfrac{1}{\beta_r}}}{1 - \rho_{vd} \dfrac{e^{-j\beta_d 2\hbar} e^{-\alpha_d 2\hbar}}{1 + \dfrac{\hbar}{r}\dfrac{1}{\beta_r}}} \right|^2$$

Note that when

$$(7.26) \qquad \rho_{vd} = \frac{e^{-j\beta_d 2\hbar} e^{-\alpha_d 2\hbar}}{1 + \dfrac{\hbar}{r}\dfrac{1}{\beta_r}}$$

the approximate radar cross section of the uniform lossy dielectric-coated metallic sphere will vanish. Since this is a conditional equation in complex variables it represents two equations in real variables defining the necessary relationships between the dielectric constant (ϵ_r), the relative conductivity (σ_r), the coating thickness ($\hbar$), the sphere radius (r), and the electromagnetic wave free-space wavelength (λ_r) that must be satisfied in order for the radar cross section as given by equation (7.25) to vanish. Equation (7.26) can be separated into the two conditional equations

$$(7.27) \quad \left(2\hbar - \frac{1}{2} \right) \pi + \arctan \left[\frac{\frac{4\pi^2}{\lambda_v^2} - \alpha_d^2 - \beta_d^2}{\frac{4\pi\alpha_d}{\lambda_v}} \right] =$$

$$\frac{\beta_d}{2\alpha_d} \ln \left\{ \frac{\left[\alpha_d^2 + \left(\frac{2\pi}{\lambda_v} + \beta_d \right)^2 \right]}{\left[\alpha_d^2 + \left(\frac{2\pi}{\lambda_v} - \beta_d \right)^2 \right]} \left(1 + \frac{\hbar}{r} \frac{1}{\beta_r} \right)^{-2} \right\}$$

$$(7.28) \quad \frac{\hbar}{\lambda_v} = \frac{1}{2\lambda_v \beta_d} \left\{ \left(2\hbar - \frac{1}{2} \right) \pi + \arctan \left[\frac{\frac{4\pi^2}{\lambda_v^2} - \alpha_d^2 - \beta_d^2}{\frac{4\pi\alpha_d}{\lambda_v}} \right] \right\}$$

where k = 1, 2, 3, ... and indicates the multiplicity of values for which the radar cross section can vanish. Equation (7.27) gives the necessary relationship between the electromagnetic properties of the dielectric material and equation (7.28) gives the necessary coating thickness.

The formulas for the detailed variation of the radar cross section of a uniform lossy dielectric-coated metallic sphere (equation (7.19) and equation (7.25) for the exact and approximate formulations, respectively) are sufficiently complex to preclude understanding of the detailed functional variations involved merely by inspection of the equations. It is therefore necessary to numerically calculate and plot the radar cross section in a suitably normalized form in order to gain insight into the detailed functional behavior.

Using equation (7.19), the radar cross section of a uniform lossy dielectric-coated metallic sphere has been calculated for certain combinations of the various parameters involved. The results of these calculations are shown in Figures A7-1 and A7-2, where the normalized radar cross section is plotted as a function of the dielectric constant with the normalized coating thickness, normalized wavelength, and relative conductivity as parameters. The normalized coating thickness ($\mathcal{R}/r$) has the same value (0.1) for all the curves shown in Figures A7-1 and A7-2. The normalized wavelength (λ_v/r) values (0.034215 and 0.25146 for Figures A7-1 and A7-2, respectively) are chosen to provide the longest wavelengths (k = 1) that cause zero radar cross section to occur for zero relative conductivity (in Figure A7-1) and for a non-zero (0.62772) relative conductivity (in Figure A7-2), respectively. Several values of relative conductivity are used to show the transitional behavior from the lossless to the highly lossy condition.

The geometrical optics approach to the determination of the radar cross section of a uniform lossy dielectric-coated metallic sphere is applicable and valid when the radius of the sphere is much larger than
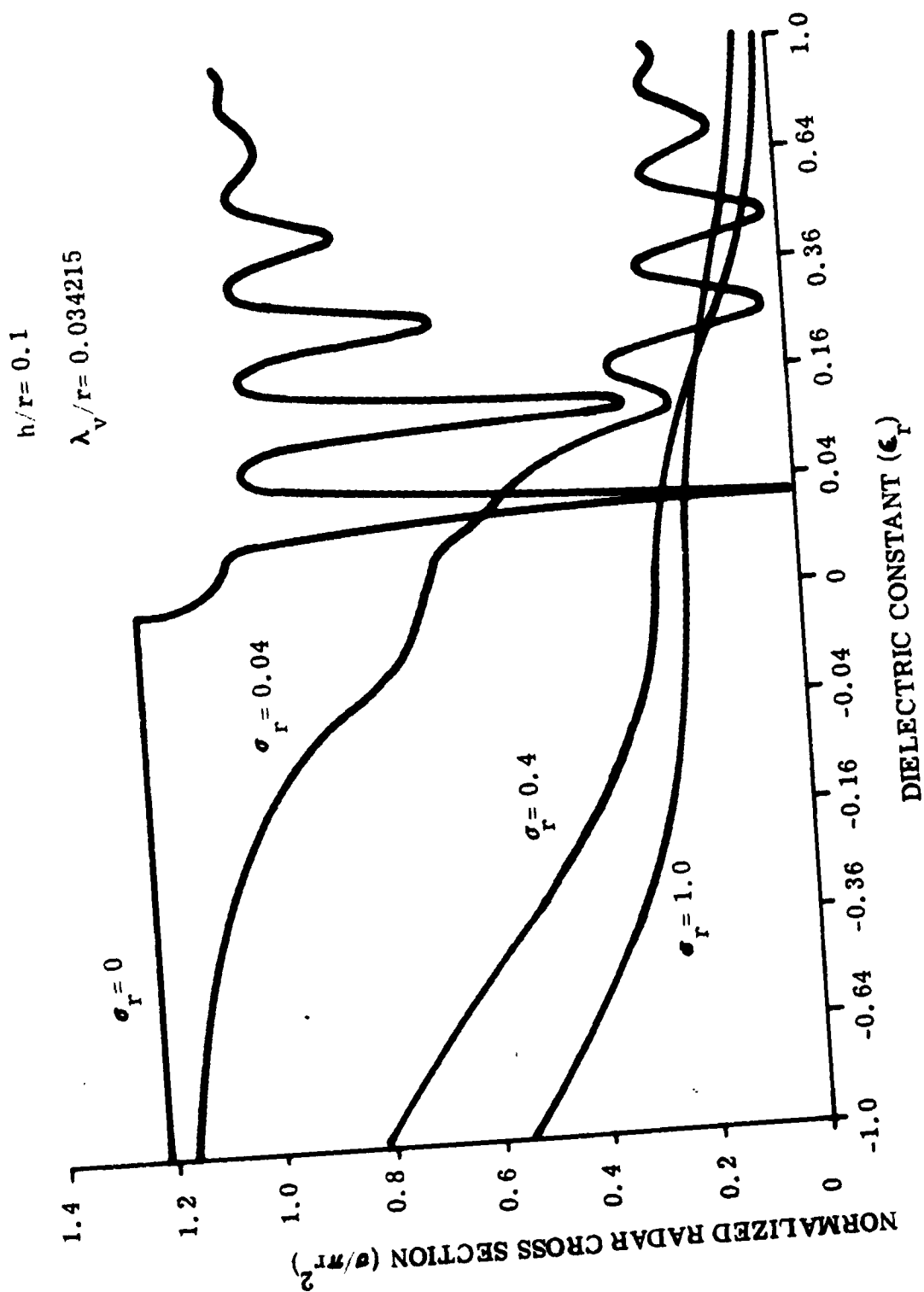
Figure A7-1   Radar Cross Section of a Uniform Lossy Dielectric-
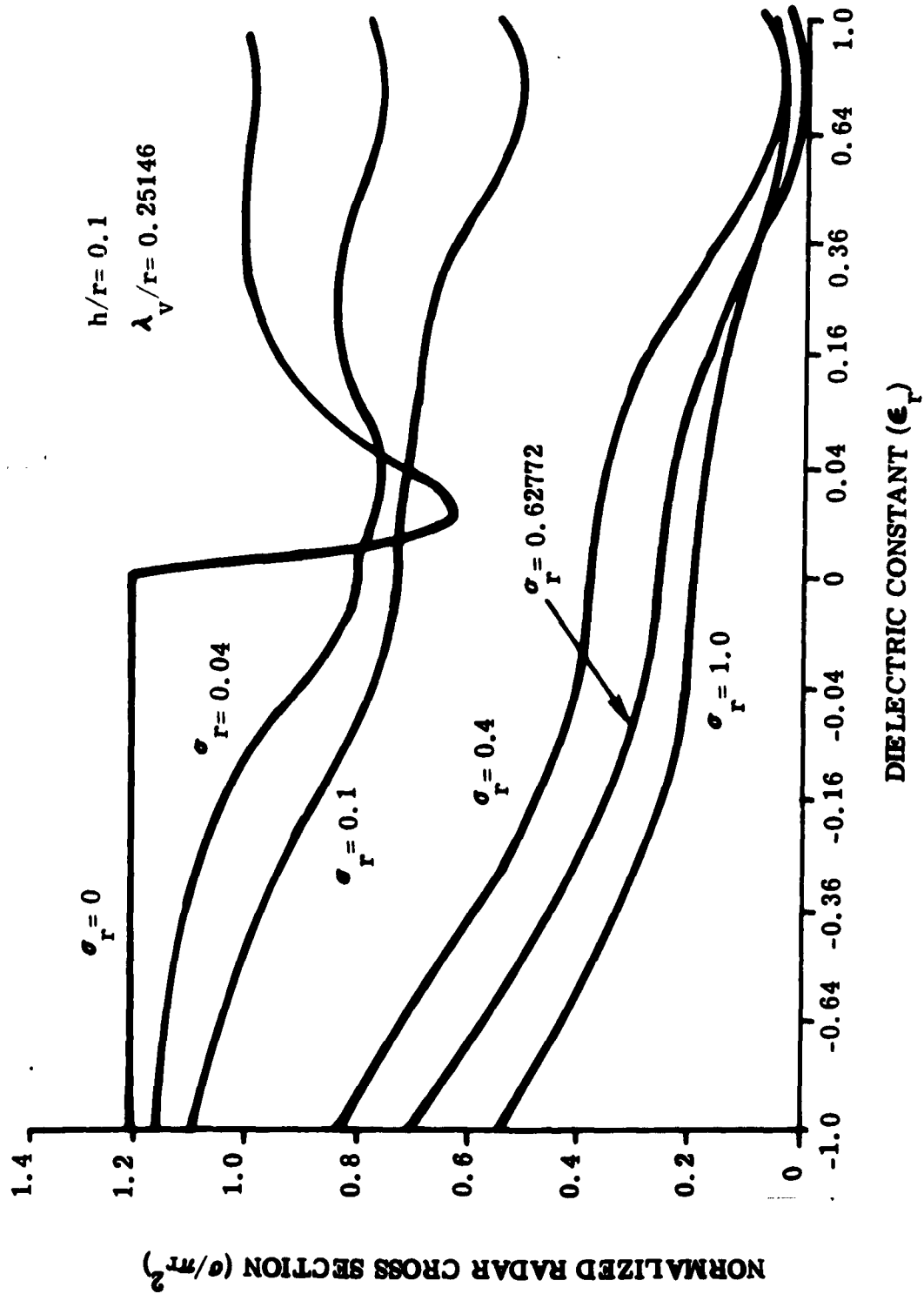Coated Metallic Sphere $\lambda_v/r = 0.034215$

Figure A7-2　Radar Cross Section of a Uniform Lossy Dielectric-Coated Metallic Sphere, $\lambda_v/r = 0.25146$

the wavelength of the incident electromagnetic wave in free space and in the dielectric. Using equation (7.18) these applicability criteria become

$$(7.29) \qquad \cdot\ \lambda_{\nu} \ <<\ r$$

and

$$(7.30) \qquad \frac{\lambda_{\nu}}{\beta_{\nu}} \ <<\ r$$

These geometrical requirements limit the applicability of the geo-metrical optics approximation when the dielectric constant and the relative conductivity both closely approach zero.

---

(1) J. A. Stratton, Electromagnetic Theory, McGraw-Hill, 1941, pp. 500–524.

ᵗ APPENDIX A-8

GEOMETRICAL OPTICS RADAR CROSS SECTION OF A
METALLIC SPHERE COATED WITH A
UNIFORM LOSSY PLASMA

The radar cross section σ , obtained by the geometrical optics approach, of a perfectly reflective (metallic) sphere of radius r covered with a uniform coating of lossy plasma is given here. The plasma is assumed to have uniform thickness h all around the sphere and no spatial variation of its electromagnetic properties throughout the coating. Furthermore, it is assumed that the plasma can be characterized (electromagnetically) by a permeability μ_p , a capacitivity ϵ_p , and a conductivity σ_p analogous to the situation for non-ionized media. Thus, the situation becomes that of a uniform lossy dielectric-coated metallic sphere. The rigorously obtained expression for the radar cross section of this composite structure is given in Appendix 2, with appropriate substitutions for the dielectric properties of the plasma from Appendix 1. However, some of the general characteristics of the behavior of the radar cross section under various parameter variations can be better seen from the geometrical optics approach. Using the results from Appendixes 1 and 7, the normalized radar cross section is given by

$$(8.1) \qquad \frac{\sigma}{\pi r^2} = \left(1 + \frac{h}{r}\right)^2 \left| \Gamma_p - \frac{(1 - \Gamma_p^2)}{\Gamma_p} \sum_{m=1}^{\infty} D_m \left(\Gamma_p \, e^{-\sigma_p 2h}\right)^m \right|^2$$

where D_m is the relative geometrical divergence factor for the mth ray path thru the plasma coating, Γ_p is the reflection coefficient for a plane transverse electromagnetic wave propagating normally from free space into a plane interface between free space and a uniform plasma having the electromagnetic properties of the coating, γ_p is the propagation factor for a plane transverse electromagnetic wave propagating thru an unbounded uniform plasma having the electromagnetic properties of the coating, and β_r is the relative phase factor for the same situation. Appendixes 1, 4 and 7 give

$$(8.2) \qquad D_m = \left(1 + m \, \frac{\ell}{r} \, \frac{1}{\beta_r} \right)^{-1}$$

$$(8.3) \qquad \Gamma_p = \frac{1 - \left(1 - \dfrac{\Omega_p^2}{1 - j\Omega_c} \right)^{1/2}}{1 + \left(1 - \dfrac{\Omega_p^2}{1 - j\Omega_c} \right)^{1/2}}$$

$$(8.4) \qquad \gamma_p = j \frac{2\pi}{\lambda_r} \left(1 - \frac{\Omega_p^2}{1 - j\Omega_c} \right)^{1/2}$$

$$(8.5) \qquad \beta_r = \left\{ \frac{\left[\Omega_c^2 + \left(1 - \Omega_p^2 \right)^2 \right]^{1/2} \left(1 + \Omega_c^2 \right)^{1/2} + \Omega_c^2 + \left(1 - \Omega_p^2 \right)}{2 \left(1 + \Omega_c^2 \right)} \right\}^{1/2}$$

where

$\Omega_p = \omega_p / \omega$ = normalized plasma frequency,

$\Omega_c = \nu_c / \omega$ = normalized electron collision frequency,

ω_p = angular plasma frequency ($2\pi f_p$),

ν_c = electron collision frequency,

ω = angular radar frequency ($2\pi f$), and

λ_r = free-space wavelength of the radar wave.

It can be seen from equation (8.1) that when the plasma coating is highly reflective ($|\Gamma_p| \cong 1$) the radar cross section σ approaches the value $\pi r^2 (1 + \hbar/r)^2$, which is the value for a perfectly reflective sphere having a radius equal to the outer radius of the plasma coating. When the plasma coating is negligibly reflective ($|\Gamma_p| \cong 0$) the radar cross section σ approaches the value πr^2, which is the value for the bare metallic sphere, as would be expected.

Note that when

$$(8.6) \qquad \Gamma_p = \frac{|1 - \Gamma_p^2|}{\Gamma_p} \sum_{m=1}^{\infty} D_m \left(\Gamma_p e^{-\gamma_p 2\hbar} \right)^m$$

the radar cross section will vanish. This condition is possible but is very difficult to express concisely in terms of the variables r, $\hbar$, λ_r, Ω_p, and Ω_c because of the infinite sum involved.

A useful approximation to equation (8.1) can be found (see Appendix 7) when

$$(8.7) \qquad \frac{\hbar}{r} \frac{1}{\beta_r} \ll 1$$

Under this condition the infinite sum in equation (8.1) can be closed approximately, giving

$$(8.8) \qquad \frac{\sigma}{\pi r^2} \cong \left(1 + \frac{\hbar}{r} \right)^2 \left| \frac{\Gamma_p - D e^{-\gamma_p 2\hbar}}{1 - \Gamma_p D e^{-\gamma_p 2\hbar}} \right|^2$$

where

$$(8.9) \qquad D = \left(1 + \frac{\hbar}{r} \frac{1}{\beta_r}\right)^{-1}$$

Equation (8.8) has the same behavior as equation (8.1) for both highly reflective and negligibly reflective plasma coatings. Also, when

$$(8.10) \qquad \Gamma_{\phi} = D e^{-\gamma_{\phi} 2 \hbar}$$

the radar cross section will vanish. This can occur only when both the magnitudes and the phase angles of the two terms are equal. These two conditions give the parametric requirements for vanishing of the radar cross section, and can be written in the form

$$(8.11) \qquad \left(2\hbar - \tfrac{1}{2}\right)\pi + \arctan\left(\frac{1 - \alpha_r^2 - \beta_r^2}{2\alpha_r}\right) = \frac{\beta_r}{2\alpha_r} \ln\left[\frac{\alpha_r^2 + \left(1 + \beta_r\right)^2}{\alpha_r^2 + \left(1 - \beta_r\right)^2} D^2\right]$$

$$(8.12) \qquad \frac{\hbar}{\lambda_v} = \frac{1}{4\pi\beta_r}\left[\left(2\hbar - \tfrac{1}{2}\right)\pi + \arctan\left(\frac{1 - \alpha_r^2 - \beta_r^2}{2\alpha_r}\right)\right]$$

where $\hbar = 1, 2, 3, \ldots$ and indicates the multiplicity of values for which the radar cross section can vanish, and α_r is the relative attenuation factor given by

$$(8.13) \qquad \alpha_r = \left\{\frac{\left[\Omega_c^2 + \left(1 - \Omega_\phi^2\right)^2\right]^{1/2}\left(1 + \Omega_c^2\right)^{1/2} - \Omega_c^2 - \left(1 - \Omega_\phi^2\right)}{2\left(1 + \Omega_c^2\right)}\right\}^{1/2}$$

Equation (8.11) gives, indirectly, the necessary relationship between the electromagnetic properties of the plasma and equation (8.12) gives the necessary plasma thickness required for the radar cross section to vanish. In a three-dimensional space whose coordinates are Ω_p, Ω_c , and $\hbar/\lambda_r$ the conditions for vanishing radar cross section are lines, one line for each value of $\hbar$. It is necessary to solve equations (8.11) and (8.12) numerically in order to see the behavior of these conditions in terms of the pertinent variables. Figures A8-1 and A8-2 show a typical solution. Note that the conditions given by both figures must be satisfied simultaneously. It can be seen from these figures that the normalized plasma frequency (ω_p/ω) required for zero reflection is of the order of unity for small (less than unity) values of normalized electron collision frequency (ν_c/ω) and varies approximately as the square root of the normalized electron collision frequency for large (greater than unity) values of normalized electron collision frequency. It is important to note that the minimum plasma layer thickness ($\hbar$) for which zero reflection can occur is of the order of one-third of the free-space wavelength of the radar wave.
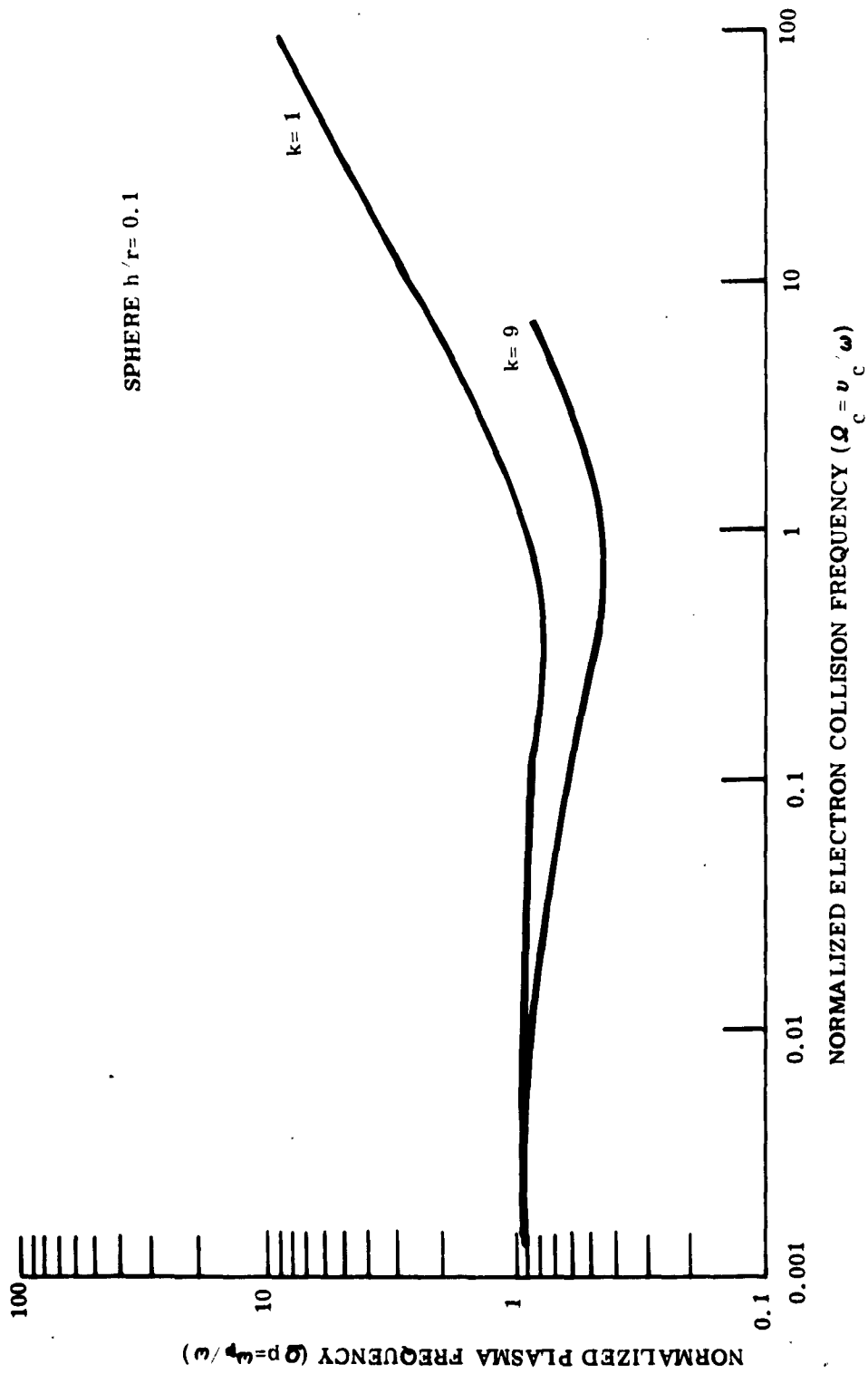
SPHERE h′/r= 0.1

k= 1

k= 9

NORMALIZED ELECTRON COLLISION FREQUENCY $(\Omega_c = \nu_c / \omega)$

NORMALIZED PLASMA FREQUENCY $(\Omega_p = \omega_p / \omega)$

Figure A8-1   Conditions for Vanishing Radar Cross Section

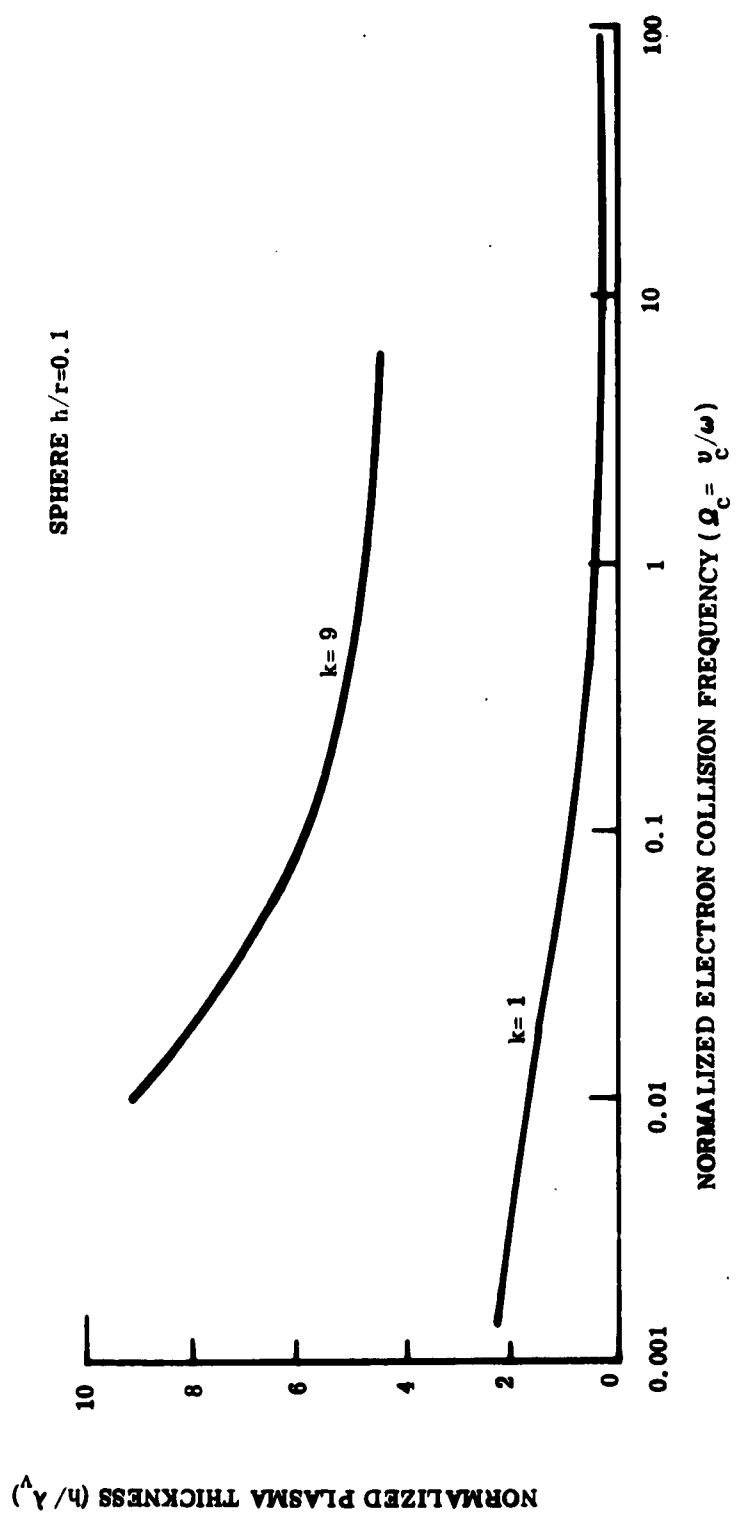$$\left(\frac{\omega_p}{\omega} \text{ vs } \frac{\nu_c}{\omega} \right)$$

Figure A8-2   Conditions for Vanishing Radar Cross Section
$$\left(\frac{h}{\lambda_v} \text{ vs } \frac{v_c}{\omega}\right)$$

APPENDIX A-9

ELECTROMAGNETIC WAVE REFLECTION AT NORMAL INCIDENCE FROM AN INFINITE METALLIC FLAT PLATE COATED WITH A UNIFORM LOSSY PLASMA

Derived here is the reflection of a plane transverse electromagnetic wave normally incident on an infinite perfectly reflective (metallic) flat plate coated with a uniform lossy plasma. The plasma coating is assumed to have a uniform thickness h, and no spatial variation of its electromagnetic properties throughout the layer. Furthermore, it is assumed that the plasma can be completely characterized electromagnetically by an equivalent permeability, dielectric constant, and conductivity as given in Appendix A-1.

In the free-space region outside the plasma layer the incident electromagnetic wave is given by the electric field ($\mathbb{E}_i$) distribution

$$(9.1) \qquad \mathbb{E}_i = 1_x \, E_i \, e^{j\omega t - \hat{\gamma}_v z}$$

and the associated magnetic field ($\mathbb{H}_i$) distribution

$$(9.2) \qquad \mathbb{H}_i = 1_y \sqrt{\frac{\epsilon_v}{\mu_v}} \, E_i \, e^{j\omega t - \gamma_v z}$$

where the wave is taken to be propagating in the positive z direction (normal to the flat plate) and has the electric field vector polarized in the positive x direction. The propagation factor in free space (γ_v) is given by

$$(9.3) \qquad \gamma_v = j \, \frac{2\pi}{\lambda_v}$$

where

$1_x ; 1_y$ = unit vectors in the x and y directions

E_i = amplitude of the electric field of the incident wave

ω = angular frequency of the incident wave ($2\pi f$)

t = time

λ_v = free-space wavelength of the incident wave

ϵ_v = capacitivity of free space

μ_v = permeability of free space.

In the free-space region outside the plasma layer the reflected wave is given by the electric field ($\mathbb{E}_r$) distribution

$$(9.4) \qquad \mathbb{E}_r = 1_x \, E_r \, e^{j\omega t + \gamma_v z}$$

and the associated magnetic field ($\mathbb{H}_r$) distribution

$$(9.5) \qquad \mathbb{H}_r = - 1_y \, \sqrt{\frac{\epsilon_v}{\mu_v}} \, E_r \, e^{j\omega t + \gamma_v z}$$

In the plasma layer the total field consists of forward-and backward-traveling waves. The forward-traveling wave is given by the electric field ($\mathbb{E}_f$) distribution

(9.6) $\quad \mathbb{E}_f = 1_x \, E_f \, e^{j\omega t - \gamma_p z}$

and the associated magnetic field ($\mathbb{H}_f$) distribution

(9.7) $\quad \mathbb{H}_f = 1_y \sqrt{\dfrac{\epsilon_r}{\mu_r}} \, (\epsilon_r - j\sigma_r)^{1/2} \, E_f \, e^{j\omega t - \gamma_p z}$

The propagation factor in plasma (γ_p) is given by

(9.8) $\quad \gamma_p = j \dfrac{2\pi}{\lambda_v} (\epsilon_r - j\sigma_r)^{1/2}$

where

ϵ_r = dielectric constant of plasma

σ_r = relative conductivity of plasma

The backward-traveling wave is given by the electric field ($\mathbb{E}_b$) distribution

(9.9) $\quad \mathbb{E}_b = 1_x \, E_b \, e^{j\omega t + \gamma_p z}$

and the associated magnetic field ($\mathbb{H}_b$) distribution

(9.10) $\quad \mathbb{H}_b = -1_y \sqrt{\dfrac{\epsilon_r}{\mu_r}} \, (\epsilon_r - j\sigma_r)^{1/2} \, E_b \, e^{j\omega t + \gamma_p z}$

The reflection coefficient (Γ) for the composite structure is defined as

(9.11) $\qquad \Gamma = \dfrac{\left|\mathbb{E}_r\right|}{\left|\mathbb{E}_i\right|}$ $\Bigg|$ at the plasma surface

Assuming the plasma surface to be at $z = 0$ and the metallic flat plate to be at $z = h$ gives

(9.12) $\qquad \Gamma = \dfrac{E_r}{E_i}$

Applying the electromagnetic boundary conditions at the plasma surface of continuous tangential electric field gives

(9.13) $\qquad E_i + E_r = E_f + E_b$

and continuous tangential magnetic field gives

(9.14) $\qquad E_i - E_r = \left(\epsilon_r - j\sigma_r\right)^{1/2}\left(E_f - E_b\right)$

Applying the electromagnetic boundary conditions at the metallic flat plate surface of zero tangential electric field gives

(9.15) $\qquad E_f\, e^{-\gamma_p h} + E_b\, e^{+\gamma_p h} = 0$

Solving equations (9.13) thru (9.15) gives

$$(9.16) \quad \frac{E_r}{E_i} = \frac{\dfrac{1 - \left(\epsilon_r - j\sigma_r\right)^{1/2}}{1 + \left(\epsilon_r - j\sigma_r\right)^{1/2}} - e^{-\gamma_p 2\ell}}{1 - e^{-\gamma_p 2\ell} \dfrac{1 - \left(\epsilon_r - j\sigma_r\right)^{1/2}}{1 + \left(\epsilon_r - j\sigma_r\right)^{1/2}}}$$

and using the definition of the reflection coefficient for a plane inter-face between free space and an unbounded plasma (Γ_p) given from Appendix 4 by

$$(9.17) \quad \Gamma_p = \frac{1 - \left(\epsilon_r - j\sigma_r\right)^{1/2}}{1 + \left(\epsilon_r - j\sigma_r\right)^{1/2}}$$

gives the overall reflection coefficient (Γ) as

$$(9.18) \quad \Gamma = \frac{\Gamma_p - e^{-\gamma_p 2\ell}}{1 - \Gamma_p e^{-\gamma_p 2\ell}}$$

It can be seen from equation (9.18) that when

$$(9.19) \quad \Gamma_p = e^{-\gamma_p 2\ell}$$

there will be no reflected wave. Using the results of Appendix 1 which give

$$(9.20) \quad \Gamma_p = \frac{1 - \left(1 - \dfrac{\Omega_p^2}{1 - j\Omega_c}\right)^{1/2}}{1 + \left(1 - \dfrac{\Omega_p^2}{1 - j\Omega_c}\right)^{1/2}}$$

and

$$(9.21) \quad \gamma_p = j\frac{2\pi}{\lambda_r}\left(1 - \frac{\Omega_p^2}{1 - j\Omega_c}\right)^{1/2}$$

where

$\Omega_p = \omega_p/\omega$ = normalized plasma frequency

$\Omega_c = \nu_c/\omega$ = normalized electron collision frequency

$\omega_p = 2\pi f_p$ = angular plasma frequency

$\nu_c =$ electron collision frequency

$\omega = 2\pi f$ = angular frequency of incident wave

the plasma properties necessary for vanishing reflection can be determined from equation (9.19). Since equation (9.19) involves complex variables it is equivalent to two ordinary algebraic equations which can be written in the forms

$$(9.22) \quad \left(2k - \frac{1}{2}\right)\pi + \arctan\left(\frac{1 - \alpha_r^2 - \beta_r^2}{2\alpha_r}\right) =$$

$$\frac{\beta_r}{2\alpha_r}\ln\left[\frac{\alpha_r^2 + (1 + \beta_r)^2}{\alpha_r^2 + (1 - \beta_r)^2}\right]$$

and

$$(9.23) \quad \frac{\hbar}{\lambda_r} = \frac{1}{4\pi\beta_r} \left\{ \left(2\hbar - \frac{1}{2}\right)\pi + \arctan\left(\frac{1 - \alpha_r^2 - \beta_r^2}{2\alpha_r}\right) \right\}$$

where $\quad \hbar = 1, 2, 3, \cdots \cdot \quad$ and

$$(9.24) \quad \alpha_r = \left\{ \frac{\left[\Omega_c^2 + \left(1 - \Omega_p^2\right)^2\right]^{1/2} \left(1 + \Omega_c^2\right)^{1/2} - \Omega_c^2 - \left(1 - \Omega_p^2\right)}{2\left(1 + \Omega_c^2\right)} \right\}^{1/2}$$

$$(9.25) \quad \beta_r = \left\{ \frac{\left[\Omega_c^2 + \left(1 - \Omega_p^2\right)^2\right]^{1/2} \left(1 + \Omega_c^2\right)^{1/2} + \Omega_c^2 + \left(1 - \Omega_p^2\right)}{2\left(1 + \Omega_c^2\right)} \right\}^{1/2}$$

Equation (9.22) gives, indirectly, the necessary relationship between Ω_p and Ω_c , and Equation (9.23) gives the necessary relationship between $\hbar$ and λ_r for vanishing reflection. The multiple values of $\hbar$ indicate the multiplicity of thicknesses for which the vanishing condition can be obtained. In a three-dimensional space whose coordinates are Ω_p, Ω_c , and $\hbar/\lambda_r$ the conditions for zero reflection are curved lines, one line for each value of k. It is necessary to solve equations (9.22) and (9.23) numerically in order to see the behavior of these conditions in terms of the pertinent variables. Figures A9-1 and A9-2 show the solution. Note that the conditions given by both figures must be satisfied simultaneously for some given k value. It can be seen from these figures that the normalized plasma frequency (Ω_p) required for zero reflection is of the order of unity for small (less than unity) values of normalized electron collision frequency (Ω_c) and varies approximately as the square root of the normalized-electron collision frequency for large (greater than unity)
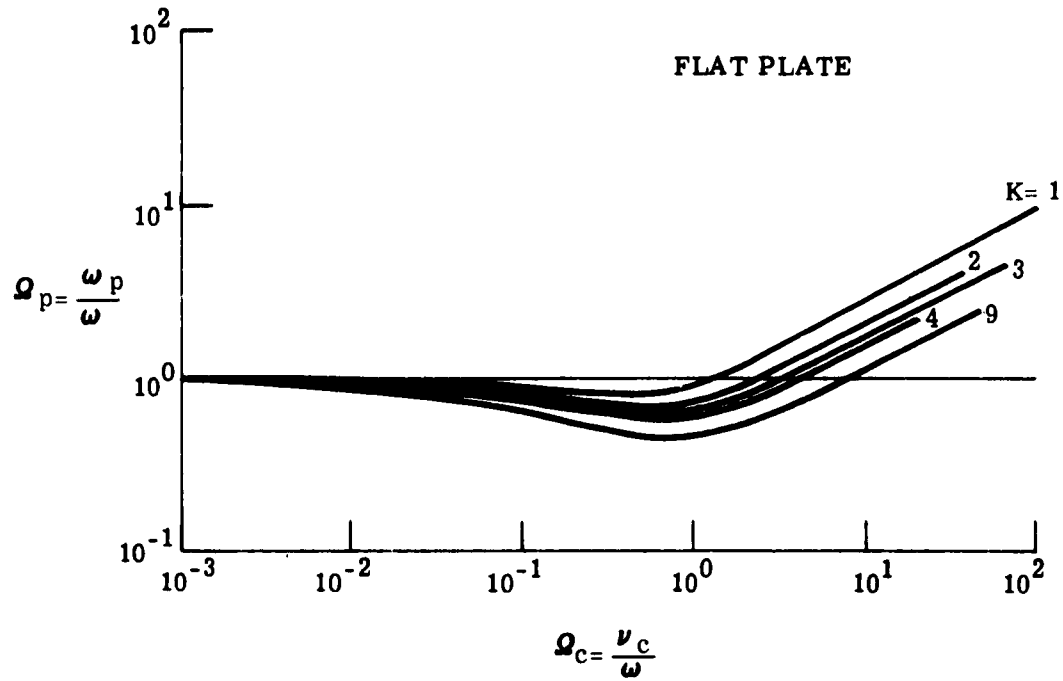
FLAT PLATE

$\Omega_{p=} \dfrac{\omega_p}{\omega}$

$\Omega_{c=} \dfrac{\nu_c}{\omega}$

Figure A9-1   Conditions for Zero Reflection (Ω_p vs Ω_c)

K= 10   FLAT PLATE

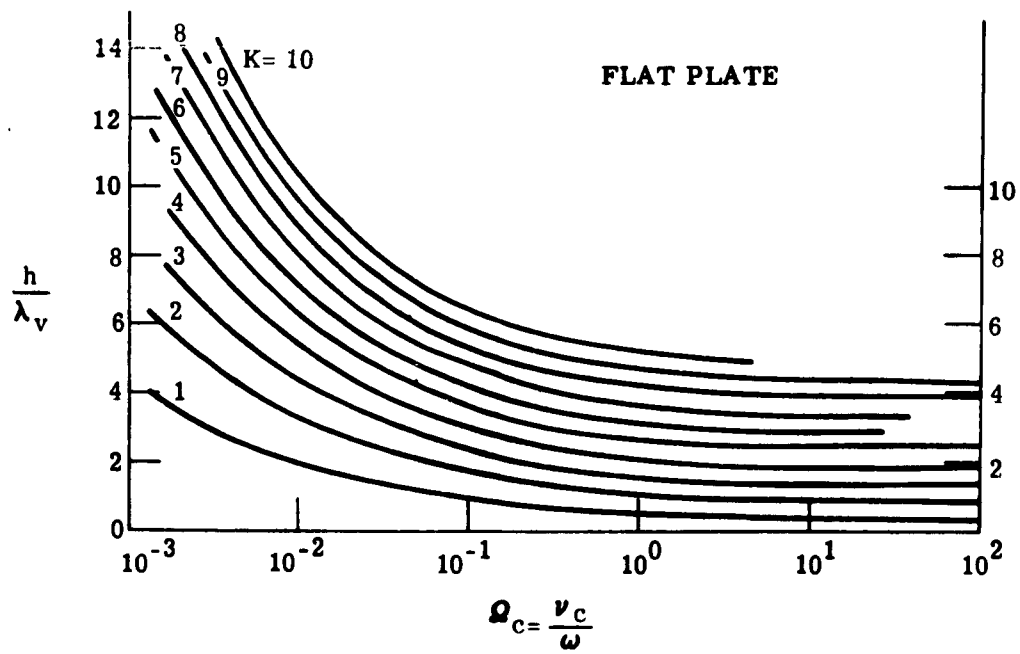$\dfrac{h}{\lambda_v}$

$\Omega_{c=} \dfrac{\nu_c}{\omega}$

Figure A9-2   Conditions for Zero Reflection ($\dfrac{h}{\lambda_v}$ vs Ω_c)

values of normalized electron collision frequency. It is important to note that the minimum plasma layer thickness ($\mathcal{A}$) for which zero reflection can occur is of the order of one-third of the free-space wavelength of the incident electromagnetic wave.

APPENDIX A-10

RAY PATHS IN NON-UNIFORM LOSSY DIELECTRIC MEDIA

The concepts of geometrical optics (ray theory) are often very useful in the general consideration of the propagation of electromagnetic waves, and sometimes can be applied to greatly simplify the method of analytical solution of electromagnetic wave propagation problems, when they are applicable. In general, the concepts of geometrical optics are applicable, and the results of solutions using these concepts are reasonably accurate, when

(1) the fractional change in the constitutive parameters of the media thru which propagation occurs is small over a distance of one wavelength in the direction of propagation (for continuously varying constitutive parameters) or if the total change in tne constitutive parameters takes place over a distance very much smaller than one wavelength (for an abrupt boundary between two regions), and

(2) the fractional change in the spacing between adjacent rays over a distance along the rays of one wavelength is small. This means that the geometrical optics solution is open to question if

(a) the rays pass thru a focus, or

(b) the rays are reflected or refracted at a surface with a size or radius of curvature that is not large compared to the wavelength.

A ray path can be considered to be the path followed by a narrow pencil beam of electromagnetic radiation as it propagates thru a medium. In uniform media ray paths are straight lines. In non-uniform media ray paths are curved toward the direction of decreasing velocity of propagation. The general vector differential equation that defines a ray path in a non-uniform isotropic lossless medium is [1]

$$(10.1) \quad \frac{d}{ds}\left(n \, \frac{d\mathbf{r}}{ds} \right) = \nabla n$$

where

S = distance along the ray path from some reference point on the ray path

$\mathbf{r}$ = position vector from some reference origin to the ray path

n = index of refraction of the medium

∇ = gradient operator.

In a non-uniform isotropic lossy medium the index of refraction as usually defined is complex. In this case the index of refraction is replaced by the electromagnetic wave relative phase factor β_r , which is

$$(10.2) \quad \beta_r = \frac{\lambda_v}{\lambda}$$

where

λ_v = wavelength of the electromagnetic wave in free-space

λ = wavelength of the electromagnetic wave in the medium

thus giving the ray path equation in a non-uniform isotropic lossy
medium as

(10.3)
$$\frac{d}{ds}\left(\beta_r \frac{d\mathbf{r}}{ds}\right) = \nabla\beta_r$$

In a lossy dielectric material with dielectric constant ϵ_r and con-
ductivity σ_d , the relative phase factor is

(10.4)
$$\beta_r = \frac{1}{\sqrt{2}}\left[\epsilon_r + \left(\epsilon_r^2 + \sigma_r^2\right)^{1/2}\right]^{1/2}$$

where

$\sigma_r = \dfrac{\sigma_d}{\epsilon_v \omega}$ = relative conductivity of the dielectric,

ϵ_v = capacitivity of free space, and

$\omega = 2\pi f$ = angular frequency of the electromagnetic wave.

It should be noted that the wavelength of an electromagnetic wave in a
lossy dielectric material depends on the conductivity as well as on the
dielectric constant of the dielectric material.

Two specific geometrical configurations of interest here are the
circular cylindrical and the spherical coordinate systems.

Consider first the circular cylindrical coordinate system, shown in
Figure A10-1. Assume that in this system β_r may be a function of
both ρ and z but not of ϕ . Now ray paths entering the
region traveling in a ϕ = constant plane will remain in that plane,
although they may bend toward or away from the z-axis as they
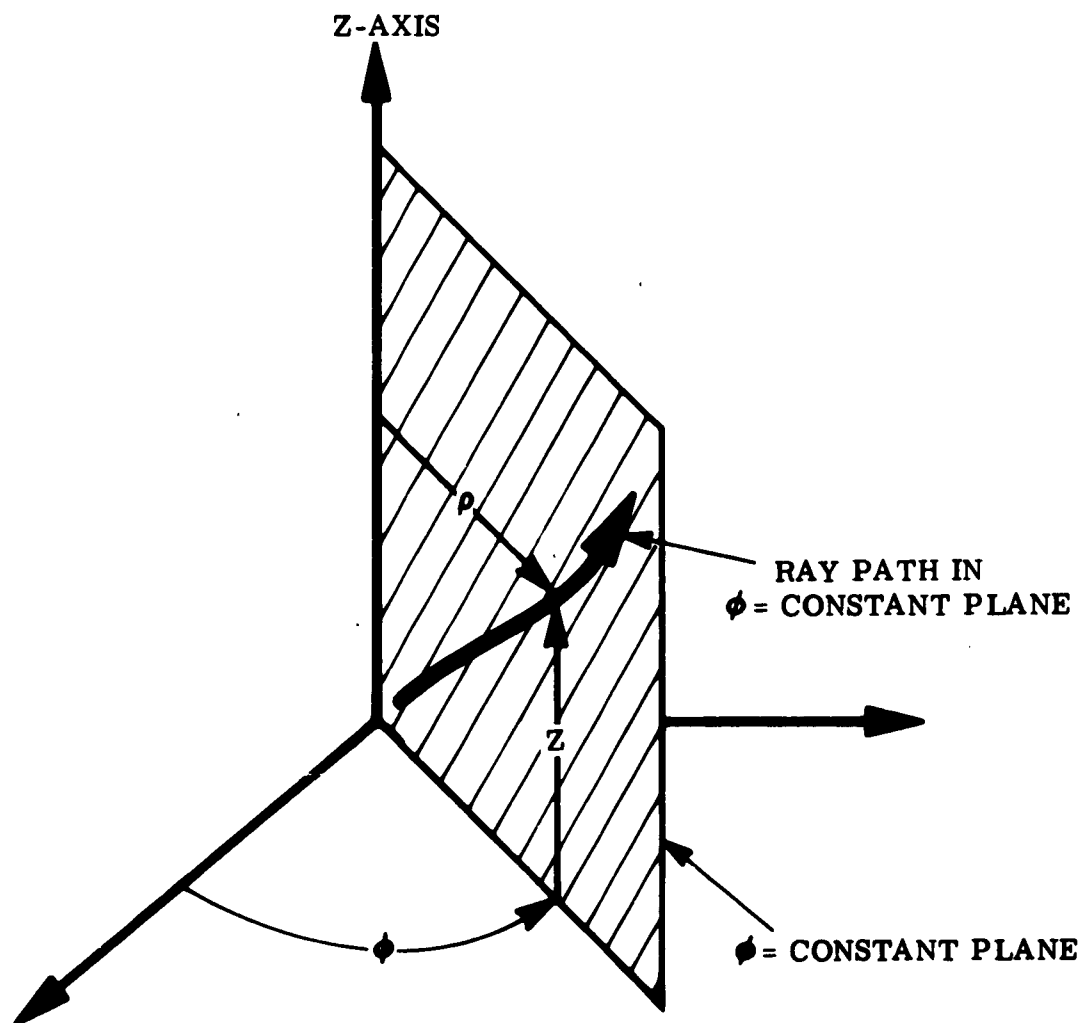progress in the z direction. In this case, the position vector from

Figure A10-1   Circular Cylindrical Coordinate System

the origin to a point on the ray path ($\mathbf{r}$) is

(10.5) $\qquad \mathbf{r} = \mathbf{1}_\rho \, \rho + \mathbf{1}_z \, z$

where $\mathbf{1}_\rho$ and $\mathbf{1}_z$ are unit vectors in the ρ and z directions, respectively. An incremental length along the ray path (ds) is given by

(10.6) $\qquad (ds)^2 = (d\rho)^2 + (dz)^2$

and the gradient of the relative phase factor ($\nabla \beta_r$) is given by

(10.7) $\qquad \nabla \beta_r = \mathbf{1}_\rho \, \dfrac{\partial \beta_r}{\partial \rho} + \mathbf{1}_z \, \dfrac{\partial \beta_r}{\partial z}$

In order to describe the ray path it is necessary to write equation (10.3) in a form such that it expresses the relationship between ρ and z along the ray path, independent of the arc length (s). The chain rule of differentiation shows that

(10.8) $\qquad \dfrac{d}{ds} \equiv \dfrac{d\rho}{ds} \, \dfrac{d}{d\rho}$

and equation (10.6) gives

(10.9) $\qquad \dfrac{d\rho}{ds} = \left[1 + \left(\dfrac{dz}{d\rho} \right)^2 \right]^{-\frac{1}{2}}$

Using equations (10.8) and (10.9) gives

(10.10) $\quad \dfrac{d\mathbf{r}}{ds} = \left[1 + \left(\dfrac{dz}{d\rho} \right)^2 \right]^{-\frac{1}{2}} \left(\mathbf{1}_\rho + \mathbf{1}_z \dfrac{dz}{d\rho} \right)$

Thus equation (10.3) becomes

(10.11) $\quad \left[1 + \left(\dfrac{dz}{d\rho} \right)^2 \right]^{-\frac{1}{2}} \dfrac{d}{d\rho} \left\{ \beta_r \left[1 + \left(\dfrac{dz}{d\rho} \right)^2 \right]^{-\frac{1}{2}} \left(\mathbf{1}_\rho + \mathbf{1}_z \dfrac{dz}{d\rho} \right) \right\}$

$$= \mathbf{1}_\rho \dfrac{\partial \beta_r}{\partial \rho} + \mathbf{1}_z \dfrac{\partial \beta_r}{\partial z}$$

Separating this vector equation into its two scalar equations gives

(10.12) $\quad \left[1 + \left(\dfrac{dz}{d\rho} \right)^2 \right]^{-\frac{1}{2}} \dfrac{d}{d\rho} \left\{ \beta_r \left[1 + \left(\dfrac{dz}{d\rho} \right)^2 \right]^{-\frac{1}{2}} \right\} = \dfrac{\partial \beta_r}{\partial \rho}$

and

(10.13) $\quad \left[1 + \left(\dfrac{dz}{d\rho} \right)^2 \right]^{-\frac{1}{2}} \dfrac{d}{d\rho} \left\{ \beta_r \left[1 + \left(\dfrac{dz}{d\rho} \right)^2 \right]^{-\frac{1}{2}} \dfrac{dz}{d\rho} \right\} = \dfrac{\partial \beta_r}{\partial z}$

Expanding the derivative in equation (10.13) and substituting equation (10.12) into it gives

(10.14) $\quad \dfrac{d^2 z}{d\rho^2} + \dfrac{dz}{d\rho} \dfrac{1}{\beta_r} \dfrac{\partial \beta_r}{\partial \rho} - \left(\dfrac{dz}{d\rho} \right)^2 \dfrac{1}{\beta_r} \dfrac{\partial \beta_r}{\partial z}$

$$+ \left(\dfrac{dz}{d\rho} \right)^3 \dfrac{1}{\beta_r} \dfrac{\partial \beta_r}{\partial \rho} = \dfrac{1}{\beta_r} \dfrac{\partial \beta_r}{\partial z}$$

In order to find the ray path it is necessary to solve equation (10.14) for z in terms of ρ .

Consider the special case where β_r is not a function of z . Then equation (10.14) simplifies to

$$(10.15) \qquad \frac{d^2 z}{d\rho^2} + \frac{dz}{d\rho} \frac{1}{\beta_r} \frac{d\beta_r}{d\rho} + \left(\frac{dz}{d\rho}\right)^3 \frac{1}{\beta_r} \frac{d\beta_r}{d\rho} = 0$$

This is a Bernoulli equation for $\dfrac{dz}{d\rho}$, which can be solved [2] to give

$$(10.16) \qquad \frac{dz}{d\rho} = \pm \left(K\beta_r^2 - 1\right)^{-\frac{1}{2}}$$

where K is a constant of integration and the algebraic sign determines the direction of propagation along the ray path. Equation (10.16) can be integrated to give

$$(10.17) \qquad z - z_0 = \pm \int_{\rho_0}^{\rho} \left(K\beta_r^2 - 1\right)^{-\frac{1}{2}} d\rho$$

where ρ_0 ; z_0 is some initial point on the ray path and β_r is a function of ρ . Note that the constant of integration (K) can be expressed as

$$(10.18) \qquad K = \frac{1}{\beta_{r_0}^2} \left[1 + \frac{1}{\left(\frac{dz}{d\rho}\right)_0^2} \right]$$

Thus, in order to define a particular ray path it is necessary to specify the location of one point on the ray path and the slope of the ray path at that point. Equation (10.18) can be put in the form

$$(10.19) \qquad K = \frac{1}{\beta_{r_o}^2} \left(1 + \tan^2 \psi_o \right)$$

where ψ_o is the angle between the z-axis and the tangent to the ray path at the initial point ρ_o ; z_o .

Consider the particular form of variation of β_r given by

$$(10.20) \qquad \beta_r^2 = \beta_{r_s}^2 \left(1 + \delta \rho^2 \right)$$

which is parabolic in β_r^2 . When δ is algebraically positive then β_r increases as ρ increases. In this case the ray paths are bent away from the z-axis (de-focused). When δ is algebraically negative then β_r decreases as ρ increases. In this case the ray paths are bent toward the z-axis (focused). Substitution of equation (10.20) into equation (10.17) and integration gives

$$(10.21) \quad z-z_o = \beta_{r_s}^{-1} \left(\delta K \right)^{-\frac{1}{2}} \operatorname{arc\,sinh} \left\{ \left[\frac{\delta}{1 - K^{-1} \beta_{r_s}^{-2}} \right] \right. \\ \left. \left[\rho \left(\frac{1 - K^{-1} \beta_{r_s}^{-2}}{\delta} + \rho^2 \right)^{\frac{1}{2}} - \rho_o \left(\frac{1 - K^{-1} \beta_{r_s}^{-2}}{\delta} + \rho^2 \right)^{\frac{1}{2}} \right] \right\}$$

when δ is algebraically positive, and

$$(10.22) \quad z-z_o = \beta_{r_s}^{-1} \left(-\delta K \right)^{-\frac{1}{2}} \operatorname{arc\,sin} \left\{ \left[\frac{-\delta}{1 - K^{-1} \beta_{r_s}^{-2}} \right] \right. \\ \left. \left[\rho \left(\frac{1 - K^{-1} \beta_{r_s}^{-2}}{-\delta} - \rho_o^2 \right)^{\frac{1}{2}} - \rho_o \left(\frac{1 - K^{-1} \beta_{r_s}^{-2}}{-\delta} - \rho^2 \right)^{\frac{1}{2}} \right] \right\}$$

when b is algebraically negative. The general behavior of these two different types of ray paths can be demonstrated by considering the special case where ρ_o is zero. Then equations (10.21) and (10.22) reduce to

$$(10.23) \qquad z - z_o = \beta_{r_s}^{-1} \left| b K \right|^{-\frac{1}{2}} \operatorname{arc\,sinh} \left\{ \rho \left(\frac{b}{1 - K^{-1} \beta_{r_s}^{-2}} \right)^{\frac{1}{2}} \right\}$$

and

$$(10.24) \qquad z - z_o = \beta_{r_s}^{-1} \left| -b K \right|^{-\frac{1}{2}} \operatorname{arc\,sin} \left\{ \rho \left(\frac{-b}{1 - K^{-1} \beta_{r_s}^{-2}} \right)^{\frac{1}{2}} \right\}$$

respectively. These can be rewritten in the form

$$(10.25) \qquad \rho = \left(\frac{1 - K^{-1} \beta_{r_s}^{-2}}{b} \right)^{\frac{1}{2}} \operatorname{sinh} \left[\beta_{r_s} \left| b K \right|^{\frac{1}{2}} \left| z - z_o \right| \right]$$

and

$$(10.26) \qquad \rho = \left(\frac{1 - K^{-1} \beta_{r_s}^{-2}}{-b} \right)^{\frac{1}{2}} \operatorname{sin} \left[\beta_{r_s} \left| -b K \right|^{\frac{1}{2}} \left| z - z_o \right| \right]$$

which show that as the ray travels in the z direction ρ increases monotonically (de-focusing) when b is algebraically positive and increases and decreases periodically (periodic focusing) when b is algebraically negative.

Now consider the spherical coordinate system, shown in Figure A10-2.
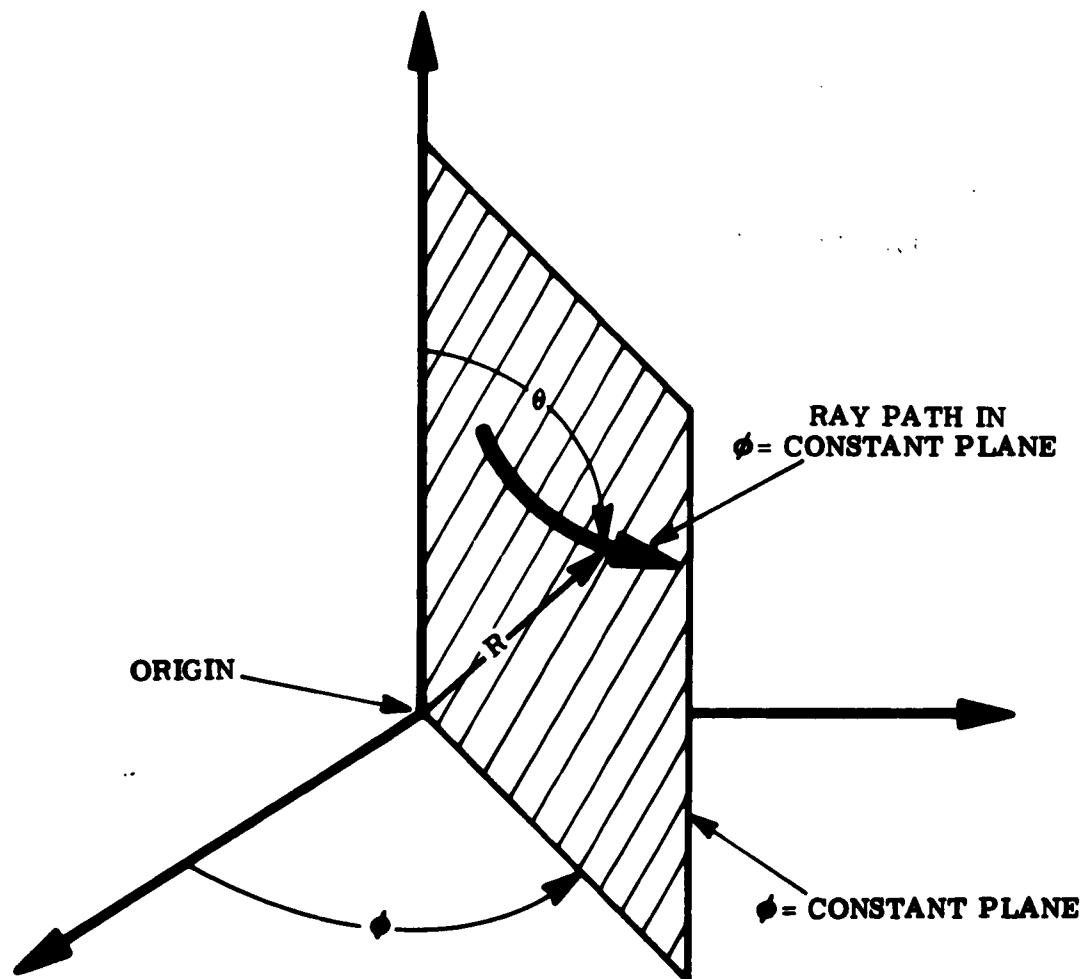
Figure A10-2   Spherical Coordinate System

Assume that in this system β_r may be a function of both R and θ but not of ϕ. Now ray paths entering the region traveling in a ϕ = constant plane will remain in that plane, although they may bend toward or away from the origin as they progress thru the region. In this case, the position vector from the origin to a point on the ray path ($\mathbf{r}$) is

$$(10.27) \qquad \mathbf{r} = 1_R \, R$$

where 1_R is a unit vector in the R direction. An incremental length along the ray path (ds) is given by

$$(10.28) \qquad ds^2 = (dR)^2 + R^2 (d\theta)^2$$

and the gradient of the relative phase factor ($\nabla\beta_r$) is given by

$$(10.29) \qquad \nabla\beta_r = 1_R \frac{\partial \beta_r}{\partial R} + 1_\theta \frac{1}{R} \frac{\partial \beta_r}{\partial \theta}$$

where 1_θ is a unit vector in the θ direction.

In order to describe the ray path it is necessary to write equation (10.3) in a form such that it expresses the relationship between R and θ along the ray path, independent of the arc length (s). The chain rule of differentiation shows that

$$(10.30) \qquad \frac{d}{ds} \equiv \frac{d\theta}{ds} \frac{d}{d\theta}$$

and equation (10.28) gives

$$(10.31) \qquad \frac{d\theta}{ds} = \left[R^2 + \left(\frac{dR}{d\theta}\right)^2 \right]^{-\frac{1}{2}}$$

Using equations (10.30) and (10.31) gives

$$(10.32) \quad \frac{d\bar{r}}{ds} = \left[R^2 + \left(\frac{dR}{d\theta} \right)^2 \right]^{-\frac{1}{2}} \left(1_R \frac{dR}{d\theta} + 1_\theta R \right)$$

Thus equation (10.3) becomes

$$(10.33) \quad \left[R^2 + \left| \frac{dR}{d\theta} \right|^2 \right]^{-\frac{1}{2}} \frac{d}{d\theta} \left\{ \beta_r \left[R^2 + \left| \frac{dR}{d\theta} \right|^2 \right]^{-\frac{1}{2}} \left(1_R \frac{dR}{d\theta} + 1_\theta R \right) \right\}$$
$$= 1_R \frac{\partial \beta_r}{\partial R} + 1_\theta \frac{1}{R} \frac{\partial \beta_r}{\partial \theta}$$

Separating this vector equation into its two scalar equations gives

$$(10.34) \quad \left[R^2 + \left(\frac{dR}{d\theta} \right)^2 \right]^{-\frac{1}{2}} \left[\!\left[\beta_r \left[R^2 + \left(\frac{dR}{d\theta} \right)^2 \right]^{-\frac{1}{2}} \left(\frac{d^2R}{d\theta^2} - R \right) \right.\right.$$
$$\left.\left. + \frac{dR}{d\theta} \frac{d}{d\theta} \left\{ \beta_r \left[R^2 + \left(\frac{dR}{d\theta} \right)^2 \right]^{-\frac{1}{2}} \right\} \right]\!\right] = \frac{\partial \beta_r}{\partial R}$$

and

$$(10.35) \quad \left[R^2 + \left(\frac{dR}{d\theta} \right)^2 \right]^{-\frac{1}{2}} \left[\!\left[\beta_r \left[R^2 + \left(\frac{dR}{d\theta} \right)^2 \right]^{-\frac{1}{2}} 2 \frac{dR}{d\theta} \right.\right.$$
$$\left.\left. + R \frac{d}{d\theta} \left\{ \beta_r \left[R^2 + \left(\frac{dR}{d\theta} \right)^2 \right]^{-\frac{1}{2}} \right\} \right]\!\right] = \frac{1}{R} \frac{\partial \beta_r}{\partial \theta}$$

Equations (10.34) and (10.35) can be combined to give

$$(10.36) \quad \frac{d^2R}{d\theta^2} + \frac{dR}{d\theta} \frac{1}{\beta_r} \frac{\partial \beta_r}{\partial \theta} - \left(\frac{dR}{d\theta} \right)^2 \left(\frac{2}{R} + \frac{1}{\beta_r} \frac{\partial \beta_r}{\partial R} \right)$$
$$+ \left(\frac{dR}{d\theta} \right)^3 \frac{1}{R^2} \frac{1}{\beta_r} \frac{\partial \beta_r}{\partial \theta} = R + R^2 \frac{1}{\beta_r} \frac{\partial \beta_r}{\partial R}$$

In order to find the ray path it is necessary to solve equation (10.36) for R in terms of θ .

Consider the special case where the region of interest is confined to the spherical shell between two closely spaced concentric spherical boundaries of radius R_1 and R_2 (where $R_2 > R_1$, and $R_2 - R_1 \ll R_1$) and where within this region β_r is not a function of R . Equation (10.36) reduces to

$$(10.37) \quad \frac{d^2 R}{d\theta^2} + \frac{dR}{d\theta} \frac{1}{\beta_r} \frac{d\beta_r}{d\theta} - \left(\frac{dR}{d\theta}\right)^2 \frac{2}{R}$$

$$+ \left(\frac{dR}{d\theta}\right)^3 \frac{1}{R^2} \frac{1}{\beta_r} \frac{d\beta_r}{d\theta} - R = 0$$

Transforming to new variables ρ and z , defined by

$$(10.38) \quad \rho = R_2 \theta$$

and

$$(10.39) \quad z = R_2 - R$$

changes equation (10.37) to the form

$$(10.40) \quad \frac{d^2 z}{d\rho^2} + \frac{dz}{d\rho} \frac{1}{\beta_r} \frac{d\beta_r}{d\rho} + \left(\frac{dz}{d\rho}\right)^2 \frac{2}{R_2 - z}$$

$$+ \left(\frac{dz}{d\rho}\right)^3 \frac{1}{\beta_r} \frac{d\beta_r}{d\rho} \frac{R_2^2}{(R_2 - z)^2} + \frac{(R_2 - z)}{R_2^2} = 0$$

and when R_z is very large and z remains small this reduces to

$$(10.41) \quad \frac{d^2z}{d\rho^2} + \frac{dz}{d\rho} \frac{1}{\beta_r} \cdot \frac{d\beta_r}{d\rho} + \left(\frac{dz}{d\rho}\right)^3 \frac{1}{\beta_r} \frac{d\beta_r}{d\rho} = 0$$

which is the same as equation (10.15) derived for the circular cylindrical geometry.

Thus, the solutions to equation (10.15) also apply approximately to equation (10.37) when the ray paths do not approach the origin closely.

(1) M. Born and E. Wolf, Principles of Optics, Pergamon, 1959, pp. 120−123.

(2) A.L. Nelson, K.W. Folley, and M. Coral, Differential Equations, Heath, 1952, pp. 44−45.

APPENDIX A-11

RAY PATH GEOMETRY FOR BACK-SCATTERING BY A NON-UNIFORM LOSSY DIELECTRIC- COATED METALLIC SPHERE

It is assumed that the scattering object consists of a perfectly reflective (metallic) sphere coated with a layer of lossy dielectric material. The thickness of the dielectric coating is assumed to be constant all around the sphere. The electromagnetic properties of the dielectric material are assumed to vary only in the angular direction away from an axis of symmetry and not angularly around the axis of symmetry nor radially from the center of the sphere. The ray path geometry of a plane electro- magnetic wave incident on these concentric spherical boundaries along the axis of symmetry, and the resultant scattered wave ray path geo- metry, necessary for the determination of the scattering cross section, can be completely defined by the ray paths in the plane of incidence (as defined in Appendix 4). A normal view of the plane of incidence, showing the equatorial section of the spherical boundaries and containing the axis of symmetry, is shown in Figure A11-1. The angles of refraction and the curvature of the ray paths in the dielectric material are indica- tive of a dielectric having a relative phase factor with a value less than unity at the axis of symmetry at the front of the sphere and increasing toward unity in the angular direction away from this location. Three characteristic ray path configurations are apparent, but only the con- tributions to the scattered wave due to "single-transit" paths through the dielectric are detailed. It should be noted that contributions to the scattered wave also come from rays that have been carried around the back of the sphere in the dielectric coating. The geometrical details of
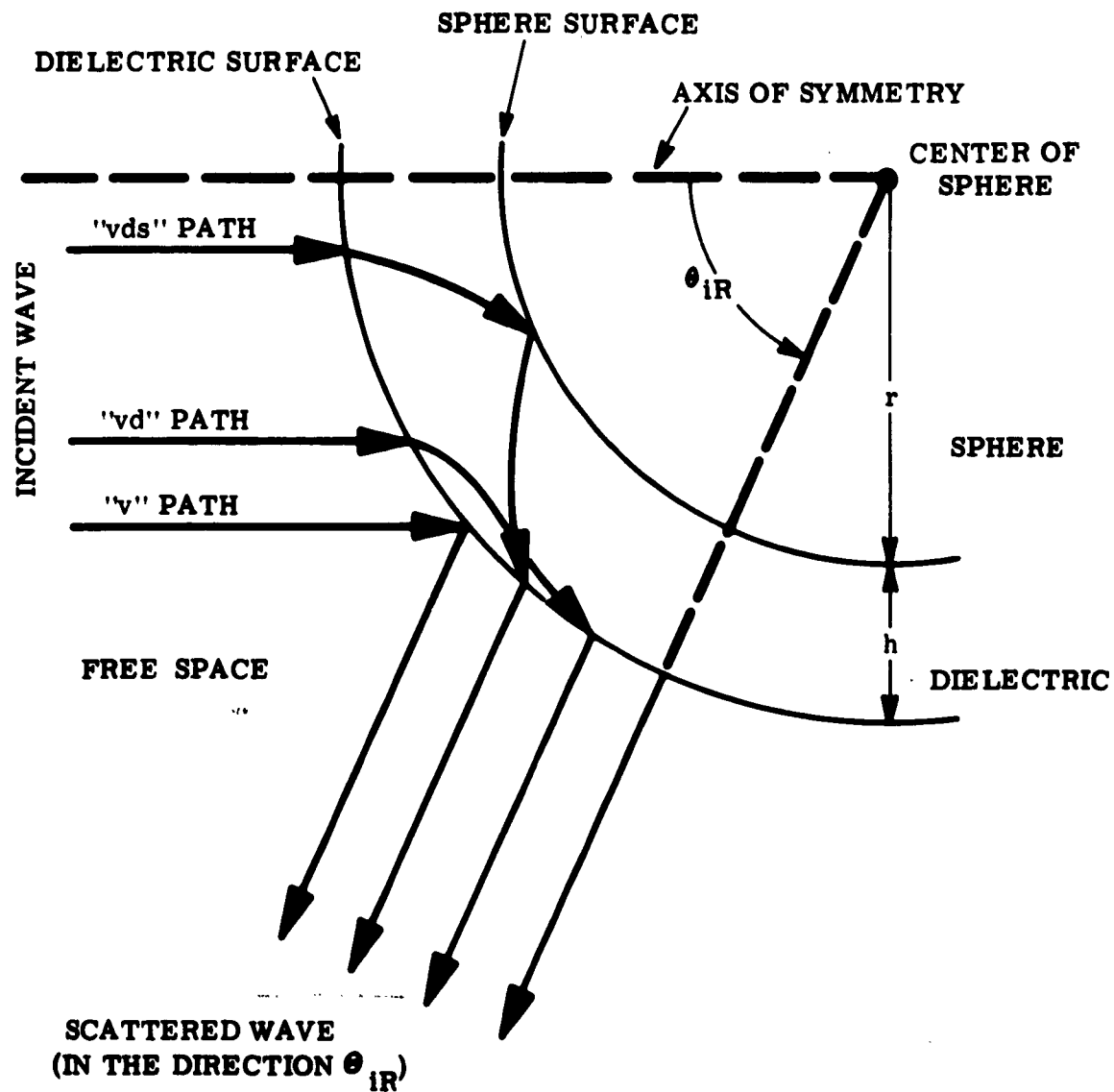
Figure A11-1   Ray Path Geometry in the Plane of Incidence

each of the three characteristic ray paths must be known in order to determine the relationship between the incident wave and the scattered wave.

The " $\vee$ " ray path in this case is identical to the " $\vee$ " ray path for the case of a uniform dielectric, the details of which are given in Appendix 5.

The " $\vee d$ " ray path, which must encircle the sphere at least once in order to contribute to back-scattering, may be neglected for thin coatings (see Appendix 5).

Consider the " $\vee d s$ " ray path, in which the ray is transmitted through the outer dielectric surface, passes through the dielectric coating until it meets the sphere surface, is reflected from the sphere surface, again passes through the dielectric coating until it meets the outer dielectric surface, and is transmitted through the outer dielectric surface to the receiver location. In general, such a ray path may traverse the dielectric coating 2 m times before emerging. This path is detailed in Figure A11-2. It is obvious from this figure for the "far-field" condition ($R_R \rightarrow \infty$) that

$$(11.1) \quad \theta_{iR} = \theta_{iv} + \theta_{tv} + \theta_1 + \theta_2$$

analogous to the situation for a uniform dielectric coating (see Appendix 5). It is necessary to express θ_{tv}, θ_1 and θ_2 in terms of θ_{iv} in order to define the ray path geometry.
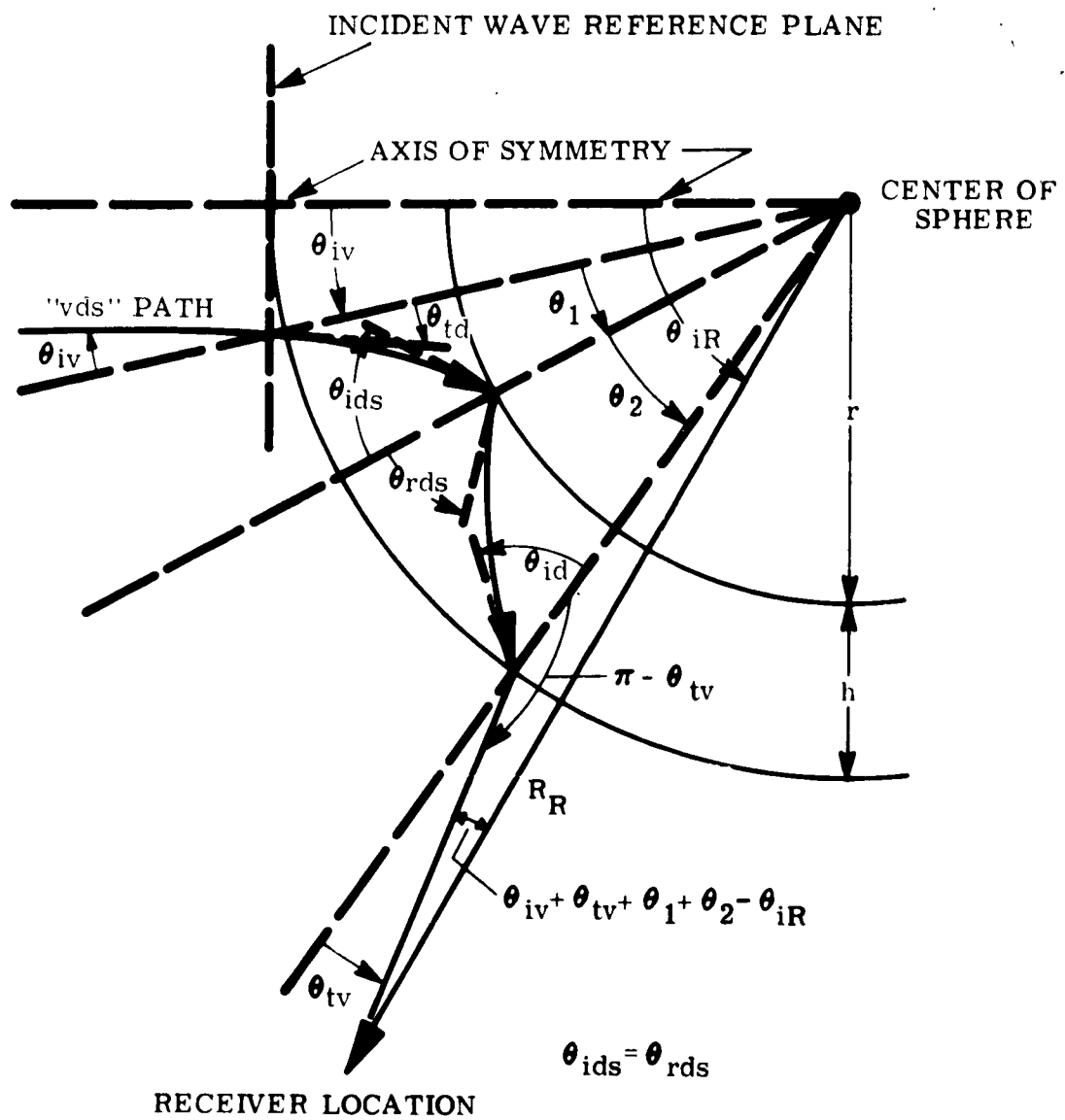
Figure A11-2   Characteristic Ray Path "vds"

Appendix A-4 gives

(11.2)
$$\sin \theta_{td} = \frac{\sqrt{2} \, \sin \theta_{iv}}{\left\{ \epsilon_r + \sin^2 \theta_{iv} + \left[\sigma_r^2 + \left(\epsilon_r - \sin^2 \theta_{iv} \right)^2 \right]^{1/2} \right\}^{1/2}}$$

and

(11.3)
$$\sin \theta_{tv} = \frac{1}{\sqrt{2}} \sin \theta_{id} \left[\epsilon_r + \left(\epsilon_r^2 + \frac{\sigma_r^2}{\cos^2 \theta_{id}} \right)^{1/2} \right]^{1/2}$$

where ϵ_r is the dielectric constant and σ_r is the relative conductivity of the dielectric material.

It is shown in Appendix A-10 that when the sphere radius r is large compared to the coating thickness $\hbar$ this spherical geometry can be approximated by a circular cylindrical geometry for small angles away from the axis of symmetry, as shown in Figure A11-3. In this coordinate system the axis of symmetry remains the same and the plasma properties vary only in the ρ direction and do not vary in the z direction nor angularly around the axis of symmetry.

The equations of transformation between these two coordinate systems (see Appendix A-10) are

(11.4)
$$\rho = \left(r + \hbar \right) \theta$$
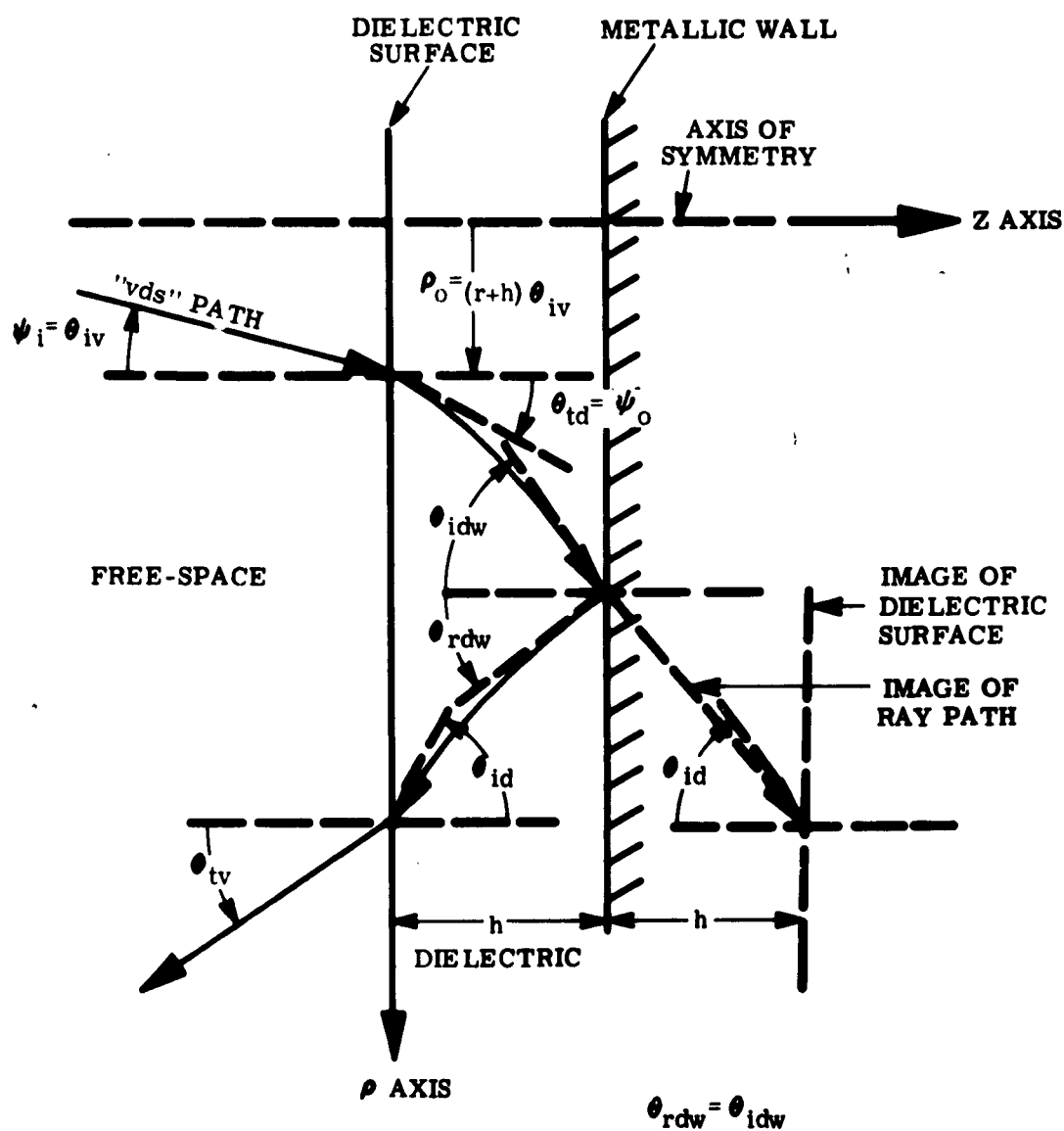
Figure A11-3   Approximation for Characteristic Ray Path "vds"

$$(11.5) \qquad z = \left(r + \hbar \right) - R$$

where R is the distance from the origin of the spherical coordinate system to a point on the ray path. Defining the angle ψ to be the angle between the positive z-axis (axis of symmetry) and the tangent to the ray path at any point (measured in the circular cylindrical system) gives

$$(11.6) \qquad \tan \psi = \frac{d\rho}{dz}$$

Using equations (11.4) and (11.5) in equation (11.6) gives

$$(11.7) \qquad \tan \psi = -\left(r + \hbar \right) \frac{d\theta}{dR}$$

Defining the angle χ to be the angle between the axis of symmetry and the tangent to the ray path at any point (measured around the origin in the spherical system) gives

$$(11.8) \qquad \tan \left(\chi - \theta \right) = R \frac{d\theta}{dR}$$

Equations (11.7) and (11.8) give

$$(11.9) \qquad \tan \psi = -\frac{\left(r + \hbar \right)}{R} \tan \left(\chi - \theta \right)$$

It can be seen from equations (11.4), (11.5), and (11.9) that a ray path in the spherical system meeting the outer spherical dielectric surface ($R = r + \hbar$) at $\theta = \theta_{i\nu}$ and parallel to the axis of symmetry (an incident wave ray path) is transformed into a ray path in the circular cylindrical system meeting the outer plane dielectric surface (z = 0) at $\rho = \rho_o$ and at an angle ψ_i to the axis of symmetry (Z- axis) where

$$(11.10) \qquad \rho_o = \left(r + \hbar \right) \theta_{i\nu}$$

$$(11.11) \qquad \psi_i = \theta_{i\nu}$$

This is shown in Figure A11-3. It can also be seen that a ray path in the circular cylindrical system leaving the outer plane dielectric surface (z = 0) at $\rho = \rho_m$ and at an angle $\psi_m = \pi - \theta_{t\nu m}$ to the axis of symmetry (z - axis) is transformed into a ray path in the spherical system leaving the outer spherical dielectric surface ($R = r + \hbar$) at $\theta = \theta_m$ and at an angle χ_m to the axis of symmetry (a scattered wave ray path) where

$$(11.12) \qquad \theta_m = \frac{\rho_m}{r + \hbar}$$

$$(11.13) \qquad \chi_m = \frac{\rho_m}{r + \hbar} + \theta_{t\nu m}$$

From equations (11.1), (11.2), and (11.13) it can be seen that χ_m is actually $\theta_{i R \nu d s m}$. Using equations (11.3) and (11.13) gives

(11.14)

$$\theta_{iRvdsm} = \frac{\rho_m}{r + h}$$

$$+ \text{ arc sin } \left\{ \frac{\sin \theta_{idm}}{\sqrt{2}} \left[\epsilon_r + \left(\epsilon_r^2 + \frac{\sigma_r^2}{\cos^2 \theta_{idm}} \right)^{1/2} \right]^{1/2} \right\}$$

Thus it is only necessary to find ρ_m and θ_{idm} in terms of θ_{iv} in order to define the scattered wave ray paths.

The actual ray path geometry in the dielectric layer involves m reflections from the metallic wall and m-1 reflections from the inner surface of the outer dielectric boundary before the ray path emerges from the dielectric layer at ρ_m . Because there is no variation of the electromagnetic characteristics of the dielectric material in the z direction (parallel to the axis of symmetry) the part of the ray path from the metallic wall back to the outer dielectric boundary can effectively be replaced by its image in the metallic wall in order to find ρ_1 and θ_{id1} , as shown in Figure A11-3. This technique can be repeated for all successive round trips through the dielectric layer. Thus, only a single effective ray path proceeding in the positive z direction need be considered. This ray path starts at the dielectric surface ($\rho = \rho_0$; $z = 0$) at some initial angle to the axis of symmetry ($\psi_0 = \theta_{td}$). The values of ρ_m and θ_{idm} for the actual path are the same as the values of ρ and ψ along the single effective ray path at the position defined by z = 2 m h.

The electromagnetic characteristics of the dielectric material
(dielectric constant, relative conductivity, and relative phase factor)
vary symmetrically with respect to θ and consequently each can
be expressed in the form of a Maclaurin's series expansion of the
form

$$(11.15) \quad y = y_0 + y_2 \, \theta^2 + y_4 \, \theta^4 + \cdots$$

which can also be written in the form

$$(11.16) \quad y = y_0 + \frac{y_2}{(r+R)^2} \rho^2 + \frac{y_4}{(r+R)^4} \rho^4 + \cdots$$

where only the first two terms of the series need be considered for
regions near the axis of symmetry. In Appendix 10 the quadratic
form of variation of the relative phase factor was analyzed and the
ray paths determined for the circular cylindrical system. Such a
ray path, with the initial conditions $\rho = \rho_0$; $z_0 = 0$ and
$\psi_0 = \theta_{td}$, is the effective ray path necessary to determine θ_{idm}
and ρ_m from which θ_{iRrdsm} may be found by equation
(11.14). Representing the functional form of the variation of the
relative phase factor β_r near the axis of symmetry by the
expression

$$(11.17) \quad \beta_r^2 = \beta_{rs}^2 \left[1 + \frac{2 R_\beta}{(r+R)^2} \rho^2 \right] = \beta_{rs}^2 \left(1 + b \rho^2 \right)$$

The equation of the effective ray path, from Appendix 10, is

(11.18)
$$\left[\frac{1-K^{-1}\beta r_s^{-2}}{b}\right] \sinh\left[\beta_{r_s}\left(bK\right)^{1/2} z\right] = \rho\left(\frac{1-K^{-1}\beta r_s^{-2}}{b}+\rho_0^2\right)^{1/2} - \rho_0\left(\frac{1-K^{-1}\beta r_s^{-2}}{b}+\rho^2\right)^{1/2}$$

when b is algebraically positive, and

(11.19)
$$\left[\frac{1-K^{-1}\beta r_s^{-2}}{-b}\right] \sin\left[\beta_{r_s}\left(-bK\right)^{1/2} z\right] = \rho\left(\frac{1-K^{-1}\beta r_s^{-2}}{-b}-\rho_0^2\right)^{1/2} - \rho_0\left(\frac{1-K^{-1}\beta r_s^{-2}}{-b}-\rho^2\right)^{1/2}$$

when b is algebraically negative, and

where

(11.20)
$$K = \frac{1+\tan^2\theta_{td}}{\beta r_s^2\left(1+b\rho_0^2\right)}$$

Note that θ_{td} can be expressed in terms of θ_{iv} by means of equation (11.2). Solving equations (11.18) and (11.19) for ρ in terms of z gives

(11.21)
$$\rho = \left(\frac{1-K^{-1}\beta r_s^{-2}}{b}+\rho_0^2\right)^{1/2} \sinh\left[\beta_{r_s}\left(bK\right)^{1/2} z\right]$$
$$+ \rho_0 \cosh\left[\beta_{r_s}\left(bK\right)^{1/2} z\right]$$

when b is algebraically positive, and

$$(11.22) \quad \rho = \left(\frac{1 - K^{-1} \beta_{r_s}^{-2}}{-b} - \rho_o^2 \right)^{1/2} \sin \left[\beta_{r_s} (-bK)^{1/2} z \right]$$

$$+ \rho_o \cos \left[\beta_{r_s} (-bK)^{1/2} z \right]$$

when b is algebraically negative. Thus, from equations (11.21) and (11.22), ρ_m is given by

$$(11.23) \quad \rho_m = \left(\frac{1 - K^{-1} \beta_{r_s}^{-2}}{b} + \rho_o^2 \right)^{1/2} \sinh \left[\beta_{r_s} (bK)^{1/2} 2mh \right]$$

$$+ \rho_o \cosh \left[\beta_{r_s} (bK)^{1/2} 2mh \right]$$

when b is algebraically positive, and

$$(11.24) \quad \rho_m = \left(\frac{1 - K^{-1} \beta_{r_s}^{-2}}{-b} - \rho_o^2 \right)^{1/2} \sin \left[\beta_{r_s} (-bK)^{1/2} 2mh \right]$$

$$+ \rho_o \cos \left[\beta_{r_s} (-bK)^{1/2} 2mh \right]$$

when b is algebraically negative.

From equations (11.21) and (11.22) it can be seen that

$$\frac{d\rho}{dz} = \beta_{r_s} \, (bK)^{1/2} \rho_o \, \sinh \left[\beta_{r_s} \, (bK)^{1/2} \, z \right]$$

(11.25)

$$+ \beta_{r_s} \, (bK)^{1/2} \left(\frac{1 - K^{-1} \beta r_s^{-2}}{b} + \rho_o^2 \right)^{1/2} \cosh \left[\beta_{r_s} \, (bK)^{1/2} \, z \right]$$

when b is algebraically positive, and

$$\frac{d\rho}{dz} = -\beta_{r_s} \, (-bK)^{1/2} \rho_o \, \sin \left[\beta_{r_s} \, (-bK)^{1/2} \, z \right]$$

(11.26)

$$+ \beta_{r_s} \, (-bK)^{1/2} \left(\frac{1 - K^{-1} \beta r_s^{-2}}{-b} - \rho_o^2 \right)^{1/2} \cos \left[\beta_{r_s} \, (-bK)^{1/2} \, z \right]$$

when b is algebraically negative. Thus, from equations (11.6), (11.25), (11.26), and the previously stated fact that θ_{idm} is equal to ψ_m , $\tan \theta_{idm}$ is given by

(11.27)

$$\tan \theta_{idm} = \beta_{r_s} (bK)^{1/2} \rho_o \sinh \left[\beta_{r_s} (bK)^{1/2} 2mh \right]$$

$$+ \beta_{r_s} (bK)^{1/2} \left(\frac{1 - K^{-1} \beta_{r_s}^{-2}}{b} + \rho_o^2 \right)^{1/2} \cosh \left[\beta_{r_s} (bK)^{1/2} 2mh \right]$$

when b is algebraically positive, and

(11.28)

$$\tan \theta_{idm} = -\beta_{r_s} (-bK)^{1/2} \rho_o \sin \left[\beta_{r_s} (-bK)^{1/2} 2mh \right]$$

$$+ \beta_{r_s} (-bK)^{1/2} \left(\frac{1 - K^{-1} \beta_{r_s}^{-2}}{-b} - \rho_o^2 \right)^{1/2} \cos \left[\beta_{r_s} (-bK)^{1/2} 2mh \right]$$

when b is algebraically negative. Thus, equations (11.14), (11.23), (11.24), (11.27), and (11.28) give θ_{iRvdsm} as

$$(11.29) \quad \theta_{iRvdsm} = \frac{\rho_0}{(r+h)} \cosh\left[\beta_{rs}(\ell K)^{1/2} 2mh\right]$$

$$+ \left(\frac{1-K^{-1}\beta_{rs}^{-2}}{\ell(r+h)^2} + \frac{\rho_0^2}{(r+h)^2}\right)^{1/2} \sinh\left[\beta_{rs}(\ell K)^{1/2} 2mh\right]$$

$$+ \arcsin\left\{\frac{1}{\sqrt{2}}\left\{\sin\arctan\left[\left[\beta_{rs}(\ell K)^{1/2}\rho_0\right.\right.\right.\right.$$

$$\sinh\left[\beta_{rs}(\ell K)^{1/2} 2mh\right]$$

$$+ \beta_{rs}(\ell K)^{1/2}\left(\frac{1-K^{-1}\beta_{rs}^{-2}}{\ell}+\rho_0^2\right)^{1/2}\cosh\left[\beta_{rs}(\ell K)^{1/2} 2mh\right]\Bigg]\Bigg]\Bigg\}$$

$$\left\{\epsilon_r + \left(\epsilon_r^2 + \sigma_r^2 \cos^{-2}\arctan\left[\left[\beta_{rs}(\ell K)^{1/2}\rho_0\right.\right.\right.\right.$$

$$\sinh\left[\beta_{rs}(\ell K)^{1/2} 2mh\right]$$

$$+ \beta_{rs}(\ell K)^{1/2}\left(\frac{1-K^{-1}\beta_{rs}^{-2}}{\ell}+\rho_0^2\right)^{1/2}\cosh\left[\beta_{rs}(\ell K)^{1/2} 2mh\right]\Bigg]\Bigg]\right)^{1/2}\Bigg\}^{1/2}\Bigg\}$$

when ℓ is algebraically positive, and

$$(11.30) \quad \theta_{iRvdsm} = \frac{\rho_0}{(r+h)} \cos\left[\beta_{rs}(-bK)^{1/2} 2mh\right]$$

$$+ \left(\frac{1-K^{-1}\beta_{rs}^{-2}}{-b(r+h)^2} - \frac{\rho_0^2}{(r+h)^2}\right)^{1/2} \sin\left[\beta_{rs}(-bK)^{1/2} 2mh\right]$$

$$+ \arcsin\left\{\frac{1}{\sqrt{2}}\left\{\sin\arctan\left[\left[-\beta_{rs}(-bK)^{1/2}\rho_0\right.\right.\right.\right.$$

$$\sin\left[\beta_{rs}(-bK)^{1/2} 2mh\right]$$

$$+ \beta_{rs}(-bK)^{1/2}\left(\frac{1-K^{-1}\beta_{rs}^{-2}}{-b} - \rho_0^2\right)^{1/2}\cos\left[\beta_{rs}(-bK)^{1/2} 2mh\right]\right]\right\}$$

$$\left\{\epsilon_r + \left(\epsilon_r^2 + \sigma_r^2 \cos^{-2}\arctan\left[\left[-\beta_{rs}(-bK)^{1/2}\rho_0\right.\right.\right.\right.$$

$$\sin\left[\beta_{rs}(-bK)^{1/2} 2mh\right]$$

$$+ \beta_{rs}(-bK)^{1/2}\left(\frac{1-K^{-1}\beta_{rs}^{-2}}{-b} - \rho_0^2\right)^{1/2}\cos\left[\beta_{rs}(-bK)^{1/2} 2mh\right]\right]\right)^{1/2}\right\}^{1/2}\right\}$$

when b is algebraically negative.

Thus, for ray paths near the axis of symmetry, and an incident wave propagating in a direction parallel to the axis of symmetry, the ray path geometry is defined for an axially-symmetric non-uniform lossy dielectric coating on a metallic sphere when $\rho_o/(r+R)$ is replaced by θ_{ir} and k is replaced by $2k_\rho/(r+R)^2$ in the preceding equations.

APPENDIX A-12

DIVERGENCE FACTOR FOR BACK-SCATTERING BY A NON-UNIFORM LOSSY DIELECTRIC-COATED METALLIC SPHERE

It is assumed that the scattering object consists of a perfectly reflective (metallic) sphere coated with a layer of lossy dielectric material. The thickness of the dielectric coating is assumed to be constant all around the sphere. The electromagnetic properties of the dielectric material are assumed to vary only in the angular direction away from an axis of symmetry and not angularly around the axis of symmetry nor radially from the center of the sphere.

The geometrical divergence factor for a plane electromagnetic wave propagating in a direction parallel to the axis of symmetry and incident on the non-uniform lossy dielectric-coated metallic sphere, necessary for the determination of the scattering cross section, is determined by the ray path geometry (as derived in Appendix A-11). The general form of the geometrical divergence factor for back-scattering from concentric spherical regions, from Appendix A-6, is

$$(12.1) \quad D_{iR} = \frac{2R_R^2}{(r+\ell)^2} \lim_{\Delta\theta_{iv} \to 0} \frac{1 - \cos\Delta\theta_{iR}}{\sin^2\Delta\theta_{iv}}$$

where it is necessary to express θ_{iR} explicitly in terms of θ_{iv} before the limit can be taken. Equation (12.1) can also be written in the form

$$(12.2) \qquad D_{iR} = \frac{4 R_R^2}{(r+\ell)^2} \lim_{\Delta \theta_{iv} \to 0} \frac{\sin^2 \frac{\Delta \theta_{iR}}{2}}{\sin^2 \Delta \theta_{iv}}$$

The two different functional relationships between θ_{iR} and θ_{iv} are given in Appendix A-11 for the two different characteristics ray paths that contribute to the back-scattering cross section, thus leading to different divergence factors for the two different characteristic ray paths.

The back-scattering geometrical divergence factor for the " $\vee$ " ray path in this case is the same as for the " $\vee$ " ray path in the case of a uniform dielectric, and is given in Appendix A-6.

The back-scattering geometrical divergence factor for the " vds " ray path is given by two different equations for the two different forms of variation of the dielectric properties near the axis of symmetry (see Appendix A-11). Substituting the formulas for θ_{iRvdsm} from Appendix A-11 into equation (12.2) and taking the limit gives

$$(12.3) \qquad D_{iRvdsm} = \frac{4 R_R^2}{(r+\ell)^2} \left\{ \coth \left[k_\beta^{\frac{1}{2}} \frac{2\sqrt{2} \, m\ell}{(r+\ell)} \right] \right.$$

$$+ \frac{1}{2\sqrt{2}} \, \beta_{r_s}^{-1} \, k_\beta^{-\frac{1}{2}} \left[1 + 2\beta_{r_s}^2 \, k_\beta \right]$$

$$\left. \sinh \left[k_\beta^{\frac{1}{2}} \frac{2\sqrt{2} \, m\ell}{(r+\ell)} \right] \right\}^2$$

when k_β is algebraically positive, and

$$(12.4) \quad D_{iRvdsm} = \frac{4R_R^2}{(r+k)^2} \left\{ \cos\left[-k_\beta^{1/2} \frac{2\sqrt{2}\, mk}{(r+k)}\right] \right.$$

$$+ \frac{1}{2\sqrt{2}} \beta_{rs}^{-1} (-k_\beta)^{-1/2} \left[1+2\beta_{rs}^2 k_\beta\right]$$

$$\left. \sin\left[(-k_\beta)^{1/2} \frac{2\sqrt{2}\, mk}{(r+k)}\right]\right\}^2$$

when k_β is algebraically negative.

APPENDIX A-13

GEOMETRICAL OPTICS ELECTROMAGNETIC WAVE
BACK-SCATTERING CROSS SECTION OF A NON-UNIFORM
LOSSY DIELECTRIC-COATED METALLIC SPHERE

Detailed here is the theoretical determination of the electromagnetic
wave back-scattering cross section (radar cross section) of a per-
fectly reflective (metallic) sphere coated with a non-uniform layer
of lossy dielectric material via the geometrical optics approach using
the ray path field intensity addition technique (see Appendix A-3). The
thickness of the dielectric coating is assumed to be constant all
around the sphere. The electromagnetic properties of the dielectric
material are assumed to vary only in the angular direction away
from an axis of symmetry and not angularly around the axis of
symmetry nor radially from the center of the sphere. The incident
electromagnetic wave is taken to be propagating in a direction parallel ·
to the axis of symmetry.

The only difference between the present situation with a non-uniform
dielectric and the situation with a uniform dielectric is the ray path
geometry, and consequently the geometrical divergence factors for
the various ray paths involved are different. The results for the
uniform dielectric situation given in Appendix A-7 can be used for the
non-uniform dielectric situation simply by substitution of the
appropriate divergence factors into the equations. Thus, using the
results from Appendixes A-7 and A-12, the normalized radar cross
section is given by

(13.1)
$$\frac{\sigma}{\pi r^2} = \left(1 + \frac{h}{r}\right)^2 \left| \rho_{vd} - \frac{(1 - \rho_{vd}^2)}{\rho_{vd}} \right.$$

$$\left. \sum_{m=1}^{\infty} D_m \left[\rho_{vd} \, e^{-j\beta_d 2h} \, e^{-\alpha_d 2h} \right]^m \right|^2$$

where

$$D_m = \left| \cosh\left[k_\beta^{1/2} \, \frac{2\sqrt{2} \, mh}{(r+h)} \right] \right.$$

(13.2)

$$+ \frac{1}{2\sqrt{2}} \, \beta_{r_s}^{-1} \, k_\beta^{-1/2} \left[1 + 2\beta_{r_s}^2 \, k_\beta \right]$$

$$\left. \sinh\left[k_\beta^{1/2} \, \frac{2\sqrt{2} \, m \, h}{r+h} \right] \right|^{-1}$$

when k_β is algebraically positive, and

(13.3)
$$D_m = \left| \cos\left[(-k_\beta)^{1/2} \, \frac{2\sqrt{2} \, mh}{(r+h)} \right] \right.$$

$$+ \frac{1}{2\sqrt{2}} \, \beta_{r_s}^{-1} (-k_\beta)^{-1/2} \left[1 + 2\beta_{r_s}^2 \, k_\beta \right]$$

$$\left. \sin\left[(-k_\beta)^{1/2} \, \frac{2\sqrt{2} \, mh}{(r+h)} \right] \right|^{-1}$$

when k_β is algebraically negative. It can be seen that when k_β is zero (uniform dielectric) equations (13.2) and (13.3) both reduce to the form

$$(13.4) \qquad D_m = \left[1 + m \frac{h}{(r+h)} \frac{1}{\beta_r} \right]^{-1}$$

This is not exactly the same as the correct form of D_m as originally derived for the uniform dielectric situation, because the ray path equation for the spherical geometry was approximated in order to solve it for the non-uniform dielectric situation. In order to preserve the correct asympotic form of D_m it is necessary to replace (r + h) by r, which is essentially one of the approximations that was made in simplifying the spherical geometry problem. Thus, the equation for the relative geometrical divergence factor becomes

$$(13.5) \qquad D_m = \left| \cosh\left[|k_\beta|^{1/2} \frac{2\sqrt{2}\, m h}{r} \right] \right.$$

$$+ \frac{1}{2\sqrt{2}} \beta_{rs}^{-1} |k_\beta|^{-1/2} \left[1 + 2\beta_{rs}^2\, k_\beta \right]$$

$$\left. \sinh\left[|k_\beta|^{1/2} \frac{2\sqrt{2}\, m h}{r} \right] \right|^{-1}$$

when k_β is algebraically positive, and

(13.6)

$$D_m = \left| \cot \left[(-k_\beta)^{1/2} \frac{2\sqrt{2}\, m\ell}{r} \right] \right.$$

$$+ \frac{1}{2\sqrt{2}} \beta_{rs}^{-1} (-k_\beta)^{-1/2} \left[1 + 2\beta_{rs}^2 k_\beta \right]$$

$$\left. \sin \left[(-k_\beta)^{1/2} \frac{2\sqrt{2}\, m\ell}{r} \right] \right|^{-1}$$

when k_β is algebraically negative. Note that the values of the dielectric properties to be used in the above equations are the values at the axis of symmetry.

Some insight into the behavior of the radar cross section as given by equations (13.1), (13.5), and (13.6) can be obtained by considering the individual terms that contribute to the overall result. Consider a thin pencil beam of electromagnetic radiation incident along the axis of symmetry on the non-uniform lossy dielectric-coated metallic sphere. At the outer dielectric surface part of the incident power is reflected in a diverging cone. This cone is the same for any spatial variation of the dielectric properties within the dielectric layer, and is shown in Figure A13-1 for a uniform dielectric, a dielectric with a de-focusing gradient (k_β positive), and a dielectric with a focusing gradient (k_β negative). This contribution to the scattered wave power is represented by ρ_{rd} , the first term in the brackets of equation (13.1). Subsequent terms (the infinite sum) in equation
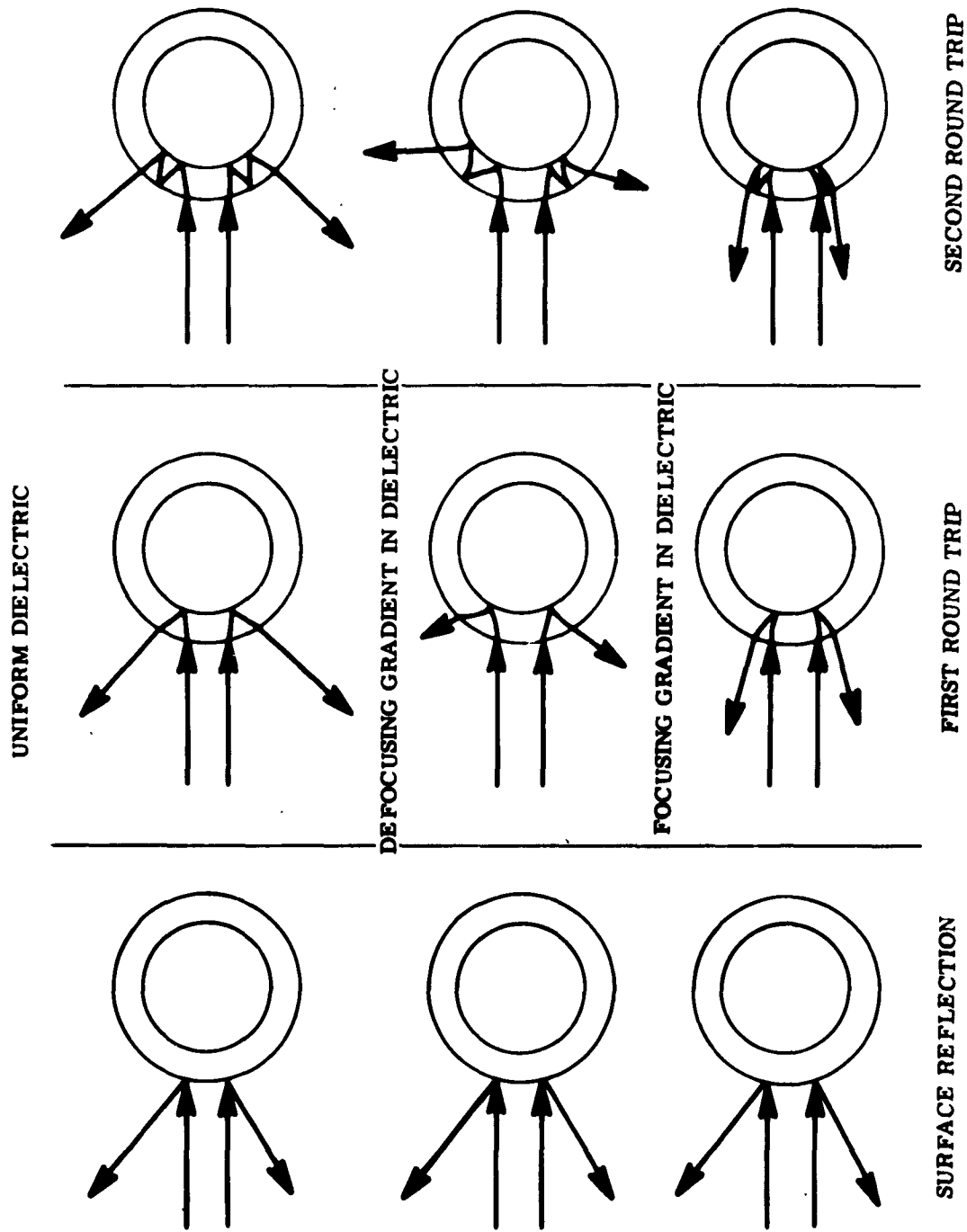
Figure A13-1   Effect of Dielectric Gradients on the Back-Scattered Power Flow from a Non-Uniform Dielectric-Coated Sphere

(13.1) represent the contributions from the part of the incident power that is transmitted into the dielectric layer and subsequently is partly transmitted out again after each successive round trip through the dielectric layer. The emergent cones after the first and second round trips through the dielectric coating are shown in Figure A13-1, for the three different forms of spatial variation of the dielectric properties within the dielectric layer. It can be seen that when a de-focusing gradient is present the emergent cone is wider and consequently the power density is smaller, and vice-versa when a focusing gradient is present. It is important to remember that the relative phasing between the electric fields associated with each of the scattered cones of power determines the resultant total scattered power density. Hence, relative to the uniform dielectric layer, the dielectric layers with either focusing or de-focusing gradients can produce either increased or decreased total back-scattered power density. However, for very thin dielectric layers the usual effect of a de-focusing gradient is a relative decrease in the radar cross section and vice-versa for the focusing gradient. As in the case of a uniform dielectric coating, conditions can be found for which the radar cross section vanishes. Also, equation (13.6) shows that when

$$(13.7) \quad \cos\left[(1-k_{\rho})^{1/2}\ \frac{2\sqrt{2}\ mk}{r}\right] + \frac{1}{2\sqrt{2}}\ \beta_{r_s}^{-1}\ (1-k_{\rho})^{-1/2}$$

$$\left[1 + 2\ \beta_{r_s}^{2}\ k_{\rho}\right]\ \sin\left[(1-k_{\rho})^{1/2}\ \frac{2\sqrt{2}\ mk}{r}\right] = 0$$

the radar cross section becomes infinitely large. This is because the mth emergent cone of power is focused to a point at the radar receiver location, producing an infinitely large power density there. This result is not valid because one of the applicability criteria for the geometrical optics solution has been violated (the solution is not good in the vicinity of a focal point). However, this condition is indicative of the fact that the back-scattered power density will be very large and consequently significant increases in the radar cross section may be observed under these conditions.

APPENDIX A-14

SPATIAL VARIATION OF PLASMA PROPERTIES IN THE SHOCK LAYER AROUND THE NOSE OF A SPHERE IN HYPERSONIC FLIGHT

The computation of the electromagnetic properties of the ionized gas (plasma) in the shock layer around the nose of a blunt body such as a sphere in hypersonic flight thru air has received considerable attention in recent years. The problem must be handled numerically and is, in general, very complicated.

When the aerodynamic parameters are such that chemical equilibrium is maintained throughout the flow field in the nose region, the situation is greatly simplified. The dependence of the plasma properties on the absolute size of the body practically disappears and consequently normalized solutions can be obtained. The aerodynamic variables involved in this situation are the composition, temperature, and density of the ambient air thru which the body flies, and the speed of the body. Charts of the flow field properties of interest for electromagnetic considerations have been prepared[1] for special locations in the flow field, such as the stagnation point. A typical example of the dependence of the plasma properties at the stagnation point on the speed of the body is shown in Figure A14-1, derived from Reference 1. Both the plasma frequency and the electron collision frequency are shown, normalized to a reference frequency of 35Gc for an ambient air pressure of 10 mm Hg, which is approximately equivalent to an altitude of 100,000 feet. The spatial variation of the plasma properties in the shock layer around the body away from the stagnation
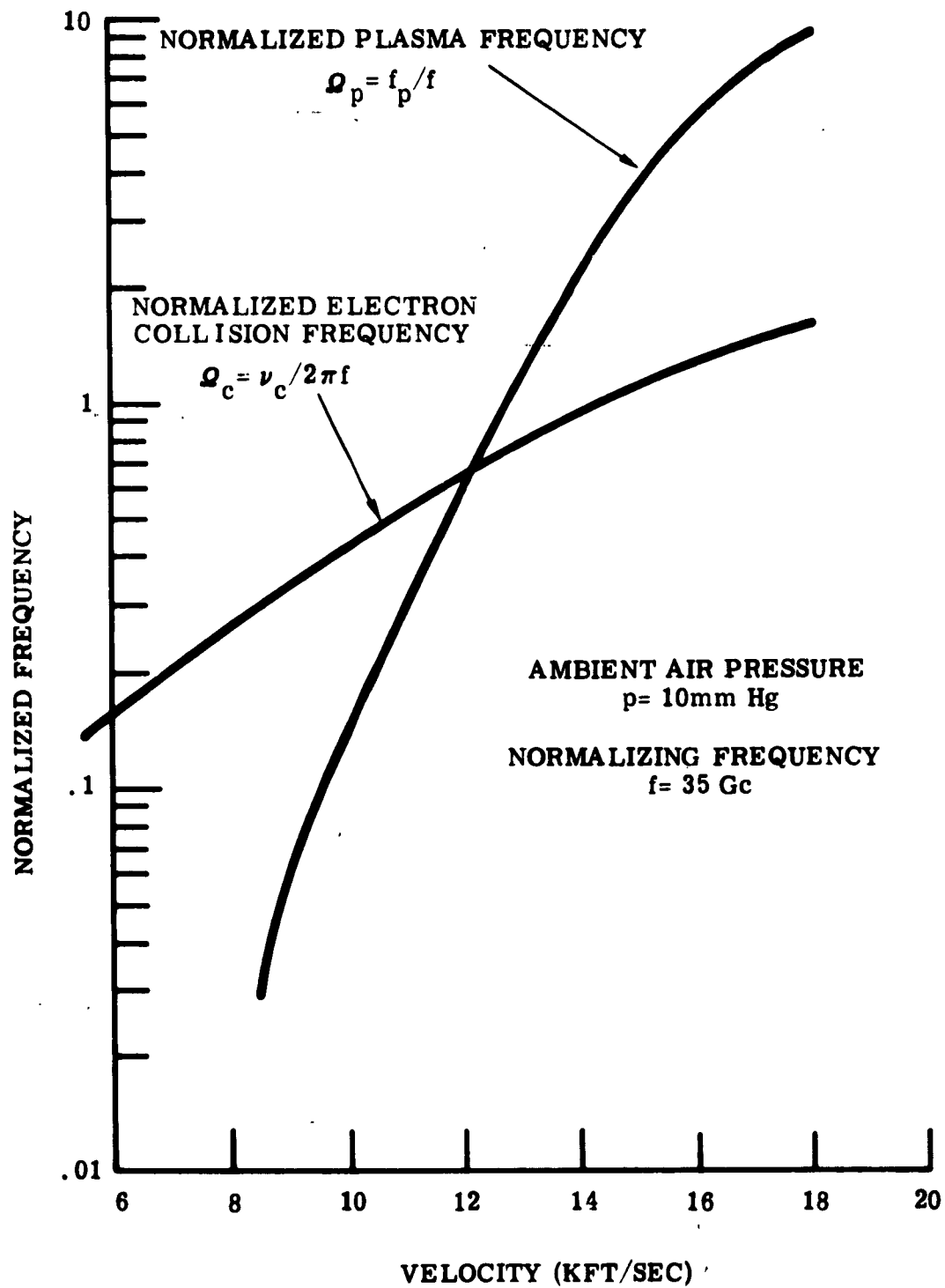
Figure A14-1   Stagnation Point Plasma Properties for Equilibrium
Conditions

point depends on the initial conditions at the stagnation point and the exact shape of the blunt nose of the body.

For a spherical nose, the pressure variation in the shock layer from the stagnation point to 45 degrees off axis approximately follows the Newtonian formula

$$(14.1) \qquad \frac{p}{p_s} = \cos^2 \theta$$

where p is the pressure in the shock layer, p_s is the pressure at the stagnation point, and θ is the angle measured around the sphere from the stagnation point. The electron collision frequency in air is almost directly proportional to the pressure, [2] hence the variation of the electron collision frequency ν_c around the nose of the sphere is given by

$$(14.2) \qquad \frac{\nu}{\nu_{cs}} \cong \cos^2 \theta$$

where ν_{cs} is the value of the electron collision frequency at the stagnation point. The expansion of the hot compressed air from the stagnation region as it flows around the body approximately follows an isentropic process. Reference to charts of high-temperature air properties [2], [3], [4] shows that for isentropic expansions over small pressure changes in the parameter regime shown in Figure A14-1, the plasma frequency f_p decreases approximately proportionally to the pressure, hence

$$(14.3) \qquad \frac{f_p}{f_{ps}} \cong \cos^2 \theta$$

where f_{ps} is the value of the plasma frequency at the stagnation point. Near the stagnation point, equations (14.2) and (14.3) can be written in the forms

$$(14.4) \qquad \frac{\nu_c}{\nu_{cs}} \cong 1 - \theta^2$$

and

$$(14.5) \qquad \frac{f_p}{f_{ps}} \cong 1 - \theta^2$$

In general, for a less restrictive situation, the plasma frequency and the electron collision frequency in the vicinity of the stagnation point can be expressed in the forms

$$(14.6) \qquad \frac{f_p}{f_{ps}} \cong 1 + k_p \theta^2$$

and

$$(14.7) \qquad \frac{\nu_c}{\nu_{cs}} \cong 1 + k_c \theta^2$$

Using the normalized plasma frequency ($\Omega_p = f_p / f$) and the normalized electron collision frequency ($\Omega_c = \nu_c / \omega$) these expressions become

(14.8)
$$\Omega_p \cong \Omega_{ps} \left(1 + k_p \theta^2 \right)$$

and

(14.9)
$$\Omega_c \cong \Omega_{cs} \left(1 + k_c \theta^2 \right)$$

where ω is the angular frequency of the incident electromagnetic wave. The electromagnetic wave relative phase factor β_r for plasma, introduced in Appendix 1, is given by

(14.10)
$$\beta_r = \left\{ \frac{\left[\Omega_c^2 + \left(1 - \Omega_p^2 \right)^2 \right]^{1/2} \left(1 + \Omega_c^2 \right)^{1/2} + \Omega_c^2 + \left(1 - \Omega_p^2 \right)}{2 \left(1 + \Omega_c^2 \right)} \right\}^{1/2}$$

Substituting equations (14.8) and (14.9) into (14.10) and neglecting powers of θ greater than the second gives

(14.11)
$$\beta_r \cong \beta_{rs} \left(1 + k_\beta \theta^2 \right)$$

where

(14.12)
$$\beta_{rs} = \left\{ \frac{\left[\Omega_{cs}^2 + \left(1 - \Omega_{ps}^2 \right)^2 \right]^{1/2} \left(1 + \Omega_{cs}^2 \right)^{1/2} + \Omega_{cs}^2 + \left(1 - \Omega_{ps}^2 \right)}{2 \left(1 + \Omega_{cs}^2 \right)} \right\}^{1/2}$$

and

(14.13)

$$\mathbb{k}_\beta = \frac{1}{2\beta_{r_s}^2} \frac{\Omega_{ps}^2}{1+\Omega_{cs}^2}$$

$$\left\{ \mathbb{k}_c \frac{\Omega_{cs}^2}{1+\Omega_{cs}^2} \left[1 + \frac{\left(1+\Omega_{cs}^2\right)^{1/2}}{\left[\Omega_{cs}^2+\left(1-\Omega_{ps}^2\right)^2\right]^{1/2}} \right] \right.$$

$$\left. - \mathbb{k}_p \left[1 + \frac{\left(1-\Omega_{ps}^2\right)\left(1+\Omega_{cs}^2\right)^{1/2}}{\left[\Omega_{cs}^2+\left(1-\Omega_{ps}^2\right)^2\right]^{1/2}} \right] \right\}$$

The variation of the relative phase factor of the plasma layer near the stagnation point is important in the determination of the nose-on radar cross section of the plasma covered blunt body. Both the plasma frequency and the electron collision frequency decrease in going away from the stagnation point in flow fields around blunt bodies ($\mathbb{k}_p$ and $\mathbb{k}_c$ are algebraically negative). This is depicted in Figure A14-2. Equations (14.11) thru (14.13) show, however, that very near the stagnation point the relative phase factor may either increase or decrease at first in going away from the stagnation point ($\mathbb{k}_\beta$ may be either positive or negative algebraically). This is also depicted, in exaggerated form, in Figure A14-2. For example, when there is no angular variation of the electron collision frequency ($\mathbb{k}_c = 0$) the variation of the relative phase factor is opposite to that of the plasma frequency when the normalized plasma frequency is less than $\sqrt{2}$, and in the same direction when the normalized
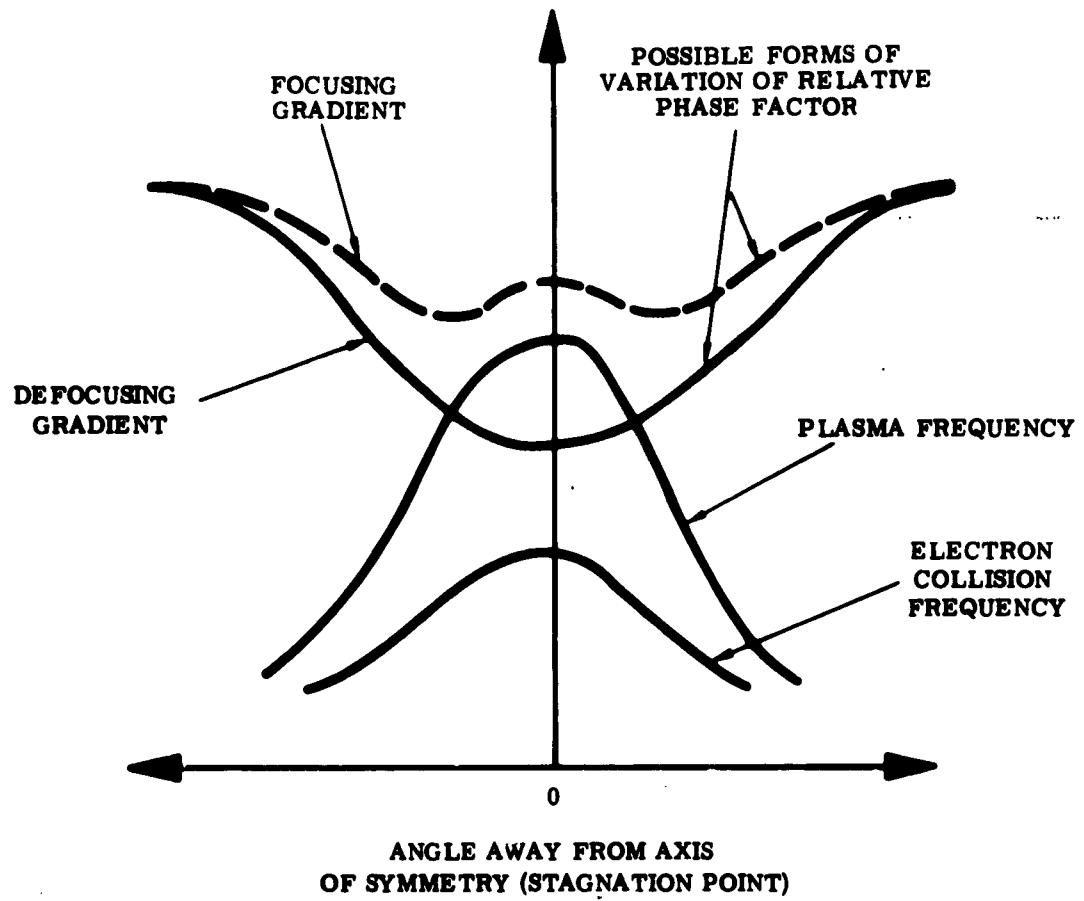
Figure A14-2   Typical Variation of Equilibrium Plasma Properties
Around a Sphere

plasma frequency is greater than $\sqrt{2}$, that is

$$(14.14) \qquad \text{sign} \left| k_\beta \right| = - \text{sign} \left| k_p \right| \quad \left\{ \begin{matrix} k_c = 0 \\ \Omega_{ps} < \sqrt{2} \end{matrix} \right.$$

$$(14.15) \qquad \text{sign} \left| k_\beta \right| = \text{sign} \left| k_p \right| \quad \left\{ \begin{matrix} k_c = 0 \\ \Omega_{ps} > \sqrt{2} \end{matrix} \right.$$

When the relative phase factor increases monotonically in going away from the stagnation point an incident electromagnetic wave is defocused relative to the back-scattering direction, as discussed in Appendix 13. When the relative phase factor decreases at first in going away from the stagnation point the part of an incident electromagnetic wave within the region of decreasing relative phase factor is focused in the back-scattering direction. Thus, in general, defocusing occurs at low values of plasma frequency and focusing occurs at high values of plasma frequency.

The prediction of the spatial variation of the plasma properties in the flow field when chemical equilibrium is not maintained throughout the flow field is extremely difficult. The composition of the gas throughout the flow field will depend on the absolute size of the body as well as its generic shape because the chemical reactions proceed at finite rates and the flow time around the body is proportional to the body size. Thus, a very large body gives long flow times and consequently near-equilibrium conditions can be maintained throughout the shock layer around the body. A very small body gives short flow times, the flow field chemical reactions will be far from equilibrium, and consequently the flow field properties will depart significantly

from the equivalent equilibrium properties. A typical calculation[5] of
the non-equilibrium flow field properties around the nose of a
sphere in hypersonic flight thru air is shown in Figure A14-3. It can
be seen from this figure that the electron collision frequency does
not change very much thru the shock layer from near the shock front
to near the body (in the radial direction), and has a slight decrease
in the angular direction away from the stagnation point. Actually,
within the angular range shown (from zero to approximately 20
degrees) the variation of the electron collision frequency follows the
form

$$(14.16) \qquad \Omega_c \cong \Omega_{cs} \left(1 - \theta^2 \right)$$

which is the same as for the equilibrium flow field. The plasma fre-
quency shows significant variation in both the radial direction thru the
shock layer and the angular direction away from the stagnation point.
Within the angular range shown, the variation of the plasma frequency
in the angular direction follows the form

$$(14.17) \qquad \Omega_p \cong \Omega_{ps} \left(1 + k_p \theta^2 \right)$$

where k_p is between -3 and -5, which gives a much more rapid change
than predicted for the equilibrium flow field.

The shock detachment distance at the stagnation point, for the same
conditions as given in Figure A14-1, is shown in Figure A14-4. As
usual, this shock layer thickness (h) is small compared to the nose
radius (r) of the body.
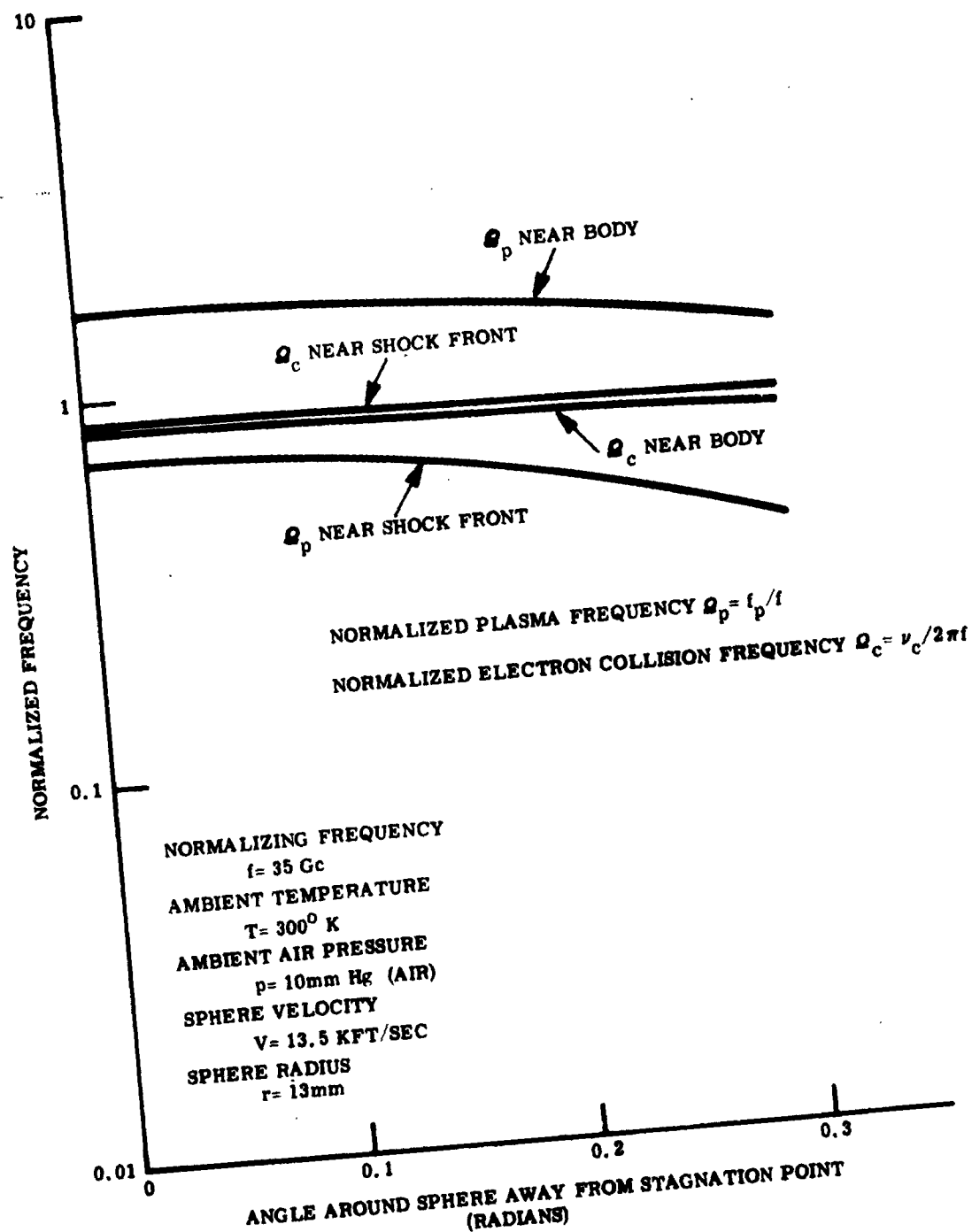
Figure A14-3   Typical Variation of Non-Equilibrium Plasma Properties Around a Sphere
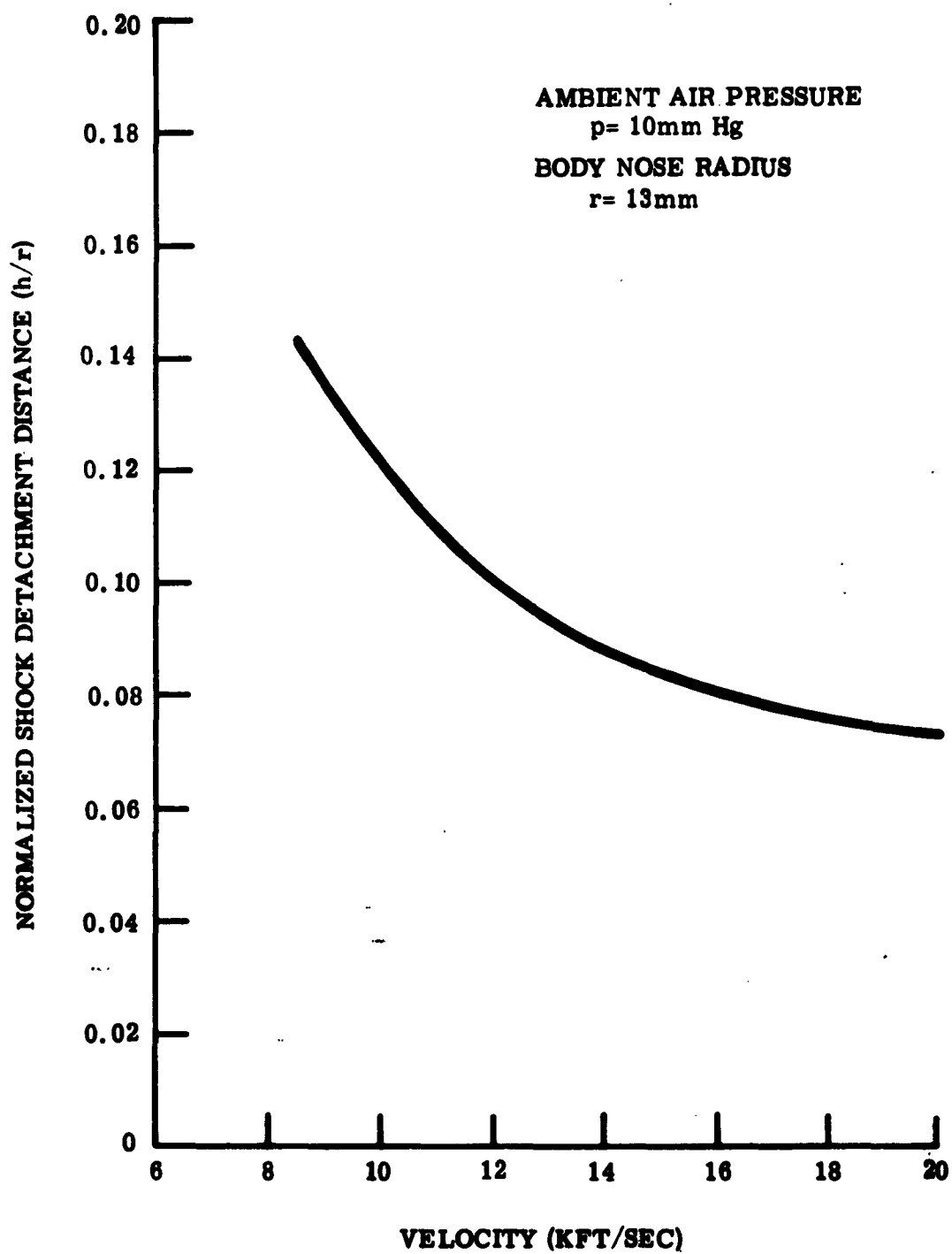
Figure A14-4   Shock Detachment Distance at Stagnation Point

(1) General Motors Corporation, Defense Research Laboratories,
     Plasma Frequency and Electron Collision Frequency Charts
     for Hypersonic Vehicle Equilibrium Flow Fields in Air, by
     H. M. Musal, Jr., SP62-232, Santa Barbara, Calif., October 1962.

(2) Bendix Corporation, Bendix Systems Division, Electron Collision
     Frequency in Equilibrium High Temperature Air, by H. M. Musal, Jr.
     Research Note 9, Ann Arbor Mich., 1 May 1960.

(3) General Dynamics Corporation, Convair Division, Air in
     Equilibrium for Normal Shocks at Hypersonic Velocities,
     by A. R. Hochstim, included with ZPh-GP-002, San Diego,
     California, January 1958.

(4) AVCO Research Laboratory, Hypersonic Gas Dynamic Charts for
     Equilibrium Air, by S. Feldman, Research Report 40, Everett,
     Mass., January 1957.

(5) Cornell Aeronautical Laboratory, Inc., Nonequilibrium Bow Shock
     Calculations for Defense Research Laboratories, General Motors
     Corporation, CAL Order No. 647, Buffalo, New York, December 6,
     1962.

APPENDIX A-15

GEOMETRICAL OPTICS NOSE-ON RADAR CROSS SECTION OF A METALLIC SPHERE COATED WITH AN ANGULARLY NON-UNIFORM LOSSY PLASMA

Given here is the radar cross section σ , obtained by the geometrical optics approach, of a perfectly reflective (metallic) sphere of radius r covered with a non-uniform coating of lossy plasma. The plasma is assumed to have uniform thickness $\hbar$ all around the sphere. The electromagnetic properties of the plasma are assumed to vary only in the angular direction around the sphere away from an axis of symmetry and not angularly around the axis of symmetry nor radially from the center of the sphere. The incident electromagnetic wave is taken to be propagating in a direction parallel to the axis of symmetry (incident nose-on). Furthermore, it is assumed that the plasma can be characterized (electromagnetically) by a permeability μ_{ϕ} , a dielectric constant ϵ_{ϕ} , and a conductivity σ_{ϕ} analogous to the situation for non-ionized media. Thus, the situation becomes that of a non-uniform lossy dielectric-coated metallic sphere. Using the results from Appendixes 1, 13, and 14, the normalized nose-on radar cross section is given by

$$(15.1) \quad \frac{\sigma}{\pi r^2} = \left(1 + \frac{\hbar}{r}\right)^2 \left| \Gamma_{\phi s} - \frac{\left(1 - \Gamma_{\phi s}^2\right)}{\Gamma_{\phi s}} \sum_{m=1}^{\infty} D_m \left(\Gamma_{\phi s} e^{-\gamma_{\phi s} 2\hbar}\right)^m \right|^2$$

where $\Gamma_{\phi s}$ is the reflection coefficient for a plane transverse electromagnetic wave propagating normally from free space into a

plane interface between free space and a uniform plasma having the electromagnetic properties of the coating at the axis of symmetry, γ_{ps} is the propagation factor for a plane transverse electromagnetic wave propagating thru an unbounded uniform plasma having the electromagnetic properties of the coating at the axis of symmetry, and D_m is the relative geometrical divergence factor for the mth ray path thru the plasma coating. Appendixes 1, 4, 13 and 14 give

$$(15.2) \quad \Gamma_{ps} = \frac{1 - \left(1 - \dfrac{\Omega_{ps}^2}{1-j\Omega_{cs}}\right)^{1/2}}{1 + \left(1 - \dfrac{\Omega_{ps}^2}{1-j\Omega_{cs}}\right)^{1/2}}$$

$$(15.3) \quad \gamma_{ps} = j\,\frac{2\pi}{\lambda_v}\left(1 - \frac{\Omega_{ps}^2}{1-j\Omega_{cs}}\right)^{1/2}$$

$$(15.4) \quad D_m = \left| \cosh\left[k_\beta^{1/2}\,\frac{2\sqrt{2}\,mh}{r}\right] \right.$$
$$\left. + \frac{1}{2\sqrt{2}}\,\beta_{r_s}^{-1}\,k_\beta^{-1/2}\left[1 + 2\beta_{r_s}^2\,k_\beta\right]\sinh\left[k_\beta^{1/2}\,\frac{2\sqrt{2}\,mh}{r}\right]\right|^{-1}$$

when k_β is algebraically positive, and

$$(15.5) \quad D_m = \left| \cos\left[(1-k_\beta)^{1/2}\,\frac{2\sqrt{2}\,mh}{r}\right] \right.$$
$$\left. + \frac{1}{2\sqrt{2}}\,\beta_{r_s}^{-1}\,(1-k_\beta)^{-1/2}\left[1 + 2\beta_{r_s}^2\,k_\beta\right]\sin\left[(1-k_\beta)^{1/2}\,\frac{2\sqrt{2}\,mh}{r}\right]\right|^{-1}$$

when k_β is algebraically negative, where

$$(15.6) \quad \beta_{r_s} = \left\{ \frac{\left[\Omega_{cs}^2 + \left(1 - \Omega_{ps}^2\right)^2\right]^{1/2} \left(1 + \Omega_{cs}^2\right)^{1/2} + \Omega_{cs}^2 + \left(1 - \Omega_{ps}^2\right)}{2\left(1 + \Omega_{cs}^2\right)} \right\}^{1/2}$$

and in the vicinity of the axis of symmetry

$$(15.7) \quad k_\beta = \frac{1}{2\beta_{r_s}^2} \cdot \frac{\Omega_{ps}^2}{1 + \Omega_{cs}^2}$$

$$\left\{ k_c \frac{\Omega_{cs}^2}{1 + \Omega_{cs}^2} \left[1 + \frac{\left(1 + \Omega_{cs}^2\right)^{1/2}}{\left[\Omega_{cs}^2 + \left(1 - \Omega_{ps}^2\right)^2\right]^{1/2}} \right] \right.$$

$$\left. - k_p \left[1 + \frac{\left(1 - \Omega_{ps}^2\right)\left(1 + \Omega_{cs}^2\right)^{1/2}}{\left[\Omega_{cs}^2 + \left(1 - \Omega_{ps}^2\right)^2\right]^{1/2}} \right] \right\}$$

when the normalized plasma frequency Ω_p and the normalized electron collision frequency Ω_c in the vicinity of the axis of symmetry are given by

$$(15.8) \quad \Omega_p \cong \Omega_{ps} \left(1 \pm k_p \, \theta^2\right)$$

(15.9)
$$\Omega_c \cong \Omega_{cs}\left(1 + k_c\,\theta^2\right)$$

where

$\Omega_p = \omega_p/\omega$ = normalized plasma frequency (subscript "s" indicates "at axis of symmetry")

$\Omega_c = \nu_c/\omega$ = normalized electron collision frequency (subscript "s" indicates "at axis of symmetry")

ω_p = angular plasma frequency ($2\pi f_p$)

ν_c = electron collision frequency

ω = angular radar frequency ($2\pi f$)

λ_r = free-space wavelength of the radar wave

θ = angle measured around sphere away from axis of symmetry.

It can be shown, as in the case of a uniform plasma coating, that when the plasma coating is highly reflective $\left(\ |\Gamma_{ps}| \cong 1\right)$ the radar cross section σ approaches the value $\pi r^2\left(1 + \ell/r\right)^2$, which is the value for a perfectly reflective sphere having a radius equal to the outer radius of the plasma coating. When the plasma coating is negligibly reflective ($|\Gamma_{ps}| \cong 0$) the radar cross section σ approaches the value πr^2 , which is the value for the bare metallic sphere, as would be expected. The radar cross section can also exhibit maxima and minima above and below these values, as discussed in Appendix A-13. Specifically, when

(15.10)
$$\Gamma_{ps} = \frac{\left(1 - \Gamma_{ps}^2\right)}{\Gamma_{ps}} \sum_{m=1}^{\infty} D_m \left(\Gamma_{ps}\, e^{-\gamma_{ps} 2\ell}\right)^m$$

the radar cross section will become vanishingly small, and when

$$(15.11) \quad \cos\left[(1-k_\beta)^{1/2} \frac{2\sqrt{2}\, m\, \hbar}{r}\right] =$$

$$-\frac{1}{2\sqrt{2}} \beta_{r_s}^{-1} (1-k_\beta)^{-1/2} \left[1+2\beta_{r_s}^2\, k_\beta\right] \sin\left[(1-k_\beta)^{1/2} \frac{2\sqrt{2}\, m\, \hbar}{r}\right]$$

the radar cross section will become infinitely large in the geometrical optics approximation. This latter condition can occur only when k_β is algebraically negative, which is the focusing regime. As pointed out earlier, the numerical results of the geometrical optics approach are not valid under this condition.

DISTRIBUTION LIST
for Analysis Reports on the
HYPERVELOCITY RANGE RESEARCH PROGRAM

Recipient	Copy No.	Recipient	Copy No.
Commanding General U.S. Army Missile Command Redstone Arsenal, Alabama ATTN: ORDXM-RRX	1–12	ARO, Incorporated von Karman Facility,Arnold AF Station Tullahoma, Tennessee ATTN: J. Lukasiewiez	34
Los Angeles Procurement District, U.S. Army 55 South Grand Avenue Pasadena, California ATTN: F.K.Whitburn, ContractingOfficer	13	Aerojet-General Corporation Azusa, California ATTN: C. Dunning	35
Director Advanced Research Projects Agency Washington 25, D.C. ATTN: F. Koether ATTN: E. Haynes ATTN: C. McLain ATTN: Lt Col Cooper	14–16 17 18 19	Armour Research Foundation 10 W. 35th Street Chicago 16, Illinois ATTN: Fluid Dynamics Research Division Battelle Memorial Institute 505 King Avenue Columbus 1, Ohio ATTN: Battelle-DEFENDER	36 37
Armed Services Technical Information Agency Arlington Hall Station Arlington 12, Virginia ATTN: J.H. Heald	20–29	Barnes Engineering Company 30 Commerce Road Stamford, Connecticut ATTN: H. Yates	38
Avco-Everett Research Laboratory 2385 Revere Beach Parkway Everett, Massachusetts ATTN: R. Taylor	30	Bell Telephone Laboratories, Inc. Whippany, New Jersey ATTN: C.W. Hoover, Room 2B-105	39
Aerospace Corporation 2400 E. El Segundo Boulevard El Segundo, California ATTN: D. Bitondo	31	Bendix Corporation Systems Division 3300 Plymouth Road Ann Arbor, Michigan ATTN: Systems Analysis and Math. Dept.	40
Aerospace Corporation P.O. Box 95085 Los Angeles 45, California ATTN: J. Logan	32	Boeing Airplane Company P.O. Box 3707 Seattle, Washington ATTN: Org. 2-5732/J. Klaimon	41
Avco Corporation Research and Advanced Development Division Wilmington, Massachusetts ATTN: H. Flickinger	33	Brown Engineering Company P.O. Drawer 917 Huntsville, Alabama ATTN: H. Crews	42

DISTRIBUTION LIST (continued)

Recipient	Copy No.	Recipient	Copy No.
Commanding General U.S. Army Materiel Command Washington 25, D.C.	43	California Institute of Technology Pasadena, California ATTN: Prof. L. Lees	57
Commander U.S. Army Missile Command Redstone Arsenal, Alabama ATTN: AMSMI-RB ATTN: AMSMI-RRX ATTN: AMSMI-RNR	44 45 46	Cornell Aeronautical Laboratory 4455 Genesee Street Buffalo 21, New York ATTN: J. Lotsof ATTN: W. Wurster	58 59
Commanding General U.S. Army Air Defense Command Colorado Springs, Colorado ATTN: Advanced Projects Division, G-3	47	Director Ames Research Center Moffett Field, California ATTN: H. Allen	60
Commanding General U.S. Army Ballistics Research Laboratories Aberdeen Proving Ground, Maryland ATTN: C.H. Murphy	48	Defense Research Corporation 4050 State Street Santa Barbara, California ATTN: W. Short	61
Commanding General U.S. Army Research and Development Washington 25, D.C. ATTN: Intl. Division ATTN: Physical Sciences Division	49 50	Director USAF Cambridge Research Laboratories Laurence Hanscom Field Bedford, Massachusetts ATTN: CRRELR, Stop 29	62
Commanding General U.S. Army Elec. and Communications Command Research and Development Fort Monmouth, New Jersey	51	Director USAF Office of Scientific Research Washington 25, D.C. ATTN: Mechanics Division/Major Terrell	63
Chief U.S. Navy Bureau of Weapons Washington 25, D.C. ATTN: RMWC-322	52	Director Electromagnetic Warfare Laboratory Wright-Patterson Air Force Base Dayton, Ohio ATTN: ASRN/W. Bahret	64
Director U.S. Naval Research Laboratory Washington 25, D.C. ATTN: Code 2027	53	Director Institute for Defense Analyses 1666 Connecticut Avenue, N.W. Washington 9, D.C. ATTN: J. Menkes ATTN: J. Martin ATTN: D. Katch , JASON Library	65 66 67
Central Intelligence Agency 2930 E Street, N.W. Washington, D.C. ATTN: OCR Standard District	54–56	Director Weapon Systems Evaluation Group Pentagon, Room 1E-800 Washington 25, D.C.	68

DISTRIBUTION LIST (continued)

Recipient	Copy No.	Recipient	Copy No.
Director Langley Research Center Langley Field, Virginia ATTN: W. Erickson	69	Headquarters, ARDC Andrews Air Force Base Washington, D.C. ATTN: Col Fazio/Intl. Programs	79
Director Marshall Space Flight Center Huntsville, Alabama ATTN: M-AERO-TS	70	Jet Propulsion Laboratory 4800 Oak Grove Drive Pasadena, California ATTN: H. Denslow	80
Electro-Optical Systems, Inc. 125 N. Vinedo Avenue Pasadena, California ATTN: R. Denison	71	Kaman Nuclear Division Colorado Springs, Colorado ATTN: A. Bridges	81
Ford Motor Company Aeronutronics Division Ford Road Newport Beach, California ATTN: H. Hall ATTN: R. Hoglund	72 73	Lockheed Corporation Missiles and Space Division Sunnyvale, California ATTN: Ray Munson	82
General Applied Sciences Laboratories Merrick and Stewart Avenues Westbury, Long Island, New York ATTN: M. Bloom	74	Martin Aircraft Company Orlando, Florida ATTN: J. Mays	83
General Dynamics Corporation Astronautics Division San Diego, California ATTN: W. Hooker 6-172	75	Massachusetts Institute of Technology Lincoln Laboratory P.O. Box 73 Lexington 73, Massachusetts ATTN: M. Herlin ATTN: R. Slattery	84 85
General Electric Company Reentry Vehicles Division 3198 Chestnut Street Philadelphia, Pennsylvania ATTN: L.I. Chaseen, Room 3446	76	Melpar, Inc. Applied Science Division 11 Galen Street Watertown 72, Massachusetts ATTN: Librarian	86
General Electric Company Valley Forge Space Technical Center P.O. Box 8555 Philadelphia 1, Pennsylvania ATTN: K. Wau	77	New York University Department of Aero Engineering University Heights New York 53, New York ATTN: L. Arnold	87
Heliodyne Corporation 2365 Westwood Boulevard Los Angeles, California ATTN: S. Feldman	78	North American Aviation Space and Information Systems Division 12214 Lakewood Boulevard Downey, California ATTN: E. Allen	88

DISTRIBUTION LIST (concluded)

Recipient	Copy No.	Recipient	Copy No.
Purdue University School of Aero and Engineering Sciences LaFayette, Indiana ATTN: I. Kvakovsky	89	The John Hopkins University Applied Physics Laboratory 8621 Georgia Avenue Silver Springs, Maryland ATTN: G. Seielstad	100
Princeton University Princeton, New Jersey ATTN: Prof. E. Frieman ATTN: Prof. S. Bogdonoff	90 91	University of California San Diego, California ATTN: Prof. N. M. Kroll	101
Rome Air Development Center Griffiss Air Force Base Rome, New York ATTN: P. Sandler	92	University of California Lawrence Radiation Laboratory Livermore, California ATTN: C. Craig	102
Radio Corporation of America Missiles and Surface Radar Division Moorestown, New Jersey ATTN: A. Gold	93	University of Chicago Laboratories for Applied Science Chicago 37, Illinois ATTN: L. M. Biberman	103
Raytheon Manufacturing Company Missile Systems Division Bedford, Massachusetts ATTN: I. Britton, Librarian	94	University of Michigan Ann Arbor, Michigan ATTN: Prof. K. M. Case	104
Space Technology Laboratories 1 Space Park Redondo Beach, California ATTN: Leslie Hromas	95	University of Michigan Willow Run Laboratories P. O. Box 2008 Ann Arbor, Michigan ATTN: BAMIRAC/B. R. George	105
Space Technology Laboratories, Inc. P. O. Box 95001 Los Angeles 45, California ATTN: L. McFadden	96	University of Michigan Radiation Laboratory 201 Catherine Ann Arbor, Michigan	106
Sylvania Elec. Products Applied Physics Laboratory Waltham, Massachusetts ATTN: R. Row	97	U.S. Air Force Ballistic Missile Division AF Unit Post Office Los Angeles 45, California ATTN: Major R. Fowler/WDTVP	107
Stanford Research Institute Menlo Park, California ATTN: Acquisitions	98	U.S. Army Liaison Office Canadian Armament Res and Dev Establishment P. O. Box 1427 Quebec, P.Q., Canada ATTN: Lt Col E.W. Kreischer	108
The Rand Corporation 1700 Main Street Santa Monica, California ATTN: Mary Romig	99	GM Defense Research Laboratories	109 and above

GM Defense Research Laboratories, General Motors Corp., Santa Barbara, Calif.
Rpt. TR63-217A, ON THE RADAR-PLASMA ABSORPTION EFFECT, H. M. Musal, Jr., July 1963. 197 p. incl. illus., tables, 33 refs.

The usual manifestation of the phenomenon known as the radar absorption effect is the drastic reduction of the radar cross section of a body when it is surrounded by a plasma sheath having certain spatial configuration and electromagnetic properties.

A brief review of the hypersonic aerodynamics, chemical physics, plasma physics, and electromagnetic wave scattering phenomena involved in the study of these effects is given. It is shown that the effect of the plasma sheath on the radar cross section of a hypersonic body can be considered separately from the effect of the plasma trail left behind the body. Several

1. Plasma physics
2. Electromagnetic waves-scattering
3. Radar absorption
4. Reentry aerodynamics
5. Reentry-aerodynamics Test Facilities.

I TR63-217A
II Contract DA 04-495-ORD-3567(Z)
III Musal, H. M., Jr.

(Descriptors) Atmosphere entry, Plasma sheath, Absorption, Radar, Hypervelocity guns, Hypervelocity projectiles Super aerodynamics, Electromagnetic waves

theoretical models of electromagnetic wave scattering from plasma-covered bodies are formulated and analyzed. The theoretical results of these analyses show both absorption and enhancement effects that could be caused by the plasma sheath.

Theoretical predictions are compared with experimental results and it is seen that the measured absorption and enhancement are both significantly greater than predicted. Possible reasons for these discrepancies between theory and experiment are discussed, and it is concluded that the physical mechanisms that cause the effects observed experimentally are not yet completely understood and consequently not completely included in the theoretical models.